Study on iron catalysis for co-gasification of low rank coal and woody biomass

(低品位炭/木質バイオマス混合ガス化における鉄の触媒作用に関する研究)

2018

Shen Lingbo

Akita University

Akita University

Contents

Chapter 1 Introduction 1

1.1 The importance of low rank coal use 1

1.2 New coal power generation technology 3

1.3 Coal pyrolysis and gasification 5

1.3.1 Coal pyrolysis 5

1.3.2 Coal gasification 6

1.4 Catalyst for gasification 7

1.4.1 Overview for gasification catalyst 7

1.4.2 Effects of iron catalyst on pyrolysis and gasification of coal 7

1.5 Co-gasification of sub-bituminous coal and woody biomass with iron catalyst 9

1.6 Purpose and composition of doctoral thesis 10

Chapter 2 Effect of iron-loaded biochar on steam gasification of sub-bituminous coal 12

2.1 Introduction 12

2.2 Experimental 13

2.2.1 Samples 13

2.2.2 Iron catalyst loading 14

2.2.3 Preparation of mixed samples of iron-loaded biochar and AD 15

2.2.4 Pyrolysis and gasification 16

2.2.5 Characterization of the pyrolyzed char and gasified residue 17

2.3 Results and discussion 18

2.3.1 Effect of iron-loaded biochar on the gasification of AD 18

2.3.2 Comparison between the amount of hydrogen evolution calculated by individual gasification and that measured by co-gasification 22

2.3.3 Effect of biomass ash on the gasification of AD 24

2.3.4 Relationship between specific rate and carbon conversion 25

2.3.5 Change of activation energy with addition of Fe-SGchar 27

2.3.6 Chemical form and crystallite size of Fe catalyst after pyrolysis and gasification of AD and SG 30

2.4 Conclusions 38

Chapter 3 Optimization of mixing conditions of subbituminous coal and iron-loaded biochar for co-gasification 39

Akita University

3.1 Introduction 39
3.2 Experimental 40
3.2.1 Preparation of mixed samples of iron-loaded biochar and AD 40
3.2.2 Pyrolysis and gasification 41
3.3 Results and Discussion 42
3.3.1 Effect of iron-loaded biochar on the gasification of AD 42
3.3.2 Influence of addition ratio of Fe-SGchar 45
3.3.3 Influence of Fe-SGchar on specific rate 46
3.3.4 Change in the form of iron during pyrolysis and steam gasification 47
3.4 Conclusion 54
Chapter 4 Effect of physical mixing of coal, biomass and Fe catalyst on the gasification 55
4.1 Introduction 55
4.2 Experimental 56
4.2.1 Samples 56
4.2.2 Preparation of mixed samples and iron catalyst loading 56
4.2.3 Pyrolysis and steam gasification 57
4.2.4 Characterization of the pyrolyzed char and gasified residue 57
4.3 Result and discussion 58
4.3.1 Weight change of weight for AD and (SG+AD) during pyrolysis 58
4.3.2 Comparison of hydrogen evolution for gasification with and without Fe catalyst 60
4.3.3 Comparison between impregnation method and physical mixing method 62
4.3.4 Interaction between SG and AD in non-catalyst co-gasification and catalytic co-gasification 63
4.3.5 Effect of iron catalyst on reactivity of char for co-gasification 65
4.3.6 Change of weight during pyrolysis by Fe_2O_3 addition 66
4.3.7 XRD patterns for Fe_2O_3-AD and Fe_2O_3-(SG+AD) during gasification 69
4.3.8 Influence of biomass mixing ratio on the co-gasification 70
4.4 Conclusion 74
Chapter 5 Conclusion 75
5.1 Conclusion 75
5.2 Future outlook 77
References 78
Acknowledgments 86

Chapter 1 Introduction

1.1 The importance of low rank coal use

Fossil resources are mainly used to produce energy. However, with more and more demand of energy, reserves of fossil resources rapidly reduce. It has already become a global problem in these years which we call “Energy shortage”.

Table1.1 shows the recoverable reserves and production for the main fossil resources [1]. The Reserves-to-production ratio (RPR or R/P) is the remaining amount of a non-renewable resource, expressed in time. While applicable to all natural resources, the RPR is most commonly applied to fossil fuels. The RPRs for oil, natural gas and coal are shown in Figure 1.1 [1]. From this figure, it can be seen that the RPRs of oil and natural gas are 56 years and 59.6 years, respectively. As the reserve of coal is the most abundant, the use of coal has attracted attention in recent years.

Coal can be divided into high rank coal and low rank coal according to coal quality. High rank coal includes bituminous coal and anthracite which are the main raw materials for power generation and iron making. This is because not only the high rank coal has characteristics of high heating value, high carbon content, low moisture content, and low ash content, but also a part of high rank coal has high caking property.

The low rank coal includes brown coal and sub-bituminous coal. Compared with the high rank coal, the low rank coal has characteristics of low heating value, low carbon content, high moisture content, and high ash content. This is a reason why it is difficult to use the low rank coal. However, the reserve of high rank coal is lower than that of low rank coal by the end of 2011 (see Table 1.2). Therefore, the low rank coal must be used in the future, and, a lot of researches on the effective utilization of low rank coal, such as pyrolysis [2]–[4], upgrading of low rank coal [5]–[7], co-combustion with different low rank coal [8]–[10] and gasification, have been carried out in these years.

Table 1.1 Recoverable reserves and production for the main fossil resource by the end of 2011 [1]

	Oil (10^6 t)	Natural gas (10^9 m^3)	Coal (10^6 t)
Recoverable reserves	223,454	209,743	891,530
Production	3,973	3,518	7,520

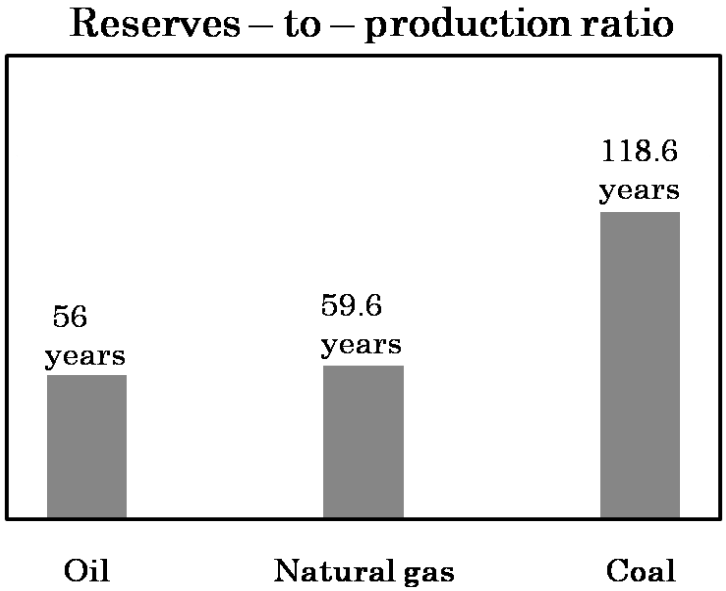

Figure 1.1 Reserves-to-production ratio for the main fossil resources by the end of 2011 [1].

Table 1.2 World's proved recoverable reserves by the end of 2011 [1]

High rank coal (10^6 t)	Low rank coal (10^6 t)	
Bituminous coal and Anthracite	Sub-bituminous coal	Brown coal
403,199	287,332	201,000

1.2 New coal power generation technology

Currently, the main power generation technology using coal is coal-fired power generation. In the coal-fired power generation, bituminous coal with a high heating value is the main raw material. Thermal energy generated by the combustion of bituminous coal is used to operate the steam turbine to produce electricity (shown in Figure 1.2(a)) [11]. However, with the rapid decrease in high rank coal reserves, low rank coal gradually becomes the main resource. In order to obtain the same amount of energy as high rank coal, a larger amount of low rank coal has to be used. Therefore, in the combustion of low rank coal, larger amounts of CO_2, which is considered to be the cause of global warming, and harmful gases such as SOx and NOx are released. On the other hand, in the power generation using the current steam turbine, the steam condition is limited to 600℃ and 24.5MPa, so the thermal efficiency has not reached 45%. In conclusion, it is not preferable to use the low rank coal in the present thermal power plant.

Compared with the coal-fired power generation technology, LNG-thermal power generation technology is known to have a high efficiency. This is because the LNG-thermal power generation is performed by combining the steam turbine and a gas turbine. Both IGCC (Integrated coal Gasification Combined Cycle) and IGFC (Integrated coal Gasification Fuel cell Combined Cycle) are considered to generate electricity with coal at the same efficiency as LNG. At present, IGCC is in the practical stage. For example, the transmission end efficiency for 1200℃ class IGCC in Nacoso city reached 42% in 2010, which was almost the same level as the present coal-fired power plant [12]. Moreover, the transmission end efficiency of the IGCC is scheduled to exceed that of coal-fired power generation in 2030 [12]. On the other hand, the IGFC is still in the development stage.

Figure 1.2(b) shows the IGCC process. From this figure, it is seen that gasification is the first step in this process. Therefore, how to increase gasification efficiency is important in this process. On the other hand, some researchers reported that low rank coal is more suitable for gasification than high rank coal [13–14]. It is believed that this is because a large amount of

oxygen-containing groups in the low rank coal helps to form a char structure that is easily gasified [13].

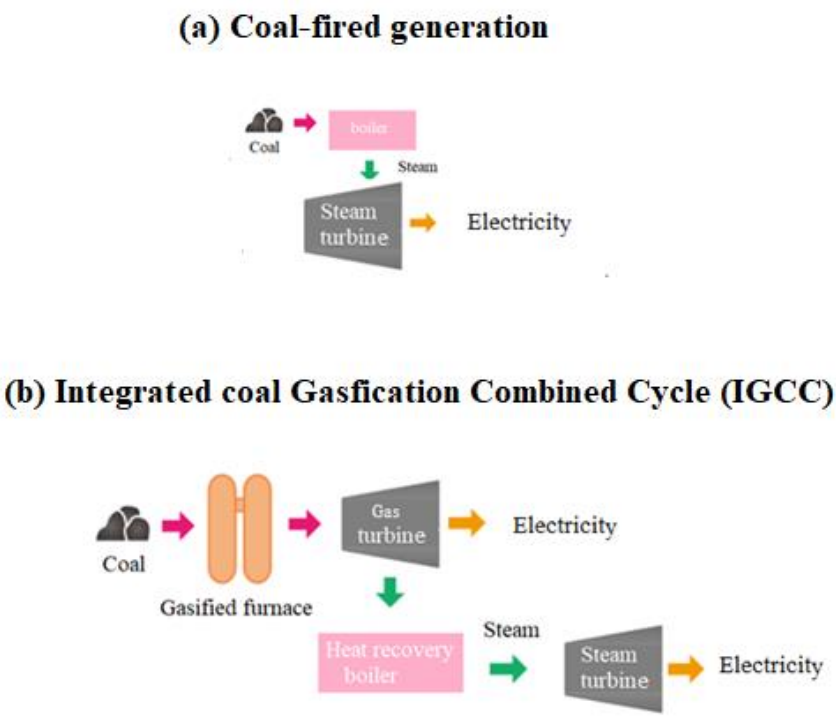

Figure 1.2 Schematic illustration of (a) present coal-fired power generation and (b) IGCC [11]

1.3 Coal pyrolysis and gasification

1.3.1 Coal pyrolysis

In general, coal pyrolysis refers to a thermochemical decomposition at high temperature in an inert atmosphere. In pyrolysis, cleavage of chemical bonds occurs basically.

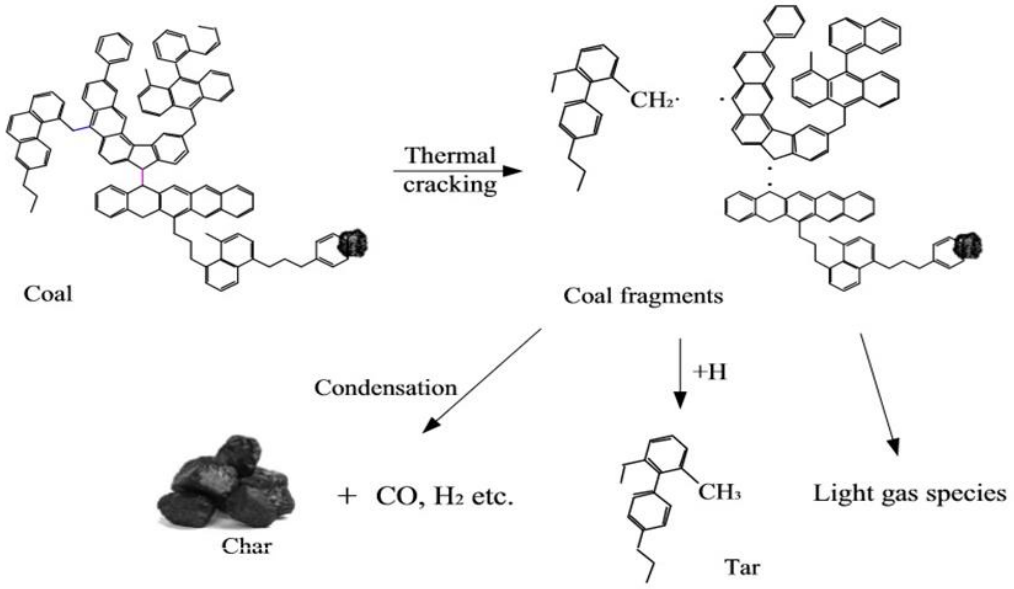

Figure 1.3 A simple diagram of coal pyrolysis process [15]

As shown in Figure 1.3, pyrolysis can be regarded as a two-step process. When the temperature increases to a certain degree, some weak chemical bonds in coal are broken. This reaction is usually called a primary pyrolysis. In this stage, coal is broken down into many smaller fragments.

In higher temperature, the products after the primary pyrolysis react to produce various compounds. This stage is usually referred to as a secondary pyrolysis. Main secondary pyrolysis is shown below.

- Cracking of small coal fragments

  Small coal fragment → Light gas species
- Hydrogenation reaction of small coal fragments

  Small coal fragment + H· → Tar
- Condensation reaction between macromolecular fragments

  Macromolecular fragment + Macromolecular fragment → Char + Gas (CO, H_2, etc)

1.3.2 Coal gasification

Coal gasification is a reaction of coal and gasifying agent at specific temperatures and pressures. Fuel gases such as CO, H_2, and CH_4 can be obtained by coal gasification. Since coal pyrolysis occurs before coal gasification, coal gasification process is substantially regarded as char gasification. A theory of oxygen exchange between gasifying agent and char is usually used to explain the gasification mechanism. When H_2O is used as the gasifying agent, the gasification mechanism of char is proposed as follows [13],

$$C_f + H_2O \rightarrow C_f(O) + H_2 , \qquad (1.1)$$

$$C_f(O) \rightarrow CO , \qquad (1.2)$$

$$CO + H_2O \rightarrow H_2 + CO_2 , \qquad (1.3)$$

where C_f represents carbon in char which H_2O is easy to adsorb, $C_f(O)$ represents an intermediate composed of carbon and oxygen produced as a result of H_2O adsorption. Reactivity of gasification is known to be affected by many factors such as ash composition, ash content, pyrolysis conditions and so on [16–19]. For example, coal contains ash, such as Na, K, Ca, which can promote gasification. Additionally, the pyrolysis temperature, pyrolysis rate and holding time during coal pyrolysis can lead to different char reactivity [18–19]. Gasification reactivity of char can also be changed by the addition of catalyst.

1.4 Catalyst for gasification

1.4.1 Overview for gasification catalyst

A lot of studies on gasification catalysts have been carried out so far [20–25]. For example, it has long been known that Na and K are excellent catalysts for char gasification. Suzuki et al. [20] previously reported the gasification mechanism by Na and K catalysts.

$$2M + H_2O \rightarrow M_2(O) + H_2 , \quad (1.4)$$

$$M_2(O) + C_f \rightarrow 2M + C_f(O) , \quad (1.5)$$

where M represents Na or K catalyst. It is also known that iron group metals such as Fe and Ni promote gasification to some extent, and the gasification mechanism by them is reported as follows [23－24],

$$M + H_2O \rightarrow M(O) + H_2 , \quad (1.6)$$

$$M(O) + C_f \rightarrow M + C_f(O) , \quad (1.7)$$

where M represents Fe and Ni catalysts. Ca also could be explained as the same mechanism [25].

Among these catalysts, there is a possibility that iron catalyst can be used in the actual gasification process [26]. This is because the iron catalyst has some advantages not found in other catalysts. Firstly, the iron catalyst is a much cheaper than other catalysts. This makes it possible to use the catalyst in a large-scale process. Secondly, the iron catalyst has a low toxicity. That is, the iron catalyst has little influence on the environment and health. From these reasons, there are many studies on the effect of iron catalyst on the pyrolysis and gasification of coal.

1.4.2 Effects of iron catalyst on pyrolysis and gasification of coal

Some researchers reported that metal oxides containing iron oxides have an effect on the decomposition of tar [27–28].

Yu et al. reported that Fe^{3+} is coordinated to a range of oxygen-containing groups such as $-OH^-$ and $-COO^-$, and this reaction offered solid carbon deposits (soot) on the char by polymerizing the tar precursors, resulting in

the char yield increases [29]. Therefore, one of the effects of Fe catalyst on coal pyrolysis is the decrease in tar yield and the increase in char yield.

On the other hand, Qi et al. indicated that the iron catalyst could change carbon crystalline structure and help to suppress the tendency of coal to graphitize during the coal pyrolysis process [30], some researchers using Raman spectroscopy reported that partially large polyaromatic ring structures converted to amorphous carbon structures by the addition of iron catalyst [30–32].

In the case of metallic iron catalyst, it is reported that the coal gasification proceeds as the above-mentioned equations (1.6) and (1.7) [30].
On the other hand, Fe_3O_4 and FeOOH catalysts, the coal gasification mechanism is proposed as follows [34],

$$Fe_xO_y + H_2O \rightarrow Fe_xO_y(O) + H_2, \quad (1.8)$$

$$Fe_xO_y(O) + C_f \rightarrow C_f(O) + Fe_xO_y, \quad (1.9)$$

$$C_f(O) \rightarrow CO. \quad (1.10)$$

From the reactions, it could be known that iron catalyst could react with both gasifying agent and carbon. And these reactions occurred more easily than the direct reaction of carbon and H_2O. Therefore, the use of iron catalyst could promote gasification.

1.5 Co-gasification of sub-bituminous coal and woody biomass with iron catalyst

Many studies on co-gasification between different fuels were carried out in these years [35-47]. For example, steam co-gasification of biochar (from corn stalk) and coal char (three different ranks of coal) was conducted, and the interactions between biochar and coal char were investigated by Ding et al. [35]. They reported that the experimental rate of carbon conversion for coal char 50/biochar 50 (the blended sample of low rank coal char and biochar at the mass ratio of 50 wt%) was higher than the rate calculated from the individual gasification. Therefore, a synergistic effect existed during co-gasification. On the other hand, co-gasification of petroleum coke and biomass was carried out by Wei et al [36]. A similar result to Ding et al.'s study was observed in their study, and they also reported that synergetic effect during co-gasification was related to active AAEM (alkali metal and alkaline earth metal) transfer between biomass and coal [36 – 37]. Co-pyrolysis/gasification of biomass (two types) and sub-bituminous coal was carried out by Krerkkaiwan et al. [38]. In their study, the synergetic effect was explained as the transferring of active OH and H radicals from the biomass to the coal in pyrolysis as well as the catalytic effect of potassium (K) from the biomass in gasification.

In previous study [48], Adaro sub-bituminous coal from Indonesia with impregnated iron catalyst was gasified with steam at 800℃. Even when the iron catalyst was loaded, the char gasification rate remained almost unchanged. On the other hand, in a previous study on the steam gasification of woody biomass (Japanese cedar) at 800 ℃, it was reported that impregnated $FeCl_2$ increased the amount of hydrogen evolution by 60% during 60 min compared to the case of the steam gasification of woody biomass without catalyst [49]. This was considered to be due to the presence of highly active iron species on the biochar. If this iron catalyst with high activity on biochar can be used for steam gasification of Adaro coal, an increase in gasification rate of Adaro coal is expected. Xiao et al. [50] ever reported a co-gasification of Ni-loaded brown coal char and waste wood biomass. With the addition of Ni-loaded brown coal char, the gas yields of H_2

and CO increased dramatically, and the total gas yield was 3.1 times larger than that for non-catalyst.

1.6 Purpose and composition of doctoral thesis

This doctoral thesis discussed the development of effective utilization technology of low rank coal and woody biomass. The steam gasification is the most practical process because both low rank coal and woody biomass can be converted to clean energy gases, such as H_2 and CO. In this thesis, the objective is to improve the gasification efficiency of low rank coal and woody biomass.

This thesis is composed of 5 chapters.

In the second chapter, the co-gasification of Fe-loaded biochar (pyrolysate of Fe-loaded Japanese cedar) and Indonesian Adaro sub-bituminous coal was carried out at 800℃ for 60 min. The main purpose was to examine the effectiveness of an iron catalyst loaded on biochar for hydrogen (H_2) evolution. It was shown that the H_2 evolution for a mixed sample of Fe-loaded biochar (20 wt%) and Adaro sub-bituminous coal increased by 20% compared with that for the Adaro coal with the same amount of iron catalyst and was approximately 1.5 times larger than that for the Adaro coal without the iron catalyst. This increase in the H_2 evolution during co-gasification was explained by the chemical form and crystallite size of the iron catalyst.

In the third chapter, Fe-loaded biochar was added to Adaro coal or coal char for steam gasification in a fixed-type reactor. The purpose was to determine the optimal content of added Fe-loaded biochar for steam co-gasification in this system and the best time to add it. The amount of hydrogen evolution observed for the mixture of Fe-loaded biochar and Adaro coal at 800 ºC for 60 min was much higher than that observed for the mixture of iron-loaded biochar and coal char. The optimal ratio of Fe-loaded Japanese cedar biochar to Indonesian Adaro sub-bituminous coal char was determined

to be 1:1 by weight. X-ray diffraction patterns of the different mixtures after pyrolysis revealed that the iron catalyst contained in the iron-loaded biochar may affect the pyrolysis of Adaro coal. The mechanism by which the iron catalyst in Fe-loaded biochar promoted the co-gasification reactivity was also discussed.

In the fourth chapter, the steam gasification of Adaro coal and Japanese cedar mixed in a 1:1 weight ratio with the physical addition of 10 wt% Fe_2O_3 in 50 vol% H_2O at ambient atmospheric pressure and 800℃ for 60 min was investigated. The objective was to examine the effectiveness of an iron catalyst on the co-gasification between Adaro coal and Japanese cedar. The study demonstrated that the H_2 evolution for co-gasification without a Fe catalyst was 100 mmol/g-char. However, the H_2 evolution for co-gasification with the addition of Fe_2O_3 was 152 mmol/g-char. The increase in the co-gasification for H_2 evolution was based on a change of the char structure during pyrolysis and gasification.

In the last chapter, the conclusions obtained in this study are summarized. Furthermore, based on the obtained findings, a guideline to the effective use of low rank coal and biomass is proposed.

Akita University

Chapter 2 Effect of iron-loaded biochar on steam gasification of sub-bituminous coal

2.1 Introduction

In my previous study, the iron catalyst was loaded with impregnation method on Indonesian Adaro sub-bituminous coal (AD) and the effect of iron on the steam gasification was examined. However, the iron catalyst did not show a positive catalytic activity unlike the steam gasification of iron-loaded brown coal [51-53]. This is because the number of cation-exchangeable functional groups such as carboxyl groups in AD coal is quite lower than those in brown coal, resulting in a low dispersion of iron catalyst on AD coal. On the other hand, in the previous study by Murakami et al. [54], it was shown that the impregnated iron catalyst considerably enhanced the amount of hydrogen evolution during steam gasification of Japanese cedar. This was considered to be because the cementite (Fe_3C) produced during the pyrolysis of iron-loaded biomass was very active for steam gasification.

Other researches have shown that the co-gasification of low rank coal and biomass is effective for promoting the amount of hydrogen evolution. For example, Howaniec et al. [55] reported that synergetic effect in the co-gasification tests of hard coal and biomass, when compared to the tests of coal and biomass gasification at all tested temperatures, and synergetic effect was attributed to the catalytic effect of K_2O present in blend ash. Jeong et al. [56] pointed out that the synergetic effect of co-gasification of coal char and biomass char increased with an increase in the amount of biomass and the reaction temperature. From above researches, it is found that the addition of biomass is very effective for the gasification of coal. This would be because the biomass has a large amount of alkali metal [57–59]. For example, Zhang et al. [57] showed that biomass ashes played an important role in catalyzing the gasification reaction of coal char and K-rich biomass had the best synergetic effect. Similar results were reported by Howaniec et al. [59] and Wei et al. [60]. Therefore, synergetic effect during co-gasification could be regarded as the interaction between the AAEM (alkali metal and alkaline earth metal) in the ash of biomass and coal.

In this chapter, the mixtures of iron-loaded biochar (pyrolysate of iron-loaded biomass) and AD coal in a weight ratio of 1:10 and 1:5 were prepared and were gasified with steam at 800℃ in a fixed-bed type reactor. The purpose of this study is to discuss the effect of iron-loaded biochar on the steam gasification of AD coal.

2.2 Experimental

2.2.1 Samples

AD was ground into powder in a mortar. AD particles used in the gasification experiment were allowed to pass through a 250 μm sieve but not through a 150 μm sieve. Japanese cedar (SG) was used as woody biomass, which was cut into small pieces in a blender and then ground into powder in a mortar. SG particles were made to pass through a 250 μm sieve. The proximate and ultimate analyses for AD and SG are shown in Tables 2.1 and 2.2, respectively. All samples were dried at 110 °C for 1 h prior to use. The ash content was calculated from the residual amount when 1 g of AD or SG was calcined at 815 °C for 1 h in air. The amount of volatile matter (VM) was determined from the weight change before and after dry distillation at 900 °C for 7 min. The fixed carbon content (FC) was obtained by subtracting the ash content (wt%) and VM content (wt%) from 100 wt%. Carbon, hydrogen, and oxygen contents were measured using a Yanaco HCN corder MT-700HCN, and the sulfur content was analyzed using a Perkin Elmer 2400II CHNS/O elemental analyzer.

Table 2.1 Proximate and ultimate analyses of AD

Prox. Analysis wt% (dry)			Ultimate Analysis wt% (daf)				
Ash	VM	FC	C	H	N	S	O(diff.)
2.5	46.7	50.8	67.8	5.1	0.44	0.14	26.5

Table 2.2 Proximate and ultimate analyses of SG

Prox. Analysis wt% (dry)			Ultimate Analysis wt% (daf)			
Ash	VM	FC	C	H	N	O(diff)
0.9	78.4	20.7	46.9	5.8	0.1	46.2

Demineralization was carried out to determine the effect of ash such as alkali metals and alkaline earth metals in the biomass on the steam gasification. A weighed amount of SG (5 g) was immersed in 200 mL of 3 mol/L HCl for 10 h with stirring. After filtration, washing with water, and drying at 110 °C for 12 h, demineralized woody biomass (Dem-SG) was obtained. Moreover, the concentrations of Na, K, and Ca in the filtrate were measured by ICP (Seiko Instruments, SPS5510).

2.2.2 Iron catalyst loading

An impregnation method was used to deposit the iron salt on the surface of AD and SG as shown in Figure 2.1. A weighed amount of AD (10 g), SG (10 g), or Dem-SG (10 g) was immersed in 200 mL of aqueous solution containing $FeCl_2$, and the suspension was stirred at 40 °C for 1 h under vacuum using a rotary evaporator. Then, the water was evaporated at 60 °C for 1 h. The impregnated samples were dried at 110 °C for 12 h prior to use. Iron catalyst loadings were determined by ICP. The prepared samples were 3.2Fe-AD, 6.7Fe-AD, 6.8Fe-SG, and 8.1Fe-Dem-SG; the numerical value in the sample name represents the iron loading (wt%).

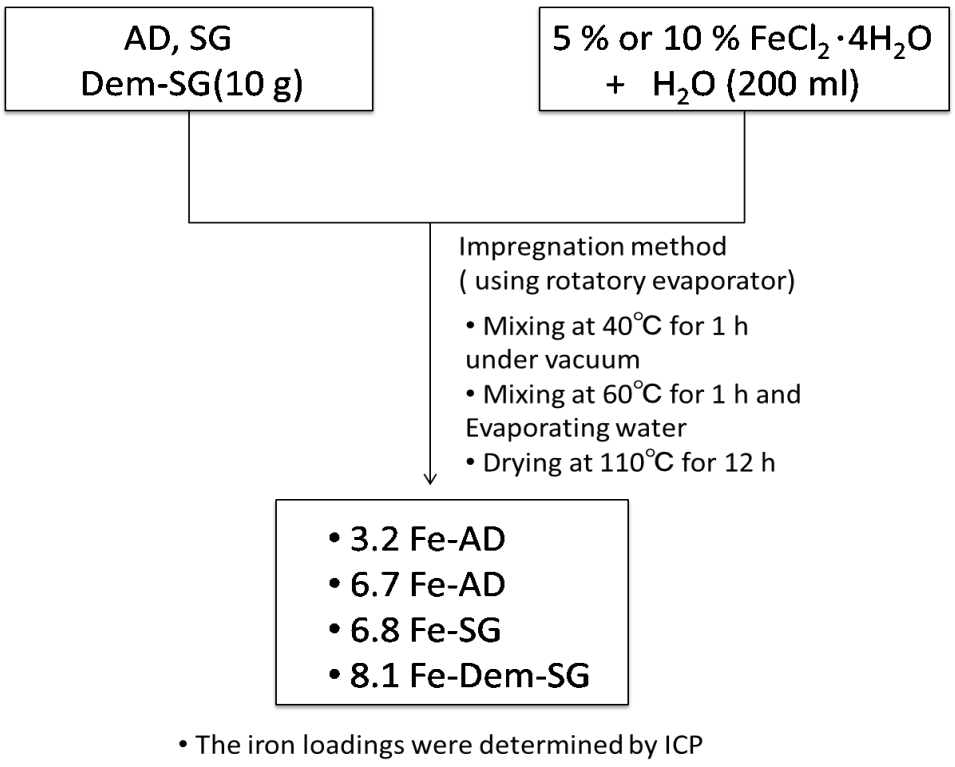

Figure 2.1 Procedure of impregnation method

2.2.3 Preparation of mixed samples of iron-loaded biochar and AD

The iron-loaded biochars were produced from 6.8Fe-SG and 8.1Fe-Dem-SG samples. The samples (0.5 g) were heated from room temperature to 800 °C at the rate of 300°C/min, under helium flow (140 mL/min), and were held at this temperature for 10 min. After cooling to room temperature, the iron-loaded biochars were preserved in nitrogen-purged polyethylene bags. These samples were designated as 6.8Fe-SGchar and 8.1Fe-Dem-SGchar, respectively. The iron content in 6.8Fe-SGchar and 8.1Fe-Dem-SG was concentrated to 23 wt% and 27 wt%, respectively, because the weight of these samples decreased to approximately 30 wt% after pyrolysis.

The four samples shown in Table 2.3 were prepared by mixing 0.5 g of AD with 0.05 g or 0.1 g of the iron-loaded biochars. The samples were well mixed by grinding in a mortar for at least 3 min. The numerical value in the sample name represents the calculated iron loading (wt%) in the mixed sample on the basis of total weight.

Table 2.3 Samples prepared by mixing AD with iron-loaded biochar

Sample	AD	6.8Fe-SGchar	8.1Fe-Dem-SGchar
1.8Fe-SG/AD	0.5g	0.05 g	—
3.5Fe-SG/AD	0.5 g	0.1 g	—
2.5Fe-Dem-SG/AD	0.5 g	—	0.05 g
4.1Fe-Dem-SG/AD	0.5 g	—	0.1 g

2.2.4 Pyrolysis and gasification

Figure 2.2 shows the fixed-bed reactor that was used for pyrolysis and gasification. At first, the sample (0.5 g for the non-mixed samples, 0.55 g or 0.6 g for the mixed samples) was heated from room temperature to 800 °C at a heating rate of 300 °C/min under a He flow of 140 mL/min in the vertical fixed-bed-type reactor and held for 10 min. The sample was taken from the reactor after cooling to room temperature. The char yield after pyrolysis was calculated by the following equation:

$$Y_{\mathrm{Char}} = \frac{W_{\mathrm{Char}}}{W_{\mathrm{sample}}} \quad , \tag{2.1}$$

where Y_{Char} is the yield of char [wt%], W_{Char} is the weight of the residue after pyrolysis [g (ash and catalyst free)], and W_{sample} is the weight of the sample before pyrolysis [g (ash and catalyst free)].

The steam gasification was performed at 800 °C for 60 min by introducing 50 vol% of steam/He into the reactor immediately after the pyrolysis of samples. The amount of steam was controlled by changing the temperature of the steam generator. The gases (H_2, CO, CO_2, CH_4, C_2H_4, and C_2H_6) produced during steam gasification were determined by on-line Micro GC (Agilent MicroGC 3000A). The gas evolution rate was calculated using the following formula:

$$R = \frac{V_{\mathrm{vol}}\% \times L}{22.4 \times m_{\mathrm{char}}} \quad , \tag{2.2}$$

where R is the gas evolution rate [mmol/g−char · min]; L is the total gas flow rate [mL/min], which was measured by a flow meter every 10 min; m_{char} is the weight of char [g], which was measured after pyrolysis; $V_{\mathrm{vol}}\%$ is the volume fraction of each produced gas measured by MicroGC. The carbon conversion was calculated using the following equation:

$$X_{\mathrm{Carbon}} = \frac{C_{gas}}{C_{Char}} \times 100 \quad , \tag{2.3}$$

where X_{Carbon} is the carbon conversion [mol%]; C_{gas} is the molar content of carbon in the total gas [mol (ash and catalyst free)], which is the sum of the molar content of all the gases containing carbon, i.e., $C_{\mathrm{gas}} = C_{\mathrm{CO}} + C_{\mathrm{CO2}} + C_{\mathrm{CH4}} + 2C_{\mathrm{C2H4}} + 2C_{\mathrm{C2H6}}$. In addition, C_{Char} is the molar content of carbon originally contained in the pyrolyzed char (mol), which was assumed to be 100% carbon.

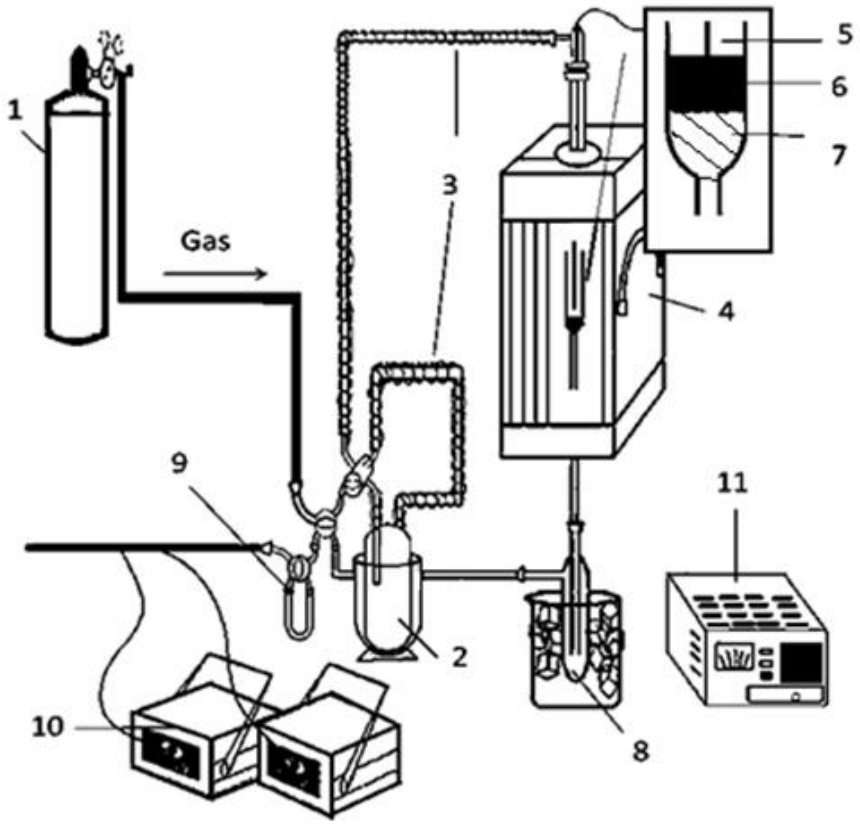

1. Carrier gas, 2. Steam generator, 3. Ribbon heater, 4. Electric furnace, 5. Thermocouple, 6. Sample, 7. Quartz wool, 8. Tar trap, 9. Dehydrating agent, 10. Micro GC, 11. Temperature controller

Figure 2.2 Fixed-bed reactor for pyrolysis and steam gasification

2.2.5 Characterization of the pyrolyzed char and gasified residue

The chemical form of the Fe catalyst after pyrolysis and gasification was evaluated by X-ray powder diffraction (XRD; Rigaku, Ultima IV) with Ni-filtered CuKα radiation. The crystallite size of the iron catalyst was calculated using the Scherrer equation.

$$L=\frac{K\lambda}{\beta\cos\theta} \quad , \qquad (2.4)$$

where L is the crystallite size [$\AA$], λ is the wavelength [$\AA$], β is the peak width at half the maximum intensity, K is equal to 0.9, and θ is the diffraction angle [°].

2.3 Results and discussion

2.3.1 Effect of iron-loaded biochar on the gasification of AD

Figure 2.3 shows the H_2, CO, and CO_2 gas evolution rates for AD, 3.2Fe-AD, 1.8Fe-SG/AD, and 3.5Fe-SG/AD during steam gasification at 800 °C. Based on the data shown in Figure 2.3, it was determined that all of the gas evolution rates reached a maximum at approximately 5 min and decreased gradually with increasing reaction time thereafter. Moreover, it was observed that the gas evolution rate increased with the addition of iron catalysts. In particular, 1.8Fe-SG/AD and 3.5Fe-SG/AD showed a higher hydrogen evolution rate than AD over the course of the entire reaction. In the case of 3.2Fe-AD, in contrast, the promotion of hydrogen evolution was limited to the initial 40 min, and the hydrogen evolution rate was almost the same as that of AD after 40 min. The CO and CO_2 evolution profiles were similar to the hydrogen evolution profile.

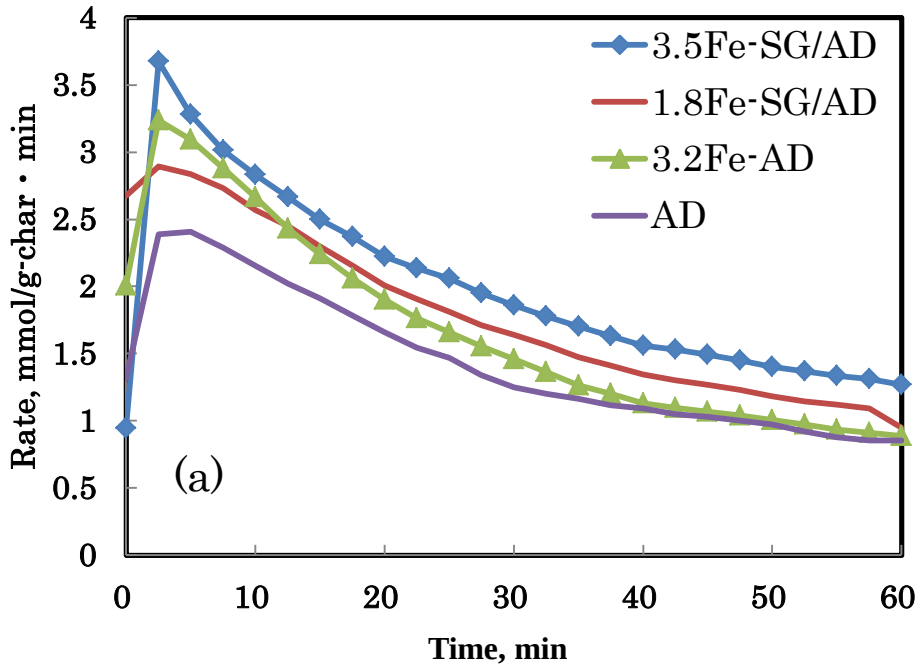

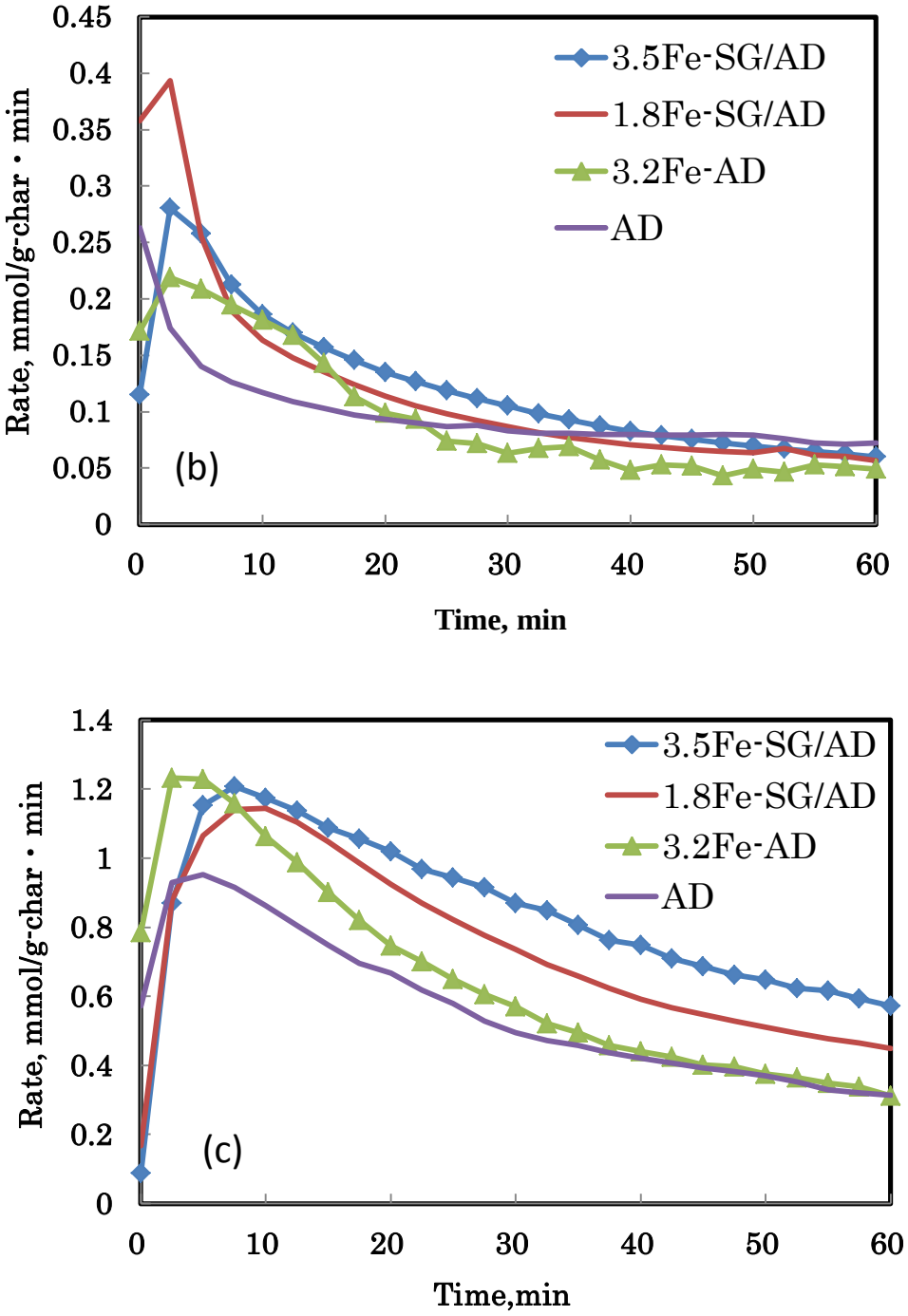

Figure 2.3 (a) H_2, (b) CO, and (c) CO_2 gas evolution profiles for AD, 3.2Fe-AD, 1.8Fe-SG/AD, and 3.5Fe-SG/AD during steam gasification at 800 °C

Table 2.4 shows the amounts of H_2, CO, CO_2, and CH_4 evolution of various samples during steam gasification at 800°C for 60min. In the steam gasification of carbonaceous materials, the following reactions are known to take place simultaneously [61]:

$$C + H_2O \rightarrow H_2 + CO \quad , \qquad (2.5)$$

$$CO + H_2O \rightarrow H_2 + CO_2 \quad , \qquad (2.6)$$

$$C + CO_2 \rightarrow 2CO \quad , \qquad (2.7)$$

$$2CO + 2H_2 \rightarrow CH_4 + CO_2 \quad , \qquad (2.8)$$

$$C + 2H_2 \rightarrow CH_4 \quad . \qquad (2.9)$$

Encinar et al. [61] described that the main reaction is only reactions (2.5) and (2.6) under an atmospheric pressure at 600–800°C among these reactions, because reaction (2.7) requires high temperature and reactions (2.8) and (2.9) require high pressure. From the results that only H_2, CO, and CO_2 were produced (Table 2.4), reactions (2.5) and (2.6) were considered to take place mainly in this experiment. As char is considered as 100% carbon in the study for gasification, 1 g-char could be regarded as 83.3 mmol carbon. When the char is converted to CO_2, the H_2 could reach the maximum of 166.6 mmol.

Table 2.4 Amount of H_2, CO and CO_2 evolution and carbon conversion after gasification (800 °C, 60 min) of samples

Sample	H_2 evolution (mmol/g-char)	CO evolution (mmol/g-char)	CO_2 evolution (mmol/g-char)	Carbon conversion (mol%)
AD	87	5.8	34	48
3.2Fe-AD	100	5.7	38	54
6.7Fe-AD	107	6.0	39	59
1.8Fe-SG/AD	107	7.1	43	62
3.5Fe-SG/AD	120	7.5	48	67
2.5Fe-Dem-SG/AD	97	5.9	36	52
4.1Fe-Dem-SG/AD	104	5.1	43	58
6.8Fe-SG	113	6.5	50	69

The relationship between carbon conversion and gas evolution of H_2, CO and CO_2 is shown in Figure 2.4.

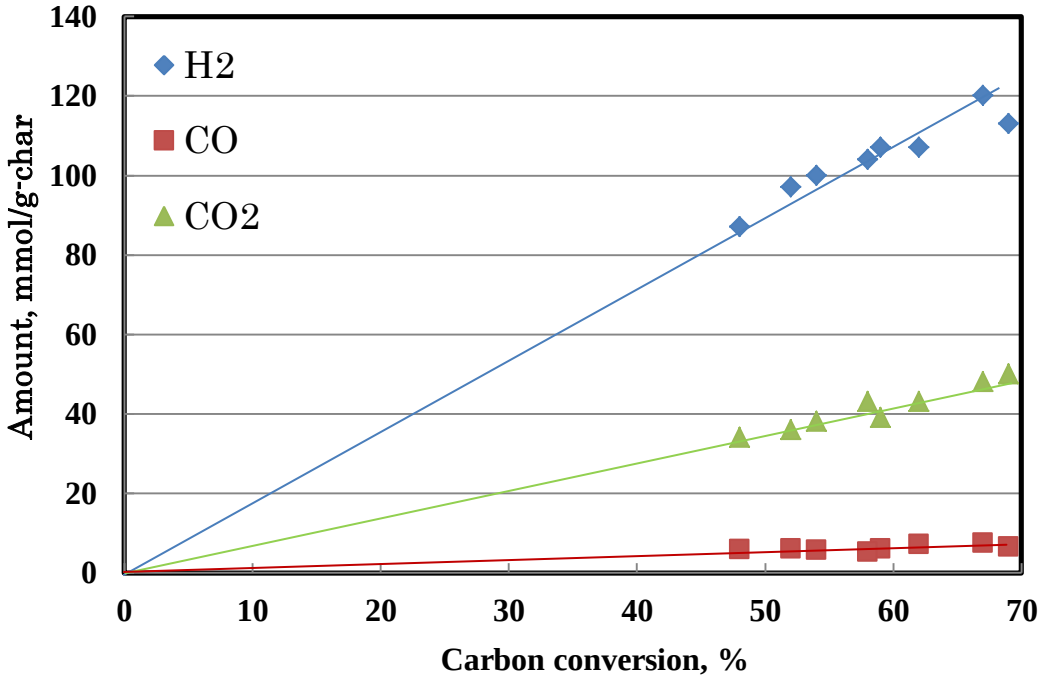

Figure 2.4 The relationship of gas evolution (H_2, CO and CO_2) and carbon conversion

From this figure, it could be seen that the relationship between carbon conversion and gas evolution is linear. This result indicated that the mechanism of gasification did not change independent of the presence of iron catalyst.

2.3.2 Comparison between the amount of hydrogen evolution calculated by individual gasification and that measured by co-gasification

A comparison between the amount of hydrogen evolution calculated by individual gasification and that measured by co-gasification was made (Figure 2.5). The amount of hydrogen evolution for 0.5 g AD + 0.05 g iron-loaded biochar shown in Figure 2.5 was calculated as follows. The amount of hydrogen evolved from 0.5 g of AD was calculated as 87 mmol/g-char × (0.5 g × 48 %) = 20.88 mmol, since the char yield was 48 wt%. The calculated amount of hydrogen evolution for 0.05 g of iron-loaded biochar was 113 mmol/g-char × (0.05 g-char − (0.01 g iron)) = 4.52 mmol. Accordingly, the amount of hydrogen evolved from 0.5 g AD + 0.05 g iron-loaded biochar was 25.4 mmol (20.88 + 4.52 mmol). Similarly, the amount of hydrogen evolution for 0.5 g AD + 0.1 g iron-loaded biochar (0.02 g iron) was 29.9 mmol. In contrast, the amount of hydrogen evolution for the case of Fe-SG/AD was approximately 8.5 mmol higher than the sum of the amount of hydrogen evolution for the individual gasification (0.5 g AD + 0.1 g iron-loaded biochar). For example, the amount of hydrogen evolution for 3.5Fe-SG/AD was 120 mmol/g-char × (0.58 g × 55 %) = 38.3 mmol, since the char yield after pyrolysis was 55 wt%. The same tendency was also seen in the case of 1.8 Fe-SG/AD. These results suggest that the Fe catalyst loaded onto biochar promoted the gasification of AD as well as SG.

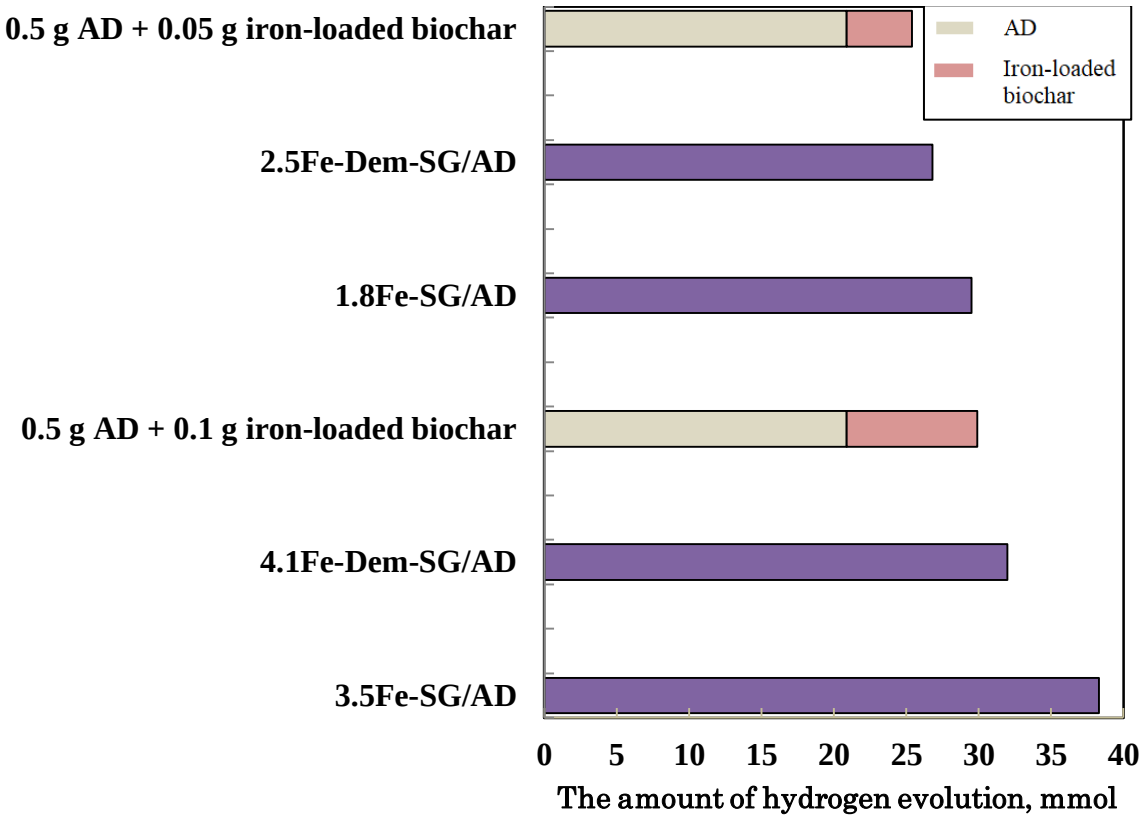

Figure 2.5 Comparison between the amount of hydrogen evolution calculated from individual gasification and measured by co-gasification

2.3.3 Effect of biomass ash on the gasification of AD

Figure 2.6 shows the hydrogen evolution profiles for samples with and without demineralization. Through demineralization, approximately 0.09 wt% Ca, 0.07 wt% K, and 0.03 wt% Na were removed from SG. Then after burned with Muffle furnace at 800℃ for 1 h. There remained 56% ash in Dem-SG after demineralization.

In the initial stage of gasification up to 10 min, the hydrogen evolution rates for 2.5Fe-Dem-SG/AD and 4.1Fe-Dem-SG/AD were almost the same as those of 1.8Fe-SG/AD and 3.5Fe-SG/AD, respectively. However, with increasing reaction time thereafter, the hydrogen evolution rate decreased and approached the hydrogen evolution rate for AD, unlike in the case of 1.8Fe-SG/AD and 3.5Fe-SG/AD.

From the amount of hydrogen evolution for 2.5Fe-Dem-SG/AD and 4.1Fe-Dem-SG/AD (Figure 2.5), it was found that the amounts of hydrogen evolution for the demineralized samples were higher than those calculated by the individual gasification but were smaller than those for the samples without demineralization. This suggests that the ash (alkali metal and alkaline metal) in SG samples plays an important role as a promoter.

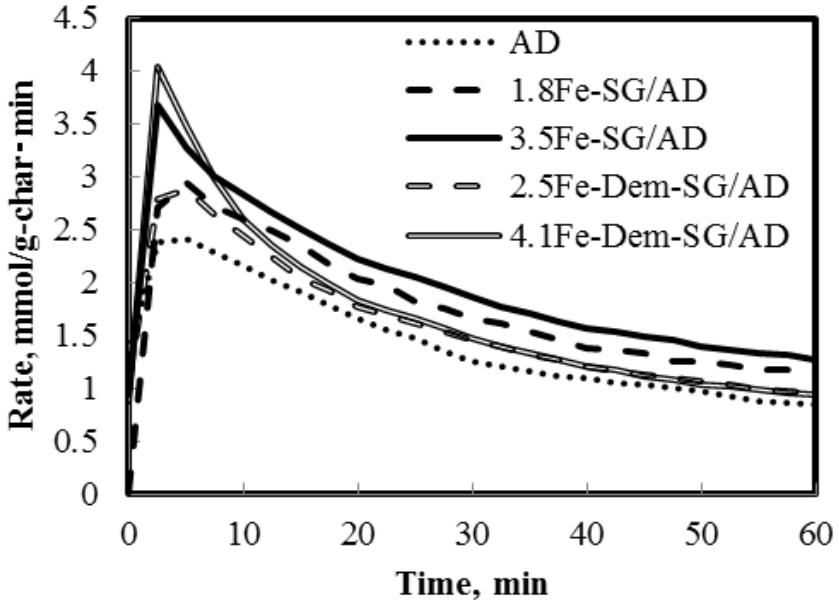

Figure 2.6 Hydrogen evolution rates for the samples with and without demineralization

2.3.4 Relationship between specific rate and carbon conversion

Specific rate was employed to investigate the change of carbon conversion to the residual amount of carbon. The specific rates were calculated as the following equation:

$$Rs = \frac{R_C}{W_{SC}} \quad , \qquad (2.10)$$

where R_s represents the specific rate [1/h], R_c represents the rate of carbon conversion [mol%/h], and W_{sc} represents the amount of residual carbon in the char [mol%].

Figure 2.7 shows the relationship between specific rate and carbon conversion. Compared 1.8Fe-SG/AD with 3.5Fe-SG/AD, it was observed that the specific rate increased with increasing in the amount of iron catalyst used. For 3.2Fe-AD, the specific rates decreased gradually with increasing carbon conversion, indicating that the activity of the iron catalyst decreased during the steam gasification. On the contrary, there was no obvious decrease in the activity of the iron catalyst in 1.8Fe-SG/AD and 3.5Fe-SG/AD. Demineralization (4.1Fe-Dem-SG/AD and 2.5Fe-Dem-SG/AD) caused the specific rates to decrease with increasing carbon conversion. From these results, it was concluded that the ash (alkali metal and alkaline metal) in SG samples had the effect of maintaining the iron catalyst activity. Compared with the findings from Asami and Ohtuska [53], it was found that the decrease in the specific rate for 3.2Fe-AD was similar to that for the pure iron catalyst used with LY brown coal. Observed increases in the late stage of 3.5Fe-SG/AD were similar to that of Fe–Ca catalyst, although the increases were not as obvious as those of the Fe–Ca catalyst because the Japanese cedar did not have a high content of AAEMs (alkali metal and alkaline earth metal) [62-63]. However, it could also be considered that the biochar ash unquestionably had a promotion effect. Therefore, it is necessary to discuss the differences between the iron catalysts on AD and SG/AD.

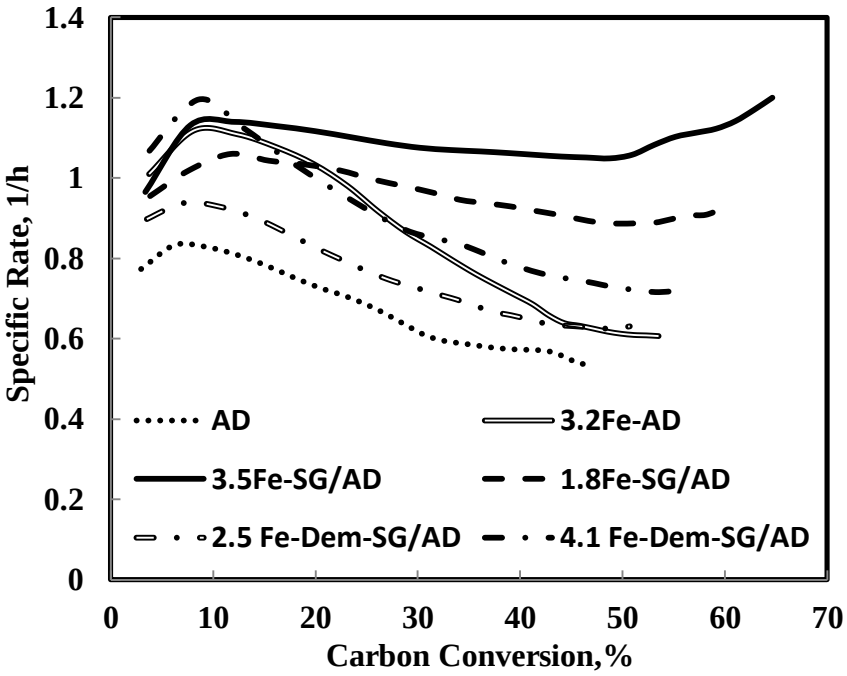

Figure 2.7 Relationship between specific rate and carbon conversion

2.3.5 Change of activation energy with addition of Fe-SGchar

Activation energy is defined as the minimum energy required to start a chemical reaction. And it could be calculated by Arrhenius equation:

$$k = Ae^{-Ea/(RT)}, \qquad (2.11)$$

where A is the frequency factor for the reaction, R (8.314 $JK^{-1}\cdot mol^{-1}$) is the universal gas constant, T (K) is the absolute temperature (973K～1123K), and k is the reaction rate constant. E_a (kJ/mol) is the activation energy for the reaction 2.5 and 2.6.

Taking the logarithm of both sides, the equation (2.11) is transformed as follows.

$$lnk = -(Ea/R)(1/T) + lnA, \qquad (2.12)$$

Combined reaction 2.5 and 2.6, the reaction for steam gasification in our experiment could be easily shown as below.

$$C + 2H_2O \rightarrow CO_2 + 2H_2 . \qquad (2.13)$$

Therefore, reaction rate could be reacted as equation (2.14):

$$r = k\,[c][H_2O]^2, \qquad (2.14)$$

Then the equation (2.14) could be transformed as below.

$$\frac{r}{[c]} = k\,[H_2O]^2 , \qquad (2.15)$$

In the experiment, steam is overused, and it won't affect the concentration. Therefore, Rs was used as k in the chapter. And equation (2.12) could be transformed as below,

$$lnRs = -(Ea/R)(1/T) + lnA. \qquad (2.16)$$

Arrhenius plot was made according to equation (2.16), where (1/T) was used as cross-rod, lnRs was used as direct-axis and was shown as Figure 2.8.

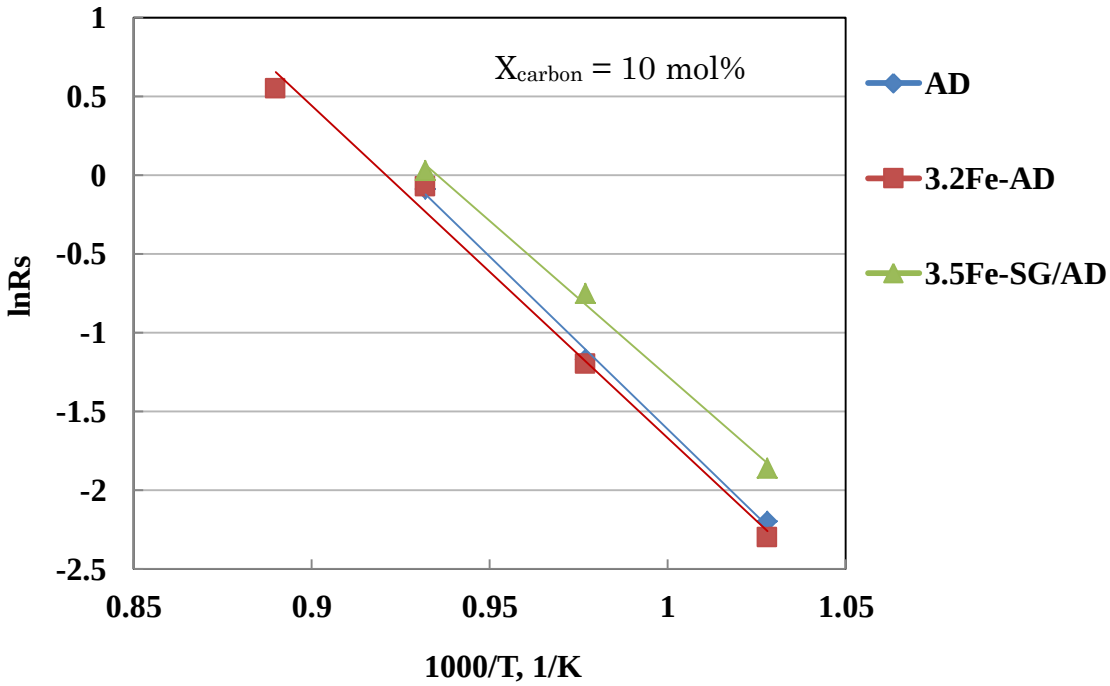

Figure 2.8 Arrhenius plot of iron-loaded sample in steam gasification when carbon conversion is 10 mol%.

Linear relationship between lnk and 1/T for AD, 3.2Fe-AD and 3.5Fe-SG/AD could be seen in Figure 2.8.

Table 2.5 Activate energy (Ea) and frequency factor A in steam gasification

X = 10 mol%

Sample	Ea, kJ/mol	A
AD	182	6.7×10^{8}
3.2Fe-AD	176	2.8×10^{8}
3.5Fe-SG/AD	164	1.03×10^{8}

Table 2.5 shows the Activate energy (Ea) and frequency factor A in steam gasification when the carbon conversion is 10 mol%. From the table, Ea(3.2Fe-AD) was just a little smaller than Ea(AD), however, Ea(3.5Fe-SG/AD) was much smaller than Ea(AD), Fe-SGchar addition decreased about 20 kJ/mol activate energy compared to AD. This expressed that Fe-SGchar addition indeed promoted AD steam gasification and the promotion was better than iron loaded coal.

Based on equation (2.15), reaction rate could be expressed as

For AD: $r = 6.7\times10^{8} \exp(-1.82\times10^{5}/RT)\,[c][H_2O]^2$, (2.17)

For 3.2 Fe-AD: $r = 2.8\times10^{8} \exp(-1.76\times10^{5}/RT)\,[c][H_2O]^2$, (2.18)

For3.5 Fe-SG/AD: $r = 1.34\times10^{8} \exp(-1.64\times10^{5}/RT)\,[c][H_2O]^2$, (2.19)

2.3.6 Chemical form and crystallite size of Fe catalyst after pyrolysis and gasification of AD and SG

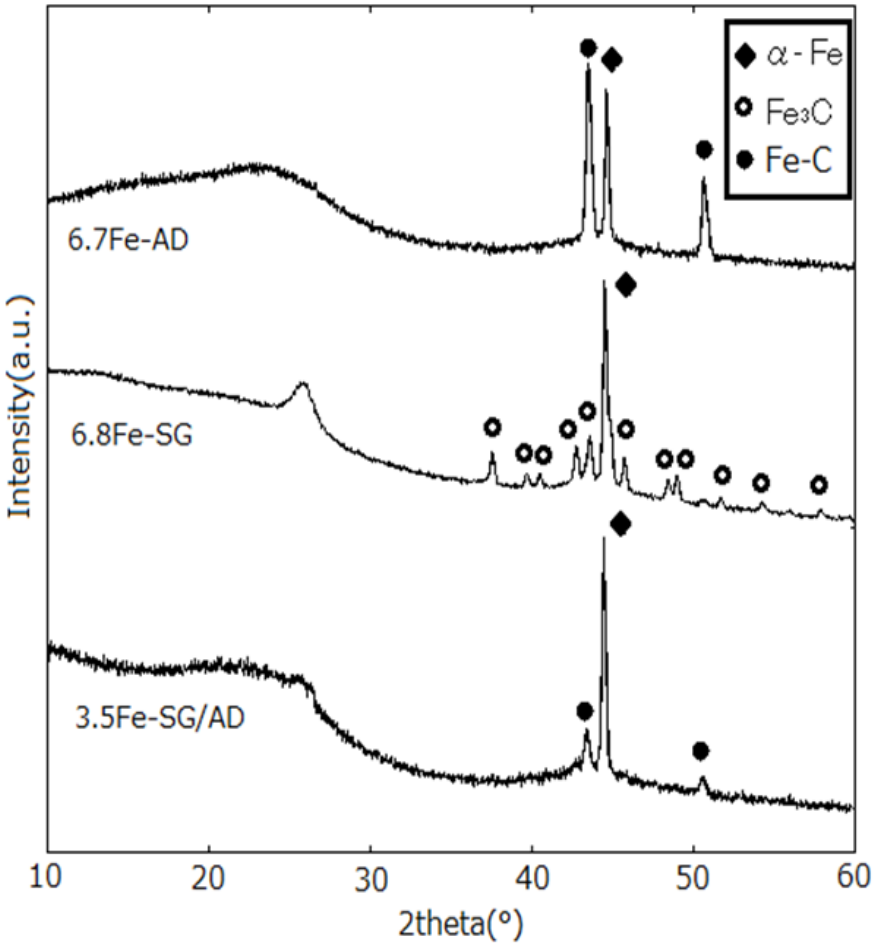

Figure 2.9 XRD patterns after the pyrolysis of 6.7Fe-AD, 6.8Fe-SG, and 3.5Fe-SG/AD

Figure 2.9 shows the XRD patterns of char after pyrolysis of 6.7Fe-AD, 6.8Fe-SG, and 3.5Fe-SG/AD. It was found that the major chemical form of iron species for all of the samples was α-Fe. In addition, a small amount of austenite (Fe–C) was present in 6.7Fe-AD and 3.5Fe-SG/AD. Interestingly, the diffraction peaks attributed to cementite (Fe_3C) were observed in the XRD pattern of 6.8Fe-SG because the tar evolved during the pyrolysis of 6.8Fe-SG (the char yield was approximately 30 wt%), which was much higher than that of SG without iron catalyst (the char yield was only 17 wt%), reacted with the iron catalyst. Accordingly, there was a possibility that cementite was also present on 3.5Fe-SG/AD after pyrolysis. However, cementite did not appear in the XRD pattern for 6.7Fe-AD.

Figures 2.10 and 2.11 show the XRD patterns of char for 3.2Fe-AD and 3.5Fe-SG/AD during steam gasification, respectively. The value in the bracket shows the carbon conversion after gasification.

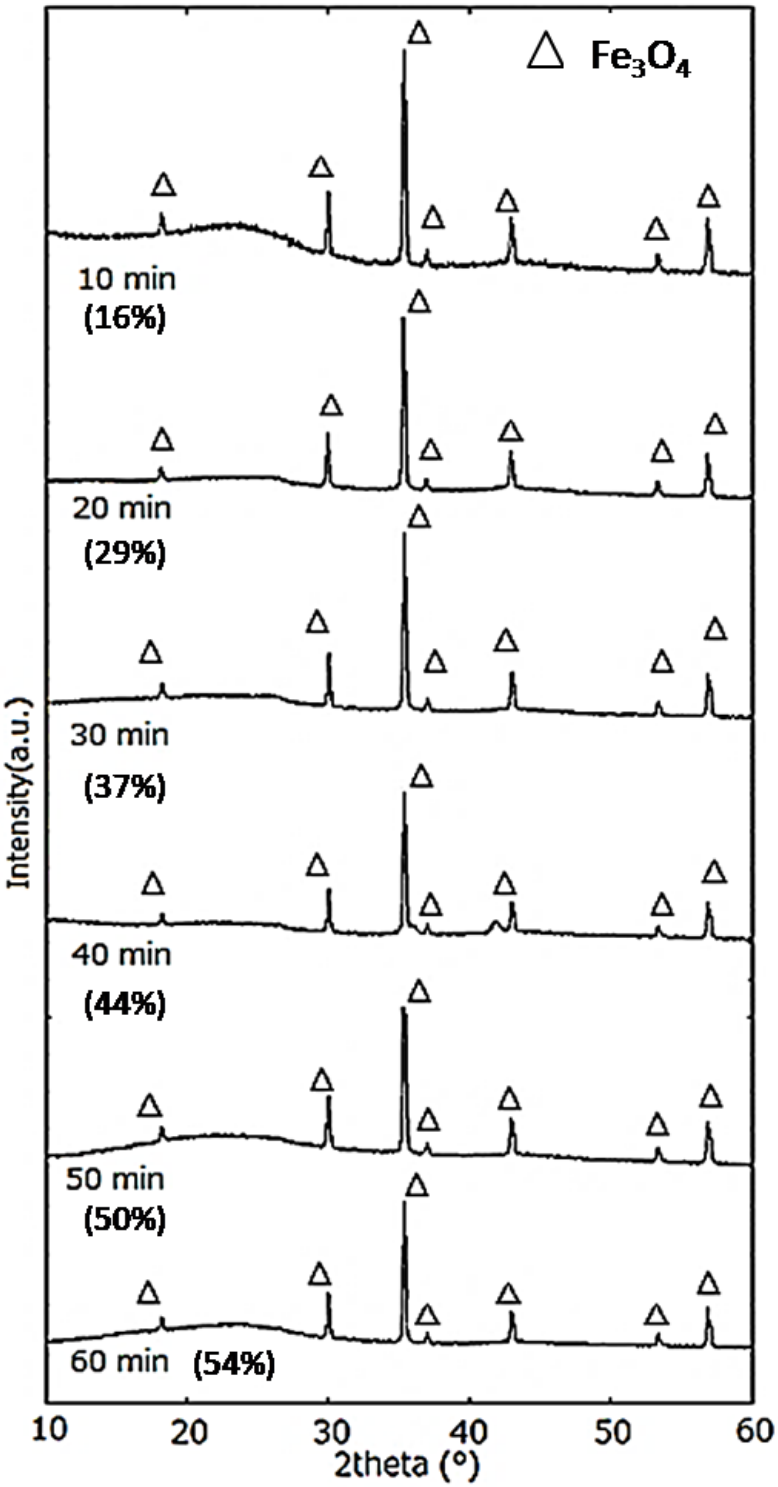

Figure 2.10 XRD patterns for 3.2Fe-AD during steam gasification

In the case of 3.2Fe-AD, the iron species changed to magnetite (Fe_3O_4) after 10 min of steam gasification. In contrast, the XRD patterns of char for 3.5Fe-SG/AD were significantly different from those for 3.2Fe-AD. The iron species in the 3.5Fe-SG/AD existed as α-Fe, Fe_3C, and Fe_2C as well as Fe_3O_4 in the first 30 min of steam gasification. It is well-known that metallic iron has higher activity for steam gasification than do other iron types [64][65].

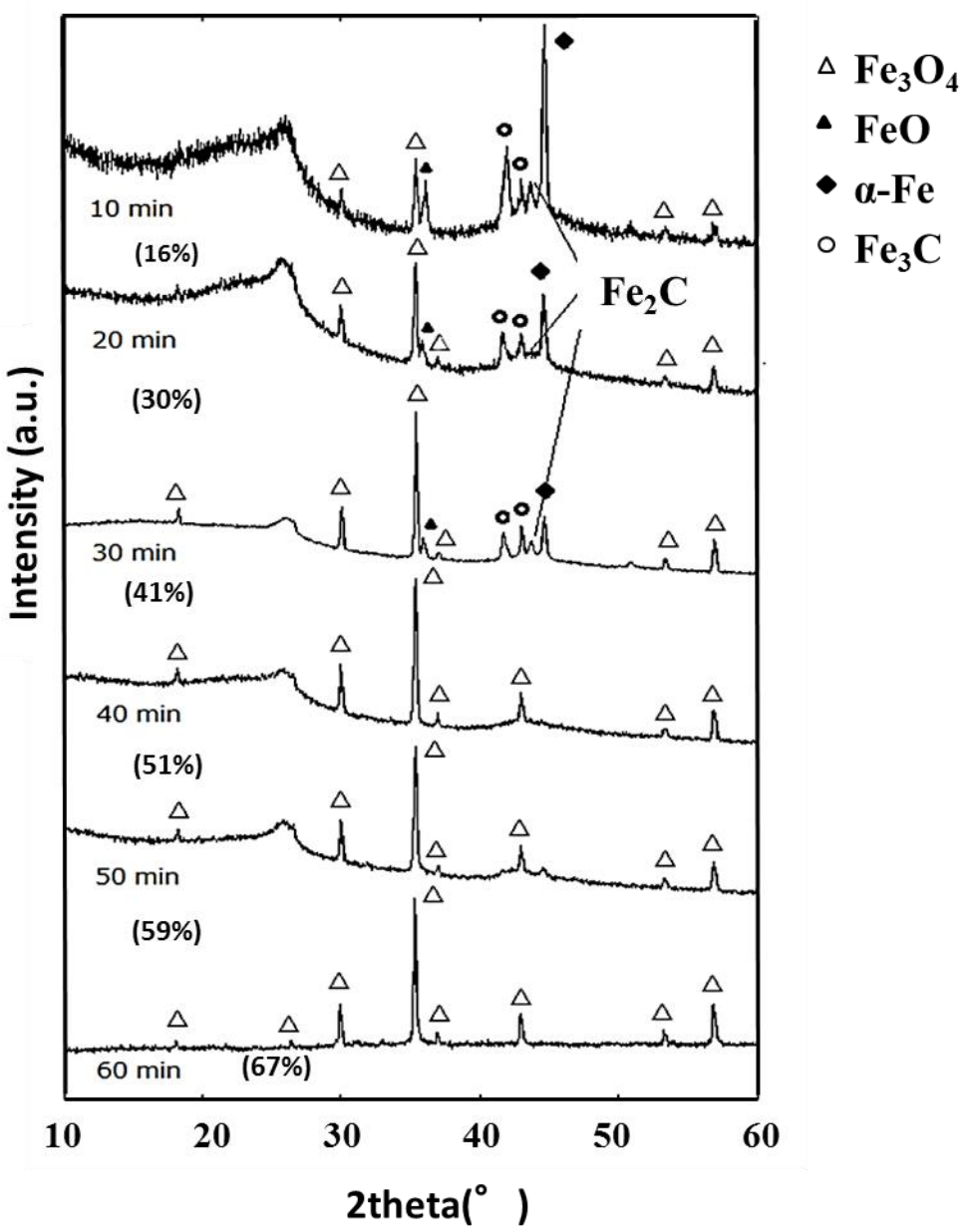

Figure 2.11 XRD patterns for 3.5Fe-SG/AD during steam gasification

Figure 2.6 demonstrated that 3.5Fe-SG/AD showed higher reactivity for steam gasification because the metallic iron species (α-Fe) existed throughout the first 30 min of steam gasification. For further clarification, XRD measurement of the char for 4.1Fe-Dem-SG/AD after steam gasification was carried out (Figure 2.12).

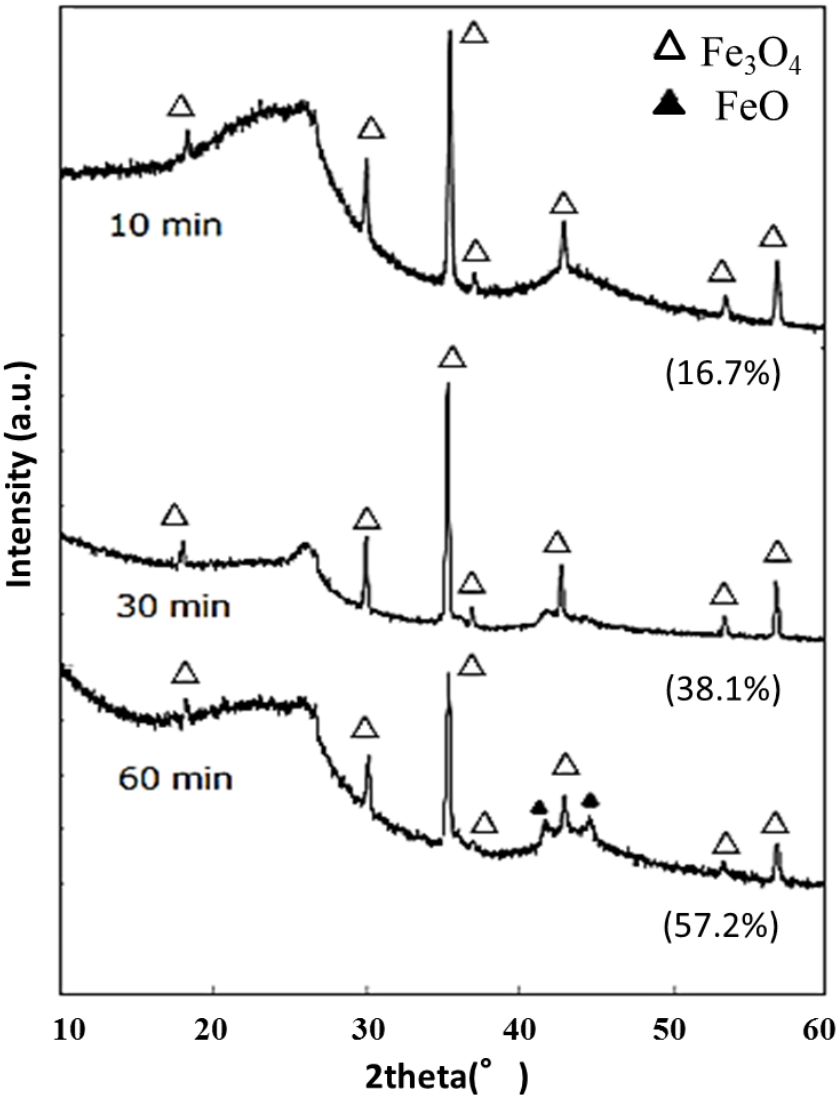

Figure 2.12 XRD patterns for 4.1Fe-Dem-SG/AD during steam gasification

In the first 30 min of steam gasification, the chemical forms of most iron species for 4.1Fe-Dem-SG/AD were Fe_3O_4, unlike those of 3.5Fe-SG/AD. Based on these results, it was believed that the ash, such as sodium, potassium, and calcium, in the biochar suppressed the oxidation of the iron catalysts. Pour et al. [64] reported that the addition of a very small amount

of co-existing calcium and magnesium (approximately 2 mol%) to iron could improve the reduction during the reduction reaction. In contrast, for co-gasification of AD and biochar without iron catalysts, the amount of hydrogen evolution (90 mmol/g-char) was just slightly larger than the hydrogen evolution in the gasification of AD (87 mmol/g-char, Table 2.5), suggesting that the ash, such as sodium, potassium, and calcium, did not promote the gasification of AD primarily because of the presence of only a small amount of ash in biochar. Accordingly, the oxidation suppression of iron species by the ash in the biochar was considered to be one of the reasons the activity of the iron catalysts did not greatly decrease.

Table 2.6 Change in crystallite diameter (nm) of Fe_3O_4 for 3.2Fe-AD and 3.5Fe-SG/AD

	10 min	20 min	30 min	40 min	50 min	60 min
3.2Fe-AD	49	50	53	49	52	57
3.5Fe-SG/AD	43	47	42	42	44	47
4.1Fe-Dem-SG/AD	40	—	48	—	—	61

Table 2.6 shows the change in the crystallite size of iron species for 3.2Fe-AD and 3.5Fe-SG/AD during steam gasification. The crystallite sizes of Fe_3O_4 for 3.5Fe-SG/AD were slightly lower than those for 3.2Fe-AD (i.e., aggregation was more difficult for the iron species on the biochar). Pour et al. [66] have also reported that the co-existing calcium and magnesium suppressed aggregation of the iron species. As the crystallite sizes of Fe_3O_4 for 4.1Fe-Dem-SG/AD was almost the same as those for 3.2Fe-AD (Table 2.6), we supposed that the Ca, K and Na present in the biochar had the effect of suppressing the aggregation of iron species. Asami and Ohtuska [53] reported that the char conversion in the steam gasification of LY brown coal at 750 ℃ increased significantly from 30% to approximately 65% with addition of iron catalyst. Observed differences between this study and their report were attributed to LY coal having a higher number of cation-exchangeable functional groups, such as carboxyl groups, compared

to AD, resulting in a higher dispersion of iron catalyst on LY coal. Asami and Ohtuska also showed that the co-existence of Ca suppressed aggregation of the iron catalyst, such that the char conversion increased from 30% to 90%. As such, char conversion during steam gasification was considered to be related to the dispersion of iron catalyst. As described above, it was considered that the alkali and alkaline earth metals in the biochar play important roles in suppressing the oxidation and aggregation of iron species.

Finally, how the iron catalyst on the biochar promoted the gasification of AD was evaluated. The steam gasification using the iron-loaded biochar and AD separately was performed. Specifically, the samples were packed in the following order: 6.8Fe-SG (0.1 g), quartz wool, and AD (shown in Figure 2.13). This order was utilized to ensure there was no direct contact between the two samples. As a result, the amount of hydrogen evolved in this experiment, approximately 33 mmol, was just slightly higher than the sum of the hydrogen evolution in the individual gasification (31 mmol, Figure 2.4). This result indicates that mixing the iron-loaded biochar and AD directly was very important to obtain the synergetic effect.

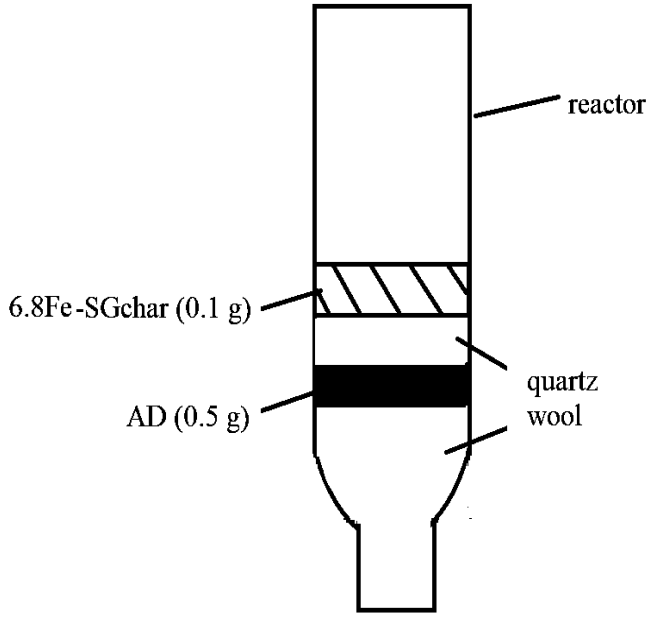

Figure 2.13 The packed sample in the separated gasification.

As above all, the mechanism for the effect of Fe-SGchar on AD could be shown as the figure below. That is, the AAEM in biomass maybe interact with Fe catalyst first. This iron catalyst will be kept as the reduced and the fine dispersed state. This may be one reason why synergetic effect appeared during co-gasification.

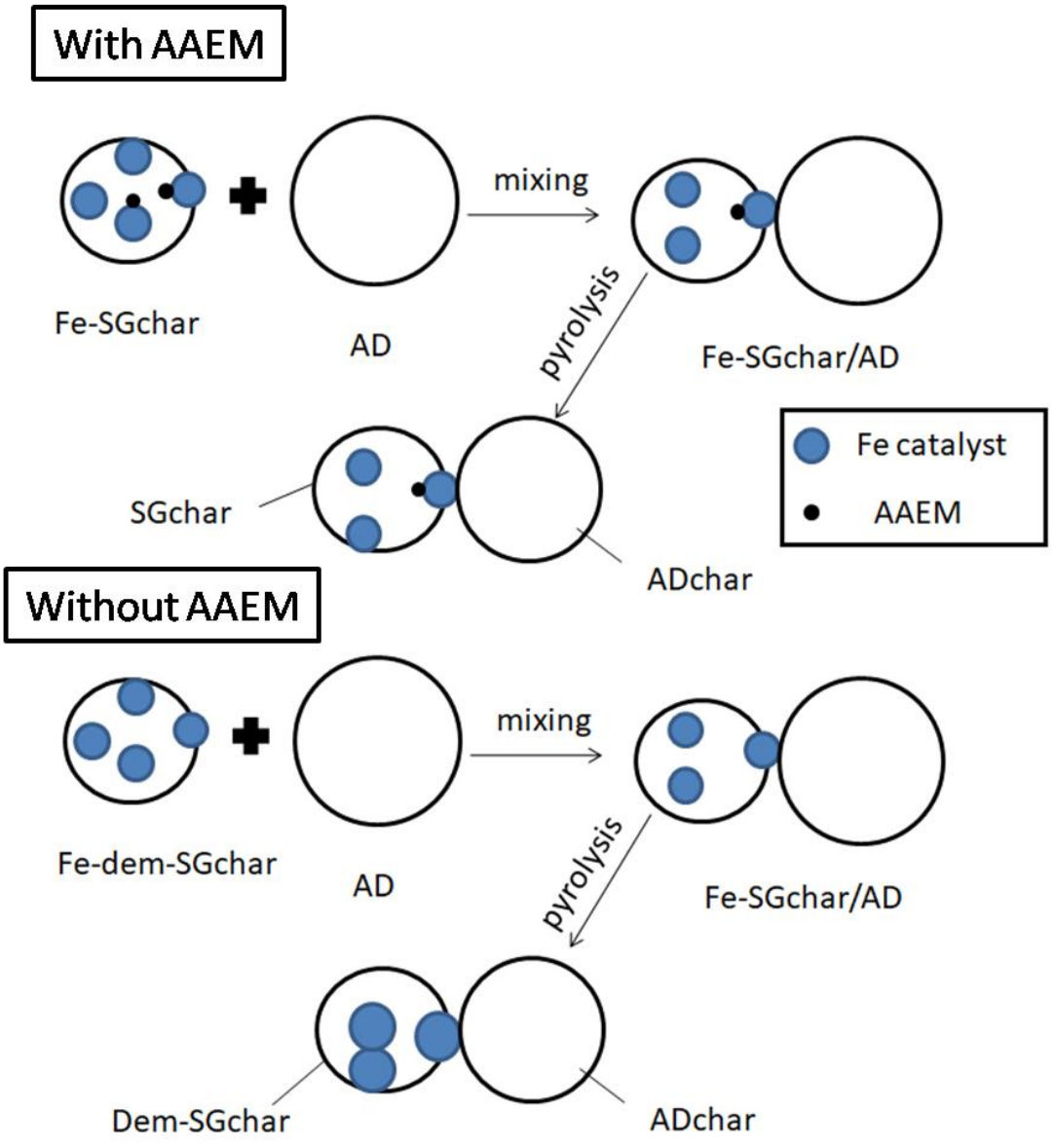

Figure 2.14 The mechanism for the effect of Fe-SGchar on AD

2.4 Conclusions

In this study, mixtures of iron-loaded biochar (pyrolysate of iron-loaded biomass) and AD with weight ratios of 1:10 and 1:5 were gasified with steam at 800 ℃ for 60 min in a fixed-bed type reactor. The conclusions are as follows:

(1) The H_2 production increased by approximately 20 mol% owing to the addition of iron-loaded biochar (20 wt%) to AD.

(2) The specific rates decreased gradually with increasing carbon conversion for AD and 3.2Fe-AD. On the contrary, there was no obvious decrease in the activity of iron catalyst in 1.8Fe-SG/AD and 3.5Fe-SG/AD.

(3) The XRD patterns of char for 3.5Fe-SG/AD were significantly different from those for 3.2Fe-AD. The metallic iron species (α-Fe) existed for the first 30 min of steam gasification for 3.5Fe-SG/AD. In the case of 3.2Fe-AD, the iron species changed to magnetite (Fe_3O_4) after 10 min of steam gasification. The crystallite sizes of Fe_3O_4 for 3.5Fe-SG/AD were slightly smaller than those for 3.2Fe-AD.

Akita University

Chapter 3 Optimization of mixing conditions of subbituminous coal and iron-loaded biochar for co-gasification

3.1 Introduction

In Chapter 2, an iron-loaded biochar (produced by the pyrolysis of 7 wt% iron-loaded Japanese cedar [SG] at 800 °C) was mixed with Indonesian sub-bituminous coal at 20 wt%, and then, the mixed sample was gasified with steam at 800 °C for 60 min. The hydrogen evolution from this system was observed to increase by 20% compared to that observed for the steam gasification of coal alone in the presence of the same amount of iron catalyst. It was also demonstrated that the small amount of alkali and alkaline earth metals contained in the biomass ash maintained the iron catalyst in an active state, even in the late stages of gasification; however, in the absence of an iron catalyst, these elements did not promote the gasification of coal to the same degree [67]. There are still two problems to be solved. First, when the iron-loaded biochar should be added must be determined. Specifically, the question of whether the iron-loaded biochar should be mixed with the coal (i.e., before pyrolysis) or coal char (i.e., after pyrolysis) to obtain higher gasification efficiency must be resolved. Second, the mixing ratio of iron-loaded biochar and coal/coal char is believed to strongly affect the co-gasification efficiency [68–70]. In Chapter 2, only two mixed samples—10 wt% and 20 wt% iron-loaded biochar in coal—were gasified with steam. Therefore, the optimum mixing ratio needed to maximize the gasification efficiency in the co-gasification of iron-loaded biochar and coal/coal char remains to be identified [67].

The purpose of this chapter is to determine the optimum time for the addition of the iron-loaded biochar and the optimum mixing ratio of iron-loaded biochar to coal/coal char for co-gasification.

3.2 Experimental

3.2.1 Preparation of mixed samples of iron-loaded biochar and AD

The iron-loaded biochar was produced from 7Fe-SG. The samples (0.5 g) were heated from room temperature to 800 °C at a rate of 300 °C/min under flowing He gas (140 mL/min) and held at this temperature for 10 min. After cooling to room temperature, the iron-loaded biochars were preserved in nitrogen-purged polyethylene bags. These samples were designated as 7Fe-SGchar. The iron content in the 7Fe-SGchar was concentrated to 23 wt% because the sample weight decreased to approximately 30 wt% after pyrolysis.

The prepared iron-loaded biochar was added to AD at ratios of 1:10 to 10:10 and were named as follows: Fe-SGchar/AD (1:10) to Fe-SGchar/AD (10:10), respectively. To determine the effectiveness of iron-loaded biochar for co-gasification, the iron-loaded biochar was also added to ADchar. ADchar was prepared by pyrolysis at 800℃ for 10 min. Because the yield of ADchar was roughly 50 wt%, the ratio of iron-loaded biochar to ADchar ranged from 1:5 to 10:5 to maintain the iron and carbon contents of Fe-SGchar/AD. These samples were named as follows: Fe-SGchar/ADchar (1:5) to Fe-SGchar/ADchar (10:5), respectively.

Iron content in the mixed samples was shown in Table 3.1 and Table 3.2.

Table 3.1 Fe content in Fe-SGchar/AD with different Fe-SGchar mixing ratio

Mixing ratio	1:10	2:10	4:10	5:10	6:10	10:10
Fe/(SGchar+AD) (wt%)	1.8	3.5	6.1	7.1	8.1	11.1

Table 3.2 Fe content in Fe-SGchar/ADchar with different Fe-SGchar mixing ratio

Mixing ratio	1:5	2:5	4:5	5:5	6:5	10:5
Fe/(SGchar+ADchar) (wt%)	3.4	6.1	9.8	11.1	12.2	15.4

3.2.2 Pyrolysis and gasification

The same fixed-bed reactor in chapter 2 was used in this chapter. Initially, approximately 0.5 g of Fe-SGchar/AD or 0.25 g ~ 0.3 g of Fe-SGchar/ADchar (Fe-SGchar/ADchar was placed in the reactor so that the sample weight after pyrolysis was the same as Fe-SGchar/AD) was placed on quartz wool in the middle of the vertical fixed-bed-type reactor. The sample was heated from room temperature to 800 °C at a heating rate of 300 °C/min under flowing He gas (140 mL/min). The Fe-SGchar/AD was held at 800 °C for 10 min to remove any volatile components. Because Fe-SGchar/ADchar contains little volatile contents, this sample was heated to 800 °C but was not held at that temperature. After cooling to room temperature, the samples were removed from the reactor. The char yield after pyrolysis was calculated with the equation 2.1.

Steam gasification was performed at 800 °C for 60 min by introducing 50 vol% of steam/He into the reactor immediately after the pyrolysis of the samples. The amount of steam was controlled by setting the temperature of the steam generator at 87 °C. The gasses (i.e., H_2, CO, CO_2, CH_4, C_2H_4, and C_2H_6) produced during steam gasification were determined by an online MicroGC instrument (Agilent Technologies MicroGC 3000A). The gas evolution rate was calculated using the equation 2.2. The carbon conversion was calculated using the equation 2.3.

The chemical form of the iron catalyst during pyrolysis and gasification was evaluated by X-ray powder diffraction (XRD; Rigaku, Ultima IV) with Ni-filtered CuKα radiation. The crystallite size of the iron catalyst was calculated using the Scherrer equation 2.4.

3.3 Results and Discussion

3.3.1 Effect of iron-loaded biochar on the gasification of AD

Figure 3.1 shows the hydrogen evolution rates of Fe-SGchar/AD (1:10–10:10) and Fe-SGchar/ADchar (1:5–10:5) during steam gasification at 800 ºC. Here, the results of Fe-SGchar/AD (x:10) are compared with those of Fe-SGchar/ADchar (x:5), where x ranged from 1 to 10. As described above, this variation occurred because the weight of AD decreased to approximately 50 wt% after pyrolysis at 800 °C for 10 min. Based on the data shown in Figure 3.1, it was determined that the hydrogen evolution rates were maximized at approximately 5 min and subsequently decreased gradually with increasing reaction time for all samples. Fe-SGchar/AD exhibited a higher hydrogen evolution rate than Fe-SGchar/ADchar for all ratios of Fe-SGchar addition.

Table 3.3 shows the amounts of hydrogen evolution and carbon conversion for Fe-SGchar/AD (1:10～10:10) and Fe-SGchar/ADchar (1:5～10:5) during steam gasification at 800 ℃ for 60 min. From Table 3.1, it can be seen that both the carbon conversion and the amount of hydrogen evolution of Fe-SGchar/AD were always higher than those of Fe-SGchar/ADchar. Table 3.1 also presents the amount of hydrogen evolution calculated using the following equation (A (sum)):

$$A(sum)=\frac{A(Fe-SGchar)\times m(Fe-SGchar)+A(ADchar)\times m(ADchar)}{m(Fe-SGchar)+m(ADchar)} \quad , \qquad (3.1)$$

where A(Fe-SGchar) [mmol/g-char] and A(ADchar) [mmol/g-char] are the amounts of hydrogen evolution observed for Fe-SGchar alone and ADchar alone, respectively; and m(Fe-SGchar) [g, dacf] and m(ADchar) [g, dacf] are the weights of Fe-SGchar and ADchar, respectively. In this calculation, these weights (i.e., m(ADchar) and m(Fe-SGchar)) were set to be equal to those used for co-gasification. Similar to Chapter 2, the amount of hydrogen evolution during steam co-gasification was higher than the sum of the amounts of hydrogen evolution produced by the individual gasification of Fe-SGchar and ADchar (A(Sum)) in all cases. The last column in Table 3.1 presents the incremental amounts of hydrogen evolution between the co-gasification and individual gasification determined using the following equation:

$$Increment\,(\%) = \frac{A(co-gasification) - A(Sum)}{A(Sum)} \times 100 \quad , \qquad (3.2)$$

where A(co-gasification) is the amount of hydrogen evolution during steam co-gasification, which is shown in Table 3.1. Based on these results, the increments for Fe-SGchar/AD (14–29%) were higher than those for Fe-SGchar/ADchar (2–13%).

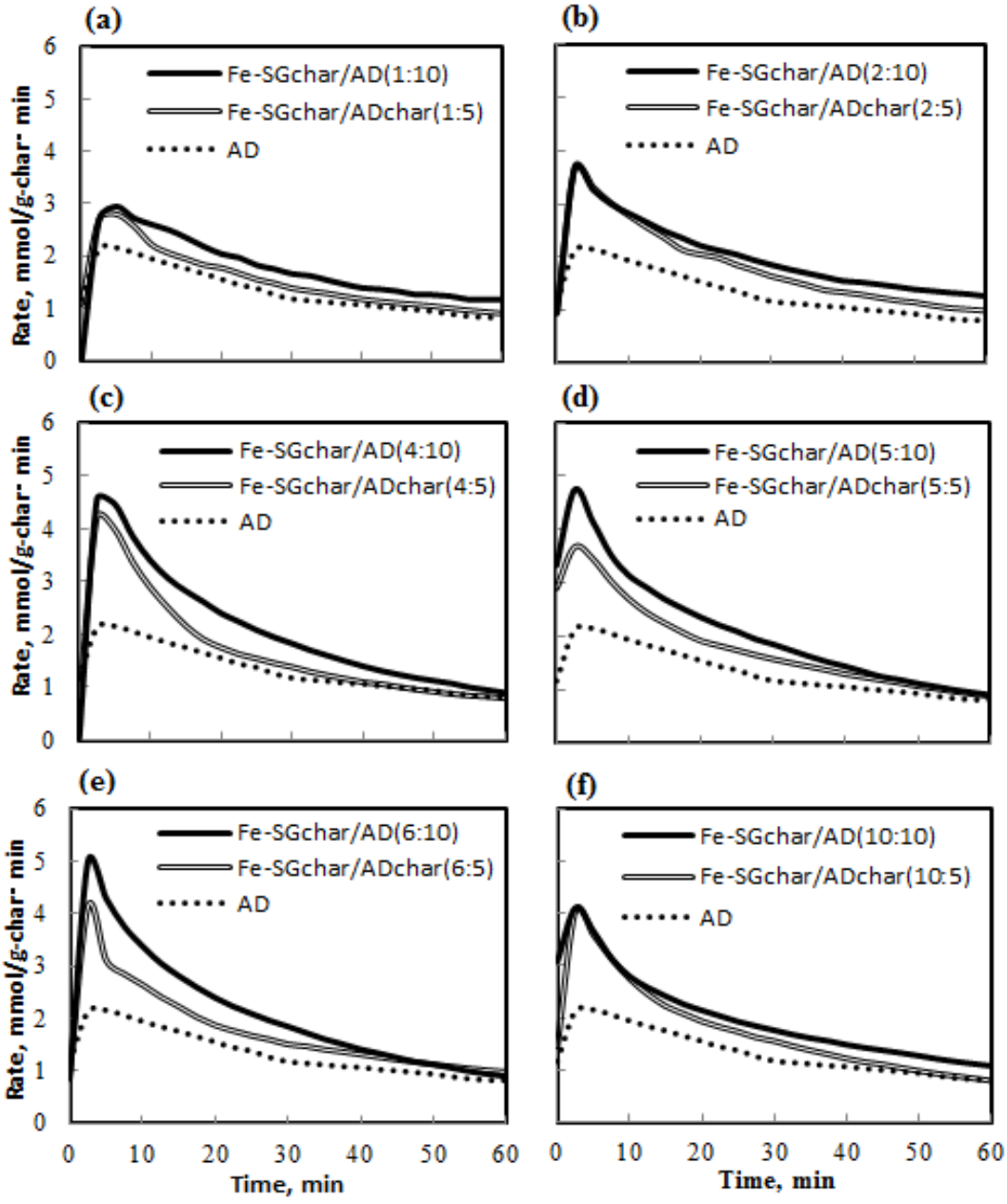

Figure 3.1 The H_2 evolution rate for Fe-SGchar/AD and Fe-SGchar/ADchar in different ratios

Table 3.1 Carbon conversion and amount of hydrogen evolution

	Carbon conversion (mol%)	Amount of hydrogen evolution		
		Co-gasification (mmol/g-char)	Sum (mmol/g-char)	Increment (%)
Fe-SGchar/AD(1:10)	61	107	91	17.5
Fe-SGchar/ADchar(1:5)	49	93		2.2
Fe-SGchar/AD(2:10)	63	113	94	20.2
Fe-SGchar/ADchar(2:5)	51	98		4.3
Fe-SGchar/AD(4:10)	65	124	97	27.8
Fe-SGchar/ADchar(4:5)	58	107		10.3
Fe-SGchar/AD(5:10)	71	126	98	28.5
Fe-SGchar/ADchar(5:5)	59	110		12.2
Fe-SGchar/AD(6:10)	65	121	99	22.2
Fe-SGchar/ADchar(6:5)	55	106		4.1
Fe-SGchar/AD(10:10)	63	119	104	14.4
Fe-SGchar/ADchar(10:5)	56	107		2.9

3.3.2 Influence of addition ratio of Fe-SGchar

From Table 3.1, it can be seen that as the amount of Fe-SGchar added increased, both the carbon conversion and the amount of hydrogen evolution initially increased and subsequently decreased. More specifically, in the steam gasification of Fe-SGchar/AD at 800 °C for 60 min, the carbon conversion was maximized (71 mol%) when the mixing ratio was 5:10. In contrast, for Fe-SGchar/ADchar, the carbon conversion was maximized (59 mol%) when the mixing ratio was 5:5. Similar to the carbon conversion, the maximum amounts of hydrogen evolution for Fe-SGchar/AD and Fe-SGchar/ADchar—126 and 110 mmol/g-char, respectively—when the mixing ratios of Fe-SGchar to AD and to ADchar were 5:10 and 5:5 by weight, respectively. Because the weight of AD decreased to approximately 50 wt% during pyrolysis at 800 ℃ for 10 min, as described above, the weight ratio of 5:10 was considered to result in the highest hydrogen evolution for the mixture of Fe-SGchar/AD. The reason will be discussed though XRD analysis of iron catalyst.

On the other hand, the relationship between carbon conversion and gas evolution was also discussed and shown in Figure 3.2. It could be seen that the relationship between carbon conversion and gas evolution is linear. This showed that the mechanism of gasification is not different between Fe-SGchar/AD and Fe-SGchar/ADchar.

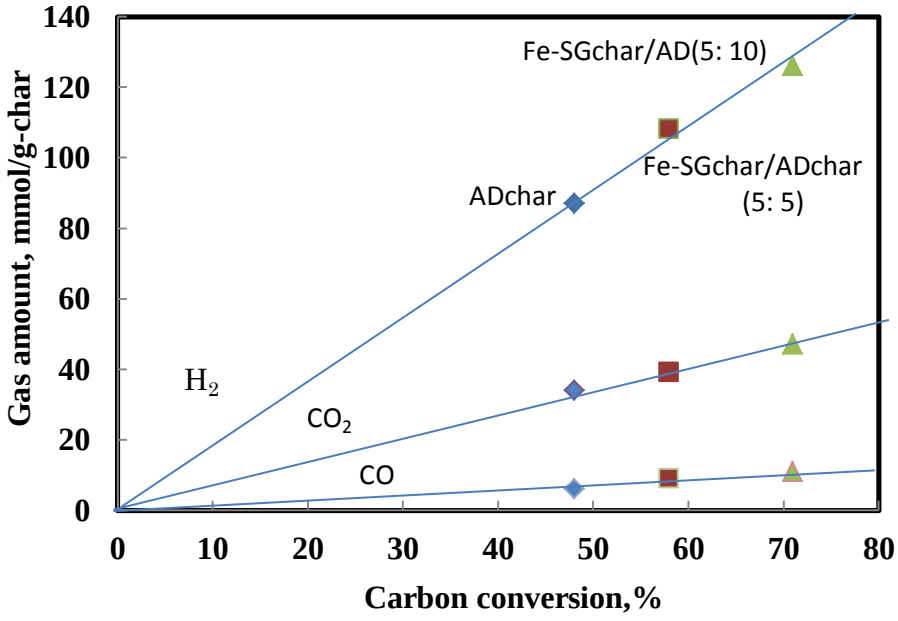

Figure 3.2 Relationship between carbon conversion and gas evolution

3.3.3 Influence of Fe-SGchar on specific rate

Figure 3.3 shows the relationship between the specific rate and carbon conversion. The specific rate, R_s [1/h], was employed to investigate the change in the carbon conversion relative to the residual amount of carbon and was calculated using the equation 2.5.

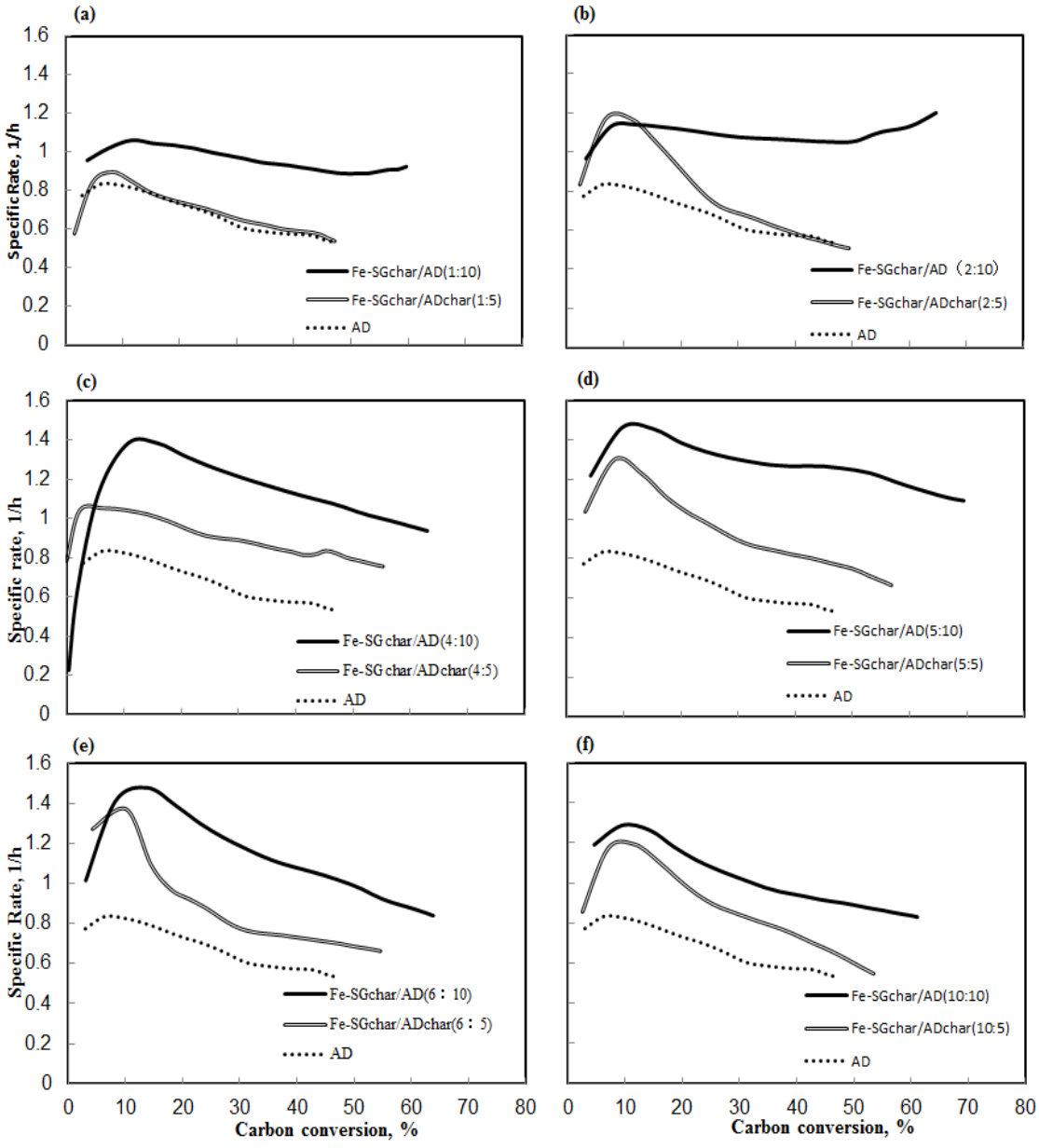

Figure 3.3 The relationship between specific rate and carbon conversion

From Figure 3.3, below approximately 10% of carbon conversion, the difference between Fe-SGchar/AD and Fe-SGchar/ADchar for the specific rate was small, whereas above 10%, the specific rates for Fe-SGchar/AD

were larger than those for Fe-SGchar/ADchar. Thus, the reactivity obtained by mixing Fe-SGchar and AD was always greater than that achieved by mixing Fe-SGchar and ADchar.

3.3.4 Change in the form of iron during pyrolysis and steam gasification

Based on the carbon conversion and hydrogen evolution data, the optimal time for the addition of iron-loaded biochar was determined to be before the pyrolysis of AD, and the optimal mixing ratio of Fe-SGchar was determined to be 1:1 by weight. Thus, two questions remained to be answered: (1) Why is the reactivity for the gasification of Fe-SGchar/AD higher than that of Fe-SGchar/ADchar? (2) Why does the mixing ratio of 1:1 exert the best effect on steam co-gasification? To answer these questions, we investigated the changes of the form of iron during pyrolysis and steam gasification.

Figures 3.4 and 3.5 present the XRD patterns of Fe-SGchar/ADchar (5:5) and Fe-SGchar/AD (5:10), respectively, pyrolyzed under various conditions. For Fe-SGchar/ADchar (5:5) (Figure 3.4), almost no changes in the form of the iron catalyst (α-Fe and Fe_3C) occur during pyrolysis. In contrast, after the pyrolysis of Fe-SGchar/AD (5:10) at 450°C, α-Fe had disappeared completely, and most of the iron species were present as Fe_3C (Figure 3.5). These results are attributable to the reaction of α-Fe with the volatile matter evolved from AD to produce Fe_3C. The iron forms differed between Fe-AD and Fe-SGchar/AD (5:10) (Figure 3.5) because of the presence of alkali and alkaline earth metals in Fe-SGchar. Martin et al. demonstrated that Ca-Fe catalyst produced more hydrogen from steam than pure Fe catalyst [71]. Moreover, Fe_3C has been reported to form readily via the reaction of the highly dispersed α-Fe with carbon [72]. In fact, the crystallite size of α-Fe on Fe-SG (26 nm) was much smaller than that on Fe-AD (45 nm). As shown in Figure 3.6, Fe_3C decomposed to form α-Fe above 700 °C. This change in the iron form is believed to occur via the following equation 2.6, which was reported by Li [73]:

$$Fe_3C \rightarrow 3Fe+C\ . \qquad (3.6)$$

The carbon formed according to this equation might be very unstable. Accordingly, because of its high reactivity, this carbon should be easily gasified with steam in the early stages of gasification, thereby increasing the hydrogen evolution rate in the early stages of gasification of

Fe-SGchar/AD (5:10) relative to that observed for Fe-SGchar/ADchar (5:5), as shown in Figure 3.3 (c), (d), and (e). In contrast, because of the availability of insufficient amounts of the catalyst or carbon from volatile matter, little Fe_3C could be generated; thus, the increases of Fe-SGchar/AD (1:10), Fe-SGchar/AD (2:10), and Fe-SGchar/AD (10:10) were not obvious (Figure 3.3 (a), (b), and (f)).

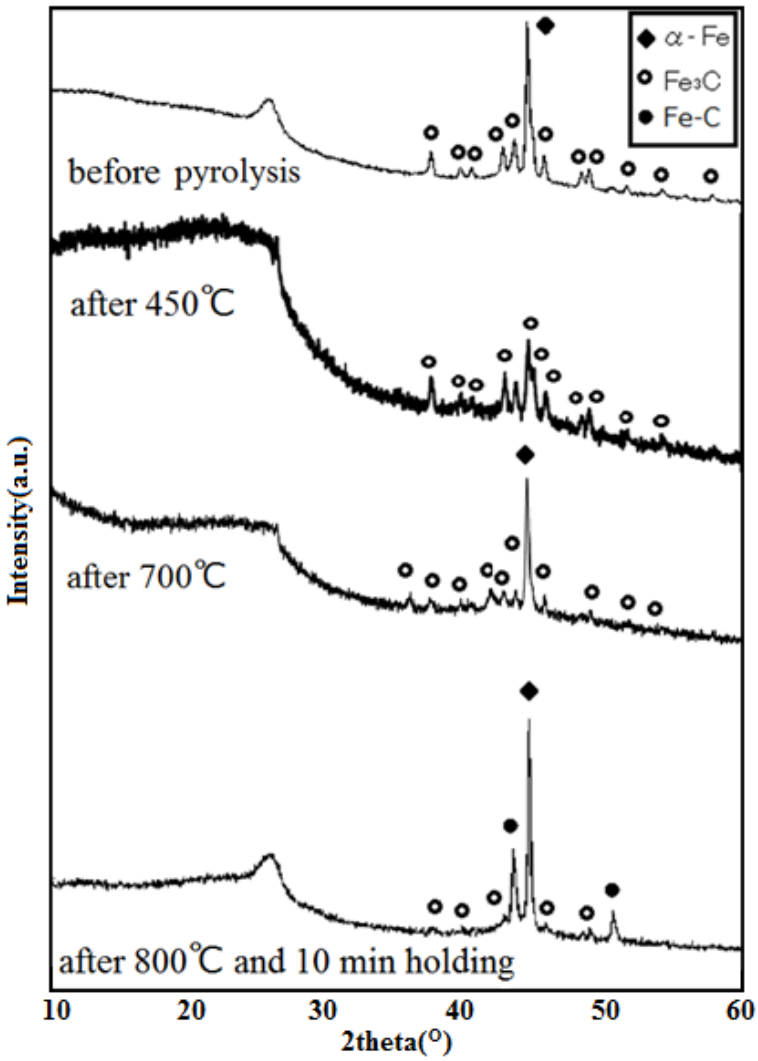

Figure 3.4 The XRD patterns of Fe-SGchar/AD with temperature rising in the processing of pyrolysis

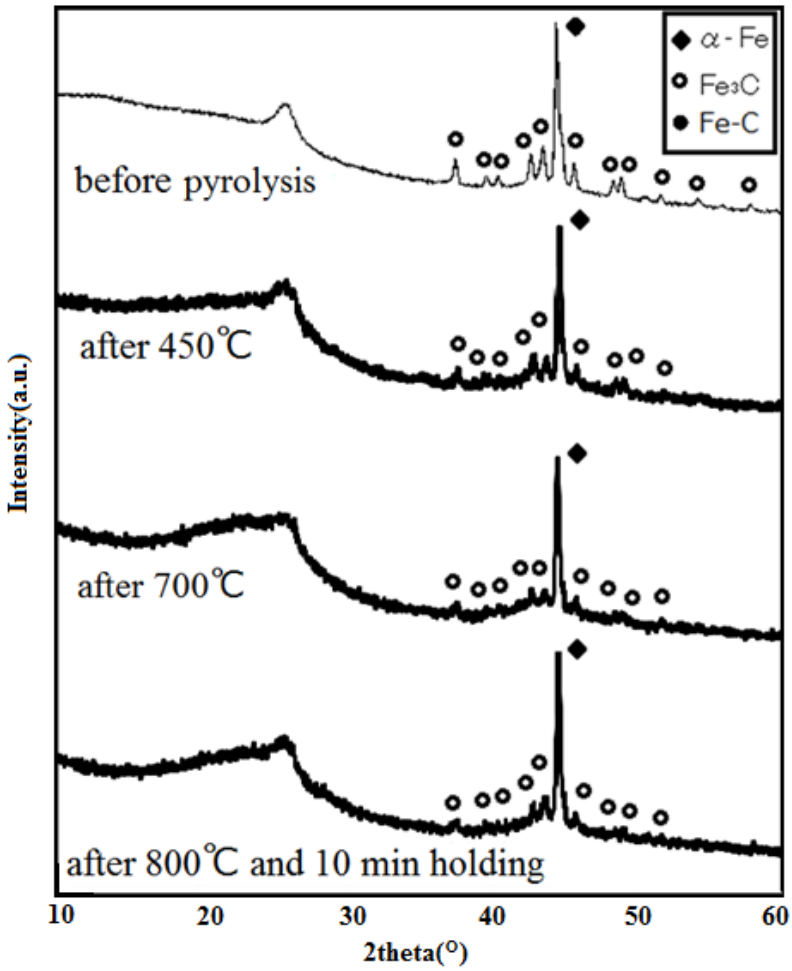

Figure 3.5 The XRD patterns of Fe-SGchar/ADchar with temperature rising in the processing of pyrolysis

Figure 3.6 shows the XRD patterns of Fe-SGchar/AD and Fe-SGchar/ADchar in and after gasification. From Figure 3.6 (b), (d) and (f), α -Fe and Fe_3C could be seen after 5 min gasification of Fe-SGchar/ADchar (2:5~10:5), and the oxidation of the iron catalyst was slower than that observed in 3.2Fe-AD (Figure 2.9). The alkali metals in Fe-SGchar have been reported to prevent the oxidation of the iron catalyst to some extent [67, 73]. Therefore, the activity of the iron catalyst in Fe-SGchar/ADchar was considered to be high, even in the later stages of gasification, relative to that of 3.2Fe-AD.

Furthermore, the iron catalyst in Fe-SGchar/AD remained in its reduced form longer than that in Fe-SGchar/ADchar. Fe-SGchar/AD and Fe-SGchar/ADchar differ in terms of whether Fe-SGchar exists during the pyrolysis of AD or not. Qi [74] reported that iron atoms could be inserted between the layers of hexagonal carbon planes produced during the pyrolysis of coal. In this study, the iron catalyst on the Fe-SGchar may have moved to the AD surface during pyrolysis. In contrast, when the mixture of Fe-SGchar and ADchar was gasified, the effect of the iron catalyst on the steam gasification of ADchar was considered to be small because the ADchar consists of carbons with low reactivity. Zhang [75] reported that alkali metals could move from biomass to the coal surface and weaken C-C bonds of coal char during pyrolysis. This is one reason why the reactivity of AD did not decrease. Therefore, Fe-SGchar/AD was believed to be more reactive than Fe-SGchar/ADchar because of the interactions between carbons and iron/alkali metals during the pyrolysis of the coal.

In addition, in this chapter, the highest amount of hydrogen evolution and the maximum char conversion were observed when the Fe-SGchar was mixed with AD or ADchar in weight ratios of 1:2 or 1:1, respectively. Because the iron catalyst and alkali and alkaline earth metals exert a promoting effect on gasification, the hydrogen evolution increases as the amount of Fe-SGchar added increases. However, there is one problem to be solved: Why did the amount of hydrogen evolution decrease when a large amount of Fe-SGchar was added? In fact, similar results have been observed previously. For example, Che et al. [76] reported that a mixing ratio of 1:1 resulted in the highest synergy during the steam gasification of a mixture of pine sawdust and lignite in air atmosphere at from 800 ℃ to 950 ℃. Additionally, Yan et al. [77] obtained similar results for the air and steam co-gasification of two types of woody biomass with brown coal at

temperatures ranging from 700 ℃ to 900 ℃. These authors attributed their results to the very low melting temperature of biomass ash: As a result, a large amount of biomass ash would cover the surface of the coal char, thereby blocking the pores of the coal char and limiting the contact between the coal char and the gasification agent. Although the biomass used in this gasification generated less ash, as the amount of biomass increased and the amount of ADchar decreased, a similar interaction between Fe-SGchar and ADchar may have occurred in this experiment. Qi [74] also investigated the relationship between iron loading and gasification reactivity and reported that a limit for the iron-loading amount exists and that, when this limit is exceeded, the gasification reactivity actually decreases. This experiment may have been affected by a similar phenomenon because the addition of large amounts of Fe-SGchar resulted in high iron-loading for AD. This may reasonably explain the decreased hydrogen evolution observed when large amounts of Fe-SGchar were added.

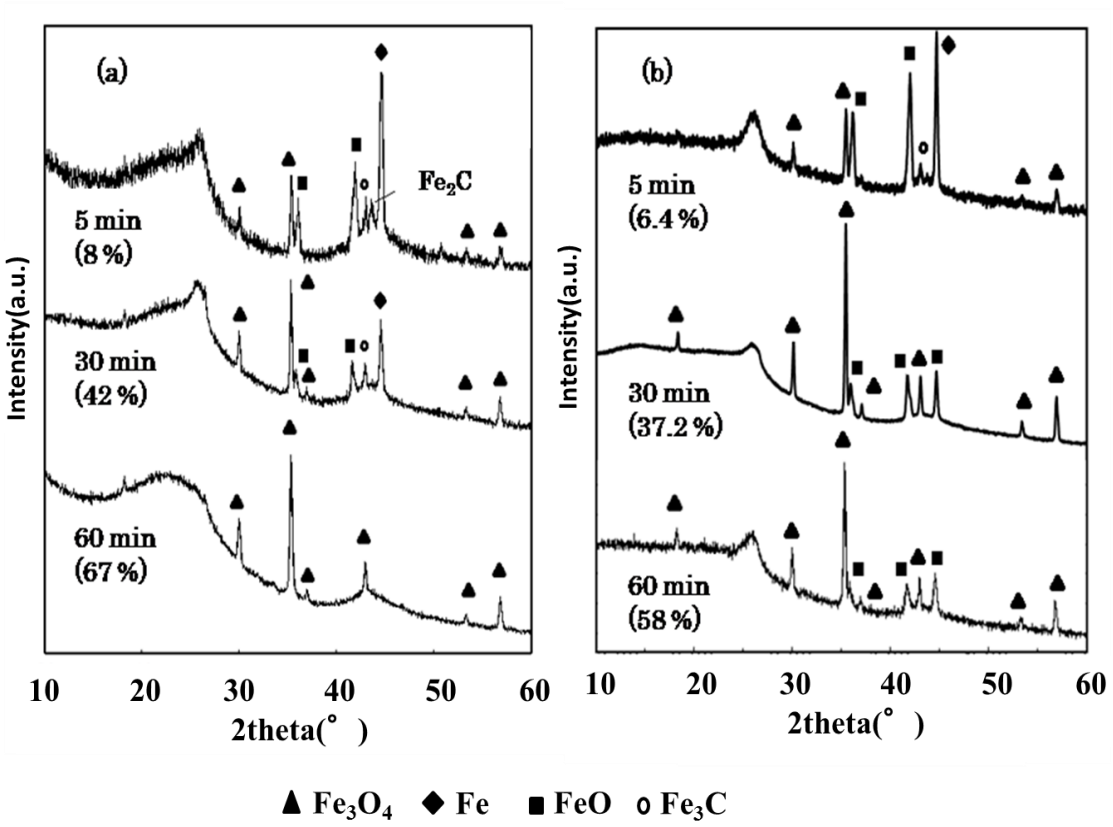

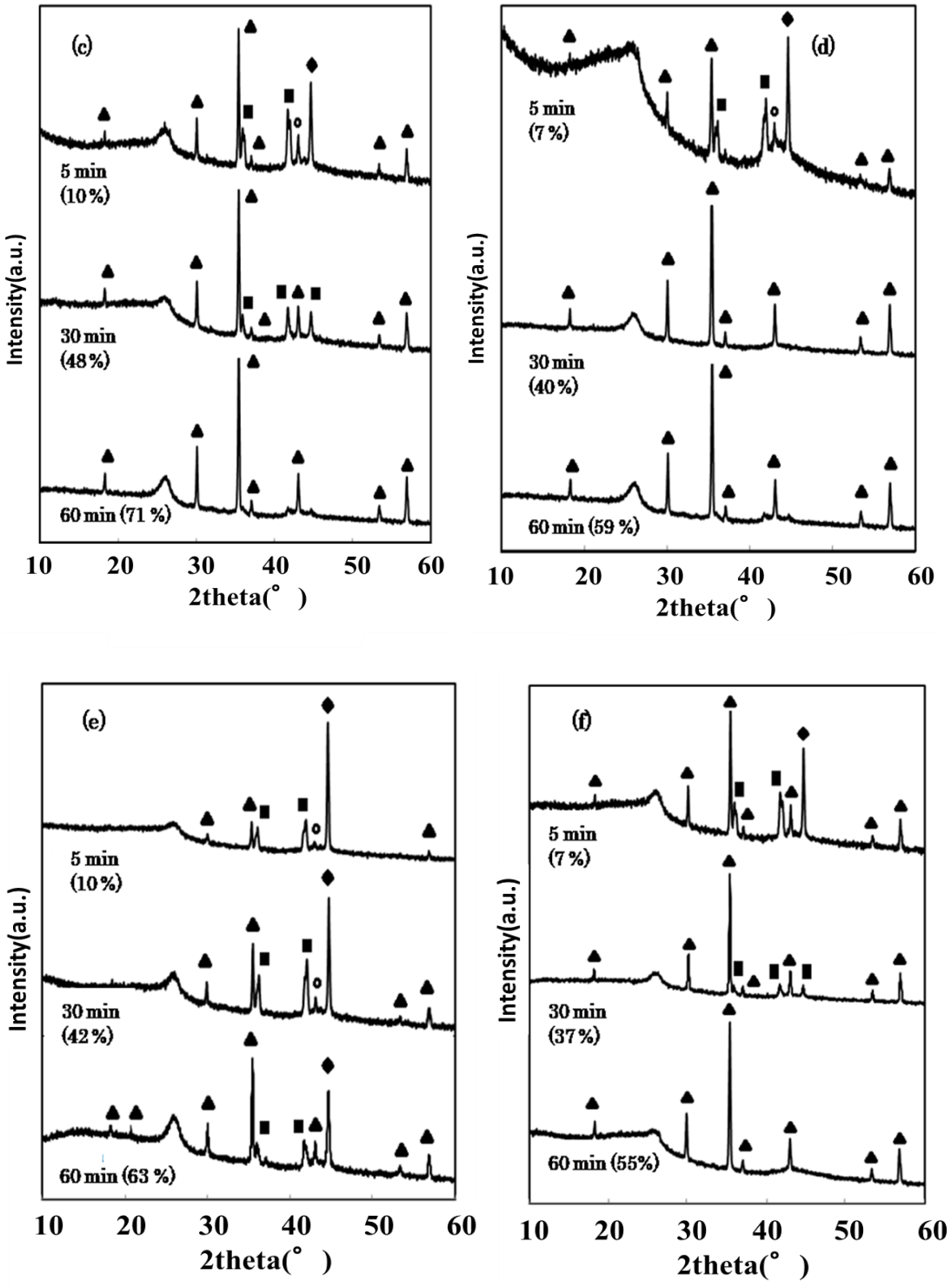

Figure 3.6 The XRD patterns of Fe-SGchar/AD and Fe-SGchar/ADchar in and after gasification. (a) Fe-SGchar/AD(2:10); (b) Fe-SGchar/ADchar(2:5); (c) Fe-SGchar/AD(5:10); (d) Fe-SGchar/ADchar(5:5); (e) Fe-SGchar/AD(10:10); (f) Fe-SGchar/ADchar(10:5)

As above all, Fe-SGchar/AD and Fe-SGchar/ADchar produced different hydrogen evolution for the same gasification time. The mechanism was shown as below in Figure 3.9. The carbon of coal could be divided into volatile matter (VM) carbon and fixed carbon. During pyrolysis, tar and light gas usually formed by VM carbon in primary pyrolysis. Char usually formed by fixed carbon in the pyrolysis during high temperature. In the case of Fe-SGchar/AD, Fe-SGchar stabilized some VM carbon of AD coal so that formed new fixed carbon. This changed char reactivity. Then AAEM in SG has an effect to keep activity of Fe catalyst. The two factors promoted AD gasification much more. On the other hand, in the case of Fe-SGchar/ADchar, Fe-SGchar could not take effect during the pyrolysis. Fe-SGchar and AAEM in SG could only take effect during the gasification so that the carbon conversion and hydrogen evolution for Fe-SGchar/ADchar were much smaller than that in Fe-SGchar/AD.

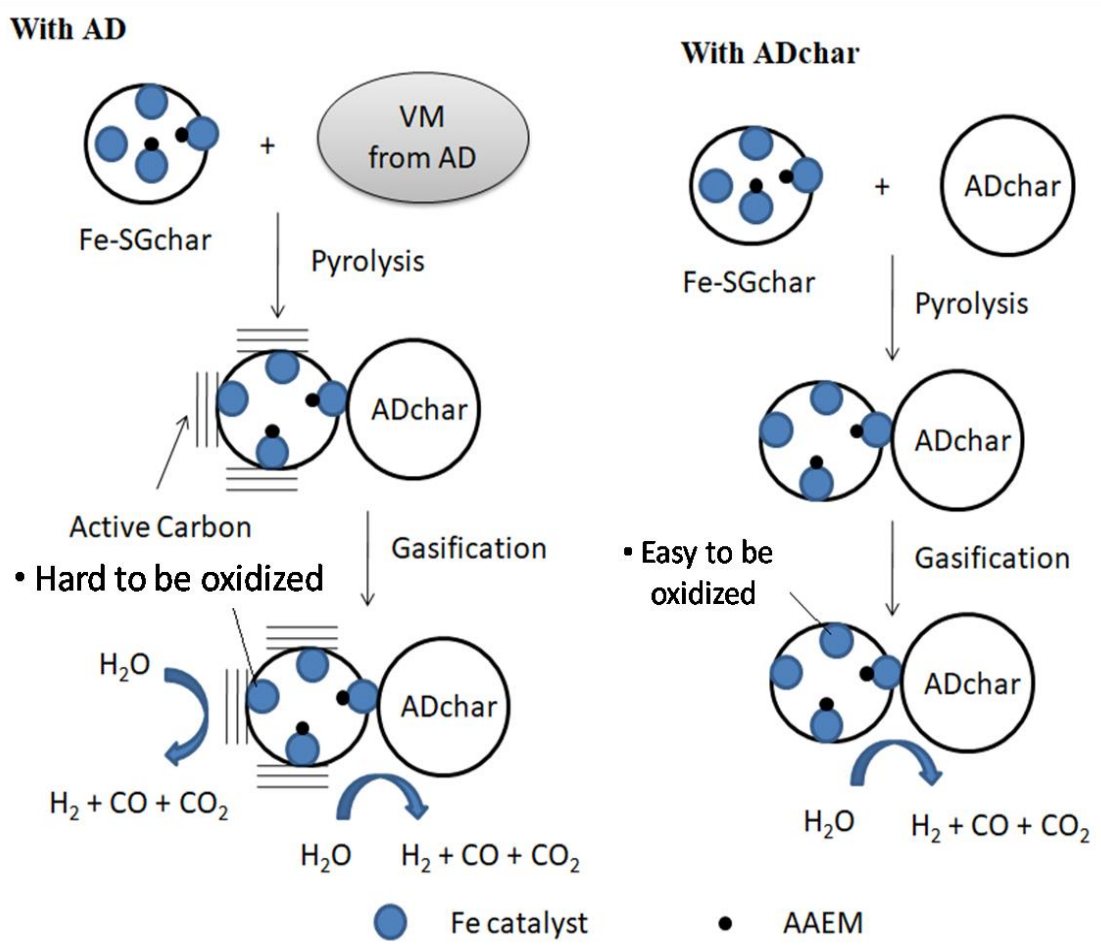

Figure 3.9 The mechanism of promotion for Fe-SGchar/AD and Fe-SGchar/ADchar

3.4 Conclusion

In this chapter, mixtures of iron-loaded biochar (the pyrolysate of iron-loaded biomass) and AD coal/ADchar with different weight ratios were gasified with steam at 800 ºC in a fixed-bed-type reactor. The conclusions obtained from this work are as follows:

(1) The optimal time to add iron-loaded biochar in this co-gasification system is before the pyrolysis of AD, and the optimal ratio for the addition of Fe-SGchar to ADchar is 1:1 by weight.

(2) Based on the relationships between the specific rate and carbon conversion obtained, the specific rate of Fe-SGchar/AD was always higher than that of Fe-SGchar/ADchar.

(3) According to the XRD patterns of chars pyrolyzed at various temperatures, a transition between α-Fe and Fe_3C occurred in Fe-SGchar/AD but not in Fe-SGchar/ADchar and produced a large amount of highly reactive carbons. Additionally, the XRD patterns of chars gasified at 800 ℃ for various times revealed that the iron catalyst can be maintained in its reduced form on both Fe-SGchar/AD and Fe-SGchar/ADchar for a longer time than that on Fe-AD. Finally, the oxidation of Fe-SGchar/AD was delayed compared to that of Fe-SGchar/ADchar in the presence of the same amount of iron catalyst.

Chapter 4 Effect of physical mixing of coal, biomass and Fe catalyst on the gasification

4.1 Introduction

In this chapter, the co-gasification of woody biomass and low rank coal was also investigated. In Chapter 2 and Chapter 3, the iron-loaded biochar (the product of iron-loaded Japanese cedar after pyrolysis) was used as an additive to AD coal or ADchar. In Chapter 2, the effectiveness for the co-gasification of iron-loaded biochar and AD coal was proved [67]. In Chapter 3, the best mixing condition of iron-loaded biochar for the co-gasification was investigated [79]. However, in this method, the iron-loaded biochar must be initially prepared. From a practical application, an easy and low cost operation is preferable. Thus, development of a co-gasification process with an easier operation in a coal/woody biomass is necessary.

In this chapter, the co-gasification of biomass and AD coal with physical mixing of an iron catalyst was investigated. Because there are a limited number of studies on catalytic co-gasification, the effect of an iron catalyst addition on the change in the interaction between biomass and AD is unknown. In this chapter, the effect of physically-mixed iron catalyst on the co-gasification of biomass and AD coal was discussed.

4.2 Experimental

4.2.1 Samples

Indonesian Adaro sub-bituminous coal (AD) and Japanese cedar (SG) were used as coal and biomass samples, respectively. The particle size, the proximate, and the ultimate analyses were identical to Chapter 2 [67]. A commercial Fe_2O_3 (α-Fe_2O_3 with 8 μm in average) was used as an iron catalyst.

4.2.2 Preparation of mixed samples and iron catalyst loading

SG and AD were mixed in a mortar with a weight ratio of 3:1, 1:1 and 1:3. After mixed, the samples were labeled (3SG + AD), (SG+AD) and (SG + 3AD).

A physical mixing method was used for iron catalyst loading. To maintain a weight fraction of 10% loading, an applicable amount of iron species was added into AD, SG, and the mixed samples. The samples were mixed thoroughly in the mortar for at least 3 min. These samples were then labeled Fe_2O_3-SG, Fe_2O_3-AD, Fe_2O_3-(3SG + AD), Fe_2O_3-(SG+AD) and Fe_2O_3-(SG + 3AD).

For the purpose of a comparative experiment, 10 wt% of Fe_2O_3 with impregnated-(SG+AD) was prepared. This sample name is shown as Fe_2O_3-(SG+AD) (I). The procedure of impregnation method was shown as below.

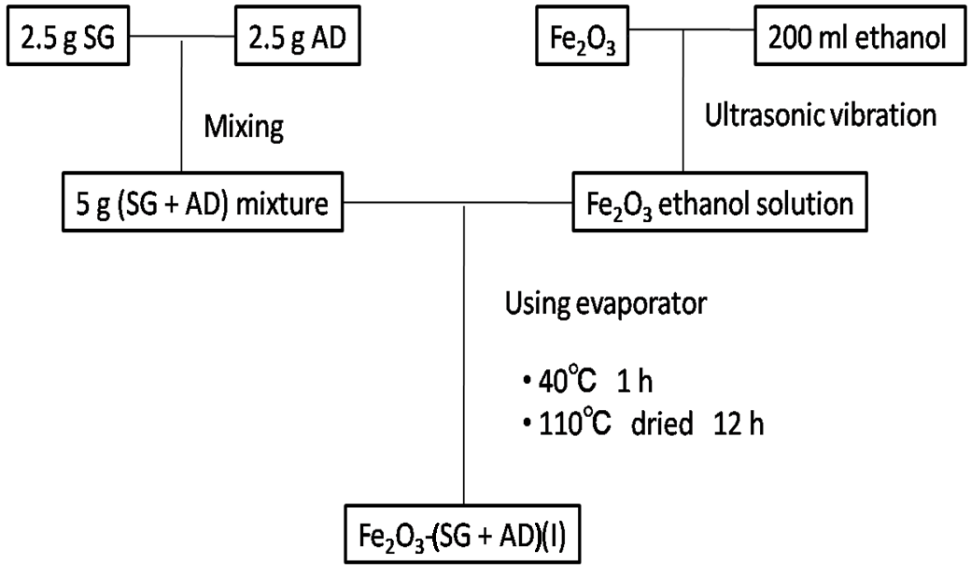

Figure 4.1 The procedure of impregnation method

As Fe_2O_3 could not be soluble in H_2O, so ethanol was used as solvent in this impregnation method. The impregnation method was almost the same as Chapter 2. Because the difference is that ethanol was easy to evaporate, the evaporating condition was set at 40℃ for 1 h. Fe content was measured using TG. As a result, Fe loading was 12.8 wt%.

4.2.3 Pyrolysis and steam gasification

Procedure of pyrolysis and gasification was the same as Chapter 2. Char yield, carbon conversion and gas evolution were calculated according to Equations (2.1), (2.2) and (2.3), respectively.

TG was used to study the weight change during pyrolysis from 25℃ to 800℃ in N_2 with a heating rate of 90℃/min.

4.2.4 Characterization of the pyrolyzed char and gasified residue

The form of iron catalyst after pyrolysis and steam gasification was measured by XRD. The measurement conditions were identical to Chapter 2 [67].

4.3 Result and discussion

4.3.1 Weight change of weight for AD and (SG+AD) during pyrolysis

Figure 4.2 shows the difference between AD and (SG+AD) during pyrolysis. It could be seen that char weight of (SG + AD) was smaller than that of AD, that is, SG addition results in large loss of char.

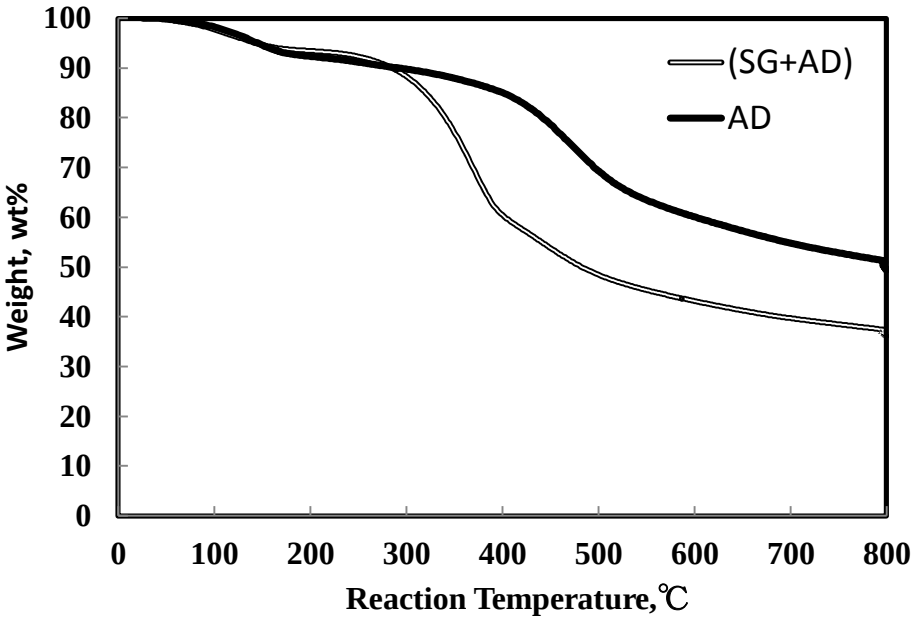

Figure 4.2 TG profiles for AD and (SG +AD) during pyrolysis

As shown in Chapter 1.4, the pyrolysis could be divided into two stages; the first stage was mainly cracking reaction. In this stage, small fragments and H radical were produced by the cracking of coal and biomass. In the second stage, condensation was the main reaction. Amount of H radical is considered to be related to tar amount. This is because tar is formed by reaction of H radicals and small fragments. Therefore, the weight loss for (SG+AD) was larger than that for AD because a large amount of H radical for SG is believed to be generated.

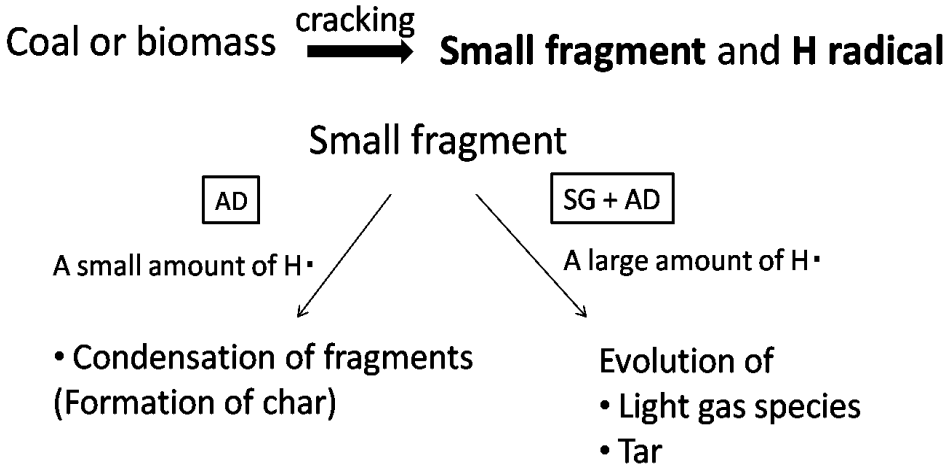

Figure 4.3 A simple for pyrolysis without catalyst.

4.3.2 Comparison of hydrogen evolution for gasification with and without Fe catalyst

Figure 4.4 shows the hydrogen evolution profiles for (SG+AD) and AD. From this figure, the hydrogen evolution of (SG+AD) was seen to be higher than that of AD for steam gasification. This shows that SG addition promotes the AD steam gasification.

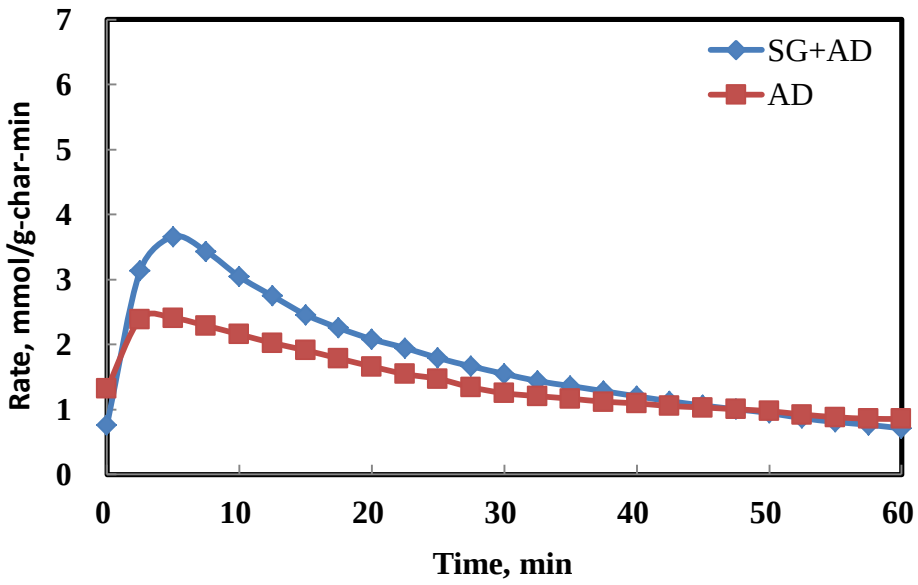

Figure 4.4 The hydrogen evolution profiles for (SG + AD) and AD

Figure 4.5 shows the hydrogen evolution profiles after Fe_2O_3 addition. Compared Fe_2O_3-AD with AD, a large difference in hydrogen evolution profile was not seen. Different from Fe_2O_3-AD, Fe_2O_3-(SG+AD) produced much more hydrogen for the same gasification time. This showed that co-existing of SG and Fe_2O_3 largely promoted AD gasification. There may be an interaction among AD, SG and Fe_2O_3 in pyrolysis and gasification.

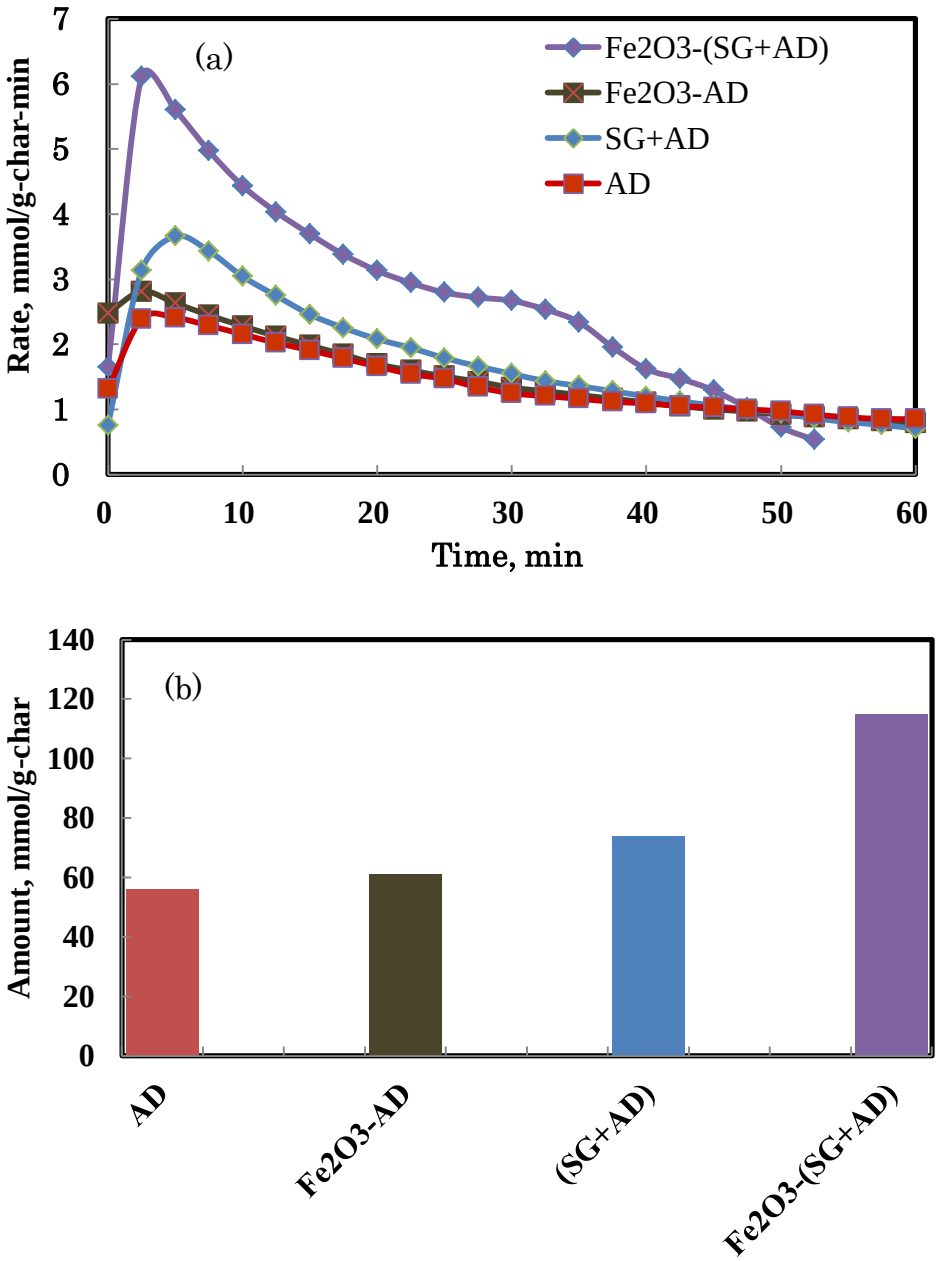

Figure 4.5 Comparison of the effect of Fe catalyst on (a) hydrogen evolution rate for AD and (SG + AD) ; (b) hydrogen amount for AD and (SG + AD) for 30 min gasification.

4.3.3 Comparison between impregnation method and physical mixing method

Comparison of gas evolution rate between Fe_2O_3-(SG+AD) (I) and Fe_2O_3-(SG+AD) was shown in Figure 4.6. From this figure, the gas evolution rate of Fe_2O_3-(SG+AD) was not smaller than Fe_2O_3-(SG+AD)(I). Especially, Fe_2O_3-(SG+AD) was slightly higher than Fe_2O_3-(SG+AD)(I) in the first stage of gasification. This also showed that the physical mixing method could be applied to co-gasification.

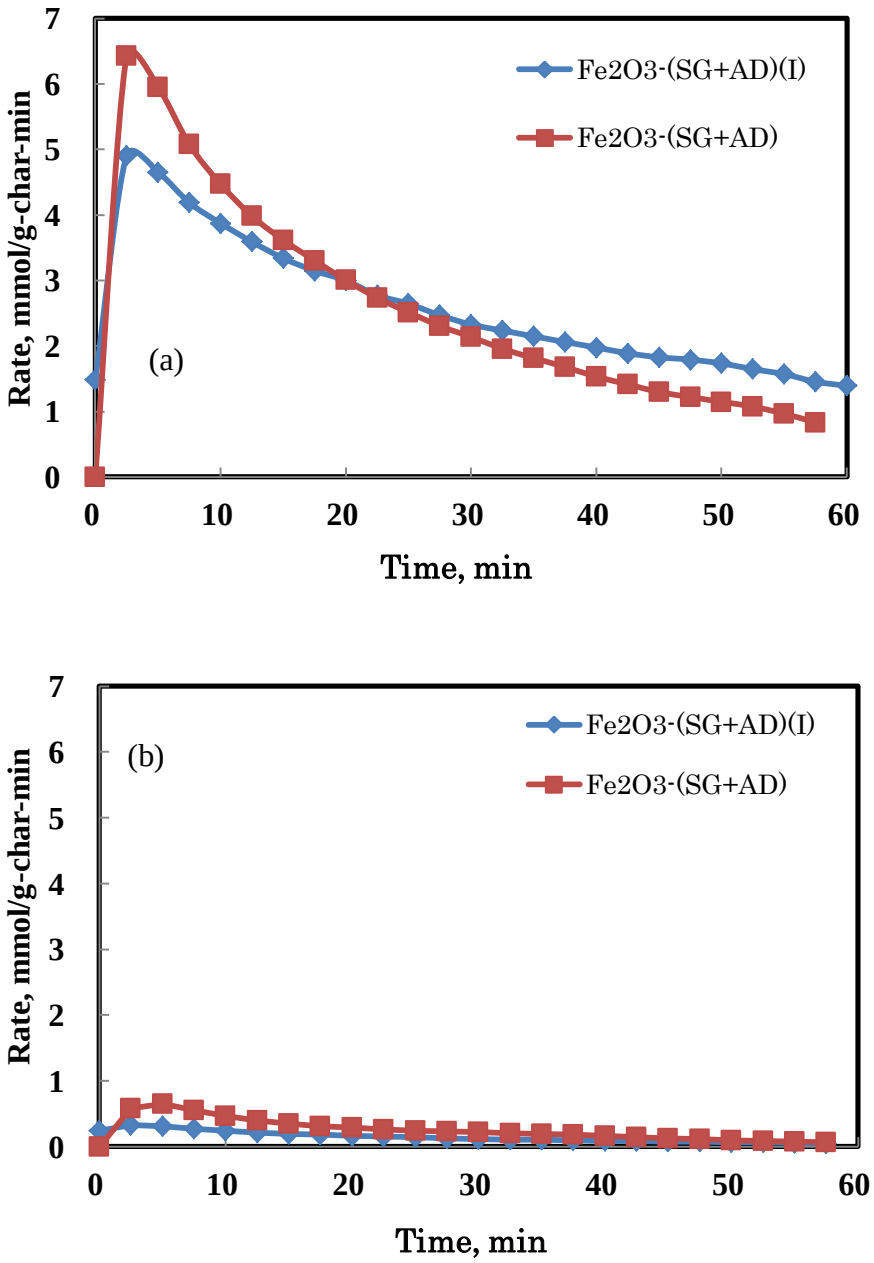

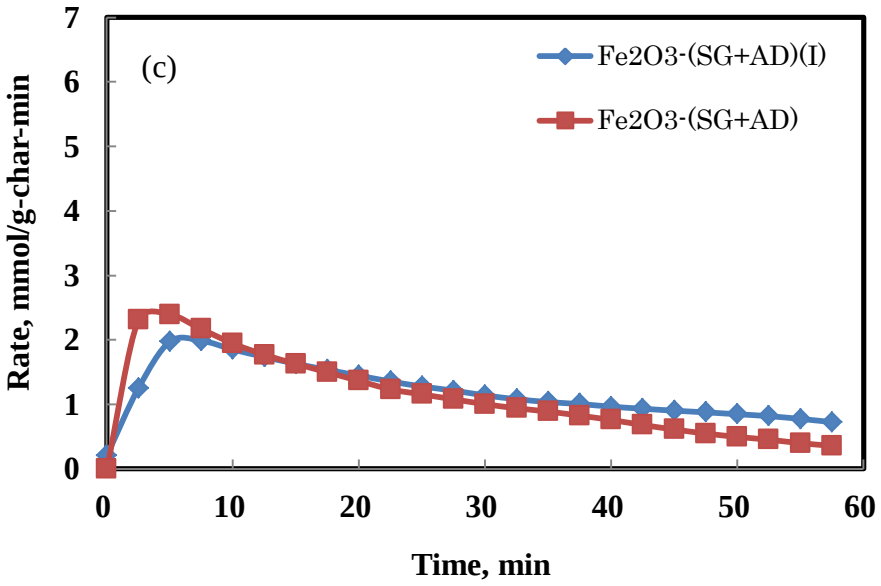

Figure 4.6 Gas evolution rate during gasification for Fe_2O_3-(SG + AD)(I) and Fe_2O_3-(SG + AD). (a) H_2, (b)CO, (c)CO_2 .

4.3.4 Interaction between SG and AD in non-catalyst co-gasification and catalytic co-gasification

The measured amount of hydrogen evolution was compared with the amount of hydrogen evolution calculated from the individual gasification. The measured amount of hydrogen evolution should be equal to the calculated amount of hydrogen evolution if there is no interaction between biomass and coal during co-gasification. If the measured amount of hydrogen evolution is larger than the calculated one, it could be described that there is an interaction between biomass and coal.

Equation 4.1 was used to calculate the without a catalyst on the assumption that there is no interaction between biomass and coal.

$$(SG + AD)_{cal} = \frac{A(AD) \times M(ADchar) + A(SG) \times M(SGchar)}{M(ADchar) + M(SGchar)}, \qquad (4.1)$$

where A (AD) is the amount of hydrogen evolution for 1 g of ADchar; A (SG) is the amount of hydrogen evolution for 1 g of SGchar; and M(ADchar) and M(SGchar) are weights of ADchar and SGchar, respectively.

For co-gasification with Fe_2O_3 Equation 4.2 was used.

$$Fe_2O_3\text{-}(SG+AD)_{cal} = \frac{A(FeAD)\times M(FeADchar)+A(FeSG)\times M(FeSGchar)}{M(FeADchar)+M(FeSGchar)}, \quad (4.2)$$

where A (FeAD) is the amount of hydrogen evolution for 1 g of Fe_2O_3-ADchar; A (FeSG) is the amount of hydrogen evolution for 1 g of Fe_2O_3-SGchar; and M(FeADchar) and M(FeSGchar) are weights of Fe_2O_3-ADchar and Fe_2O_3-SGchar, respectively.

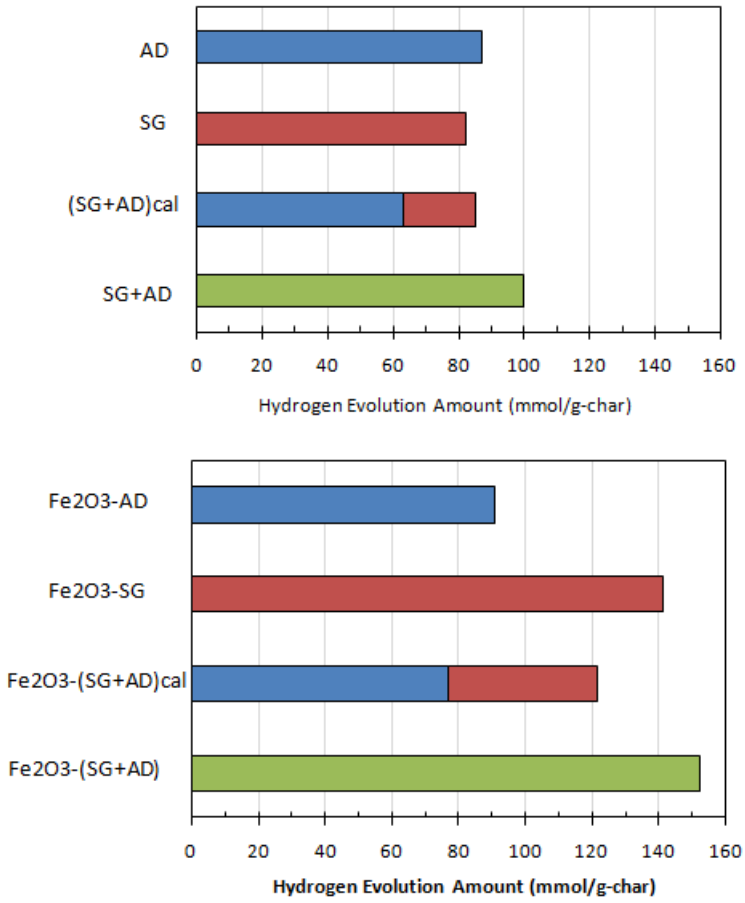

Figure 4.7 Comparison of the measured amount and calculated amount of hydrogen evolution for co-gasification (a) without Fe_2O_3, (b) with Fe_2O_3

Figure 4.7 shows the comparison of the measured amount and calculated amount of hydrogen evolution for co-gasification. For co-gasification without catalyst, the measured amount of (SG+AD) is 100 mmol/g-char and the calculated amount is 85 mmol/g-char. Therefore, the interaction between biomass and coal results in 15 mmol/g-char increase of H_2.

For Fe_2O_3-(SG+AD) the measured amount of hydrogen evolution is 152

mmol/g-char and the calculated amount is 121 mmol/g-char. Therefore, the interaction among SG, AD and Fe_2O_3 results in 31 mmol/g-char increase of H_2, which is significantly higher than that of (SG+AD). This indicated that Fe_2O_3 addition to mixture of SG and AD promotes the gasification further.

4.3.5 Effect of iron catalyst on reactivity of char for co-gasification

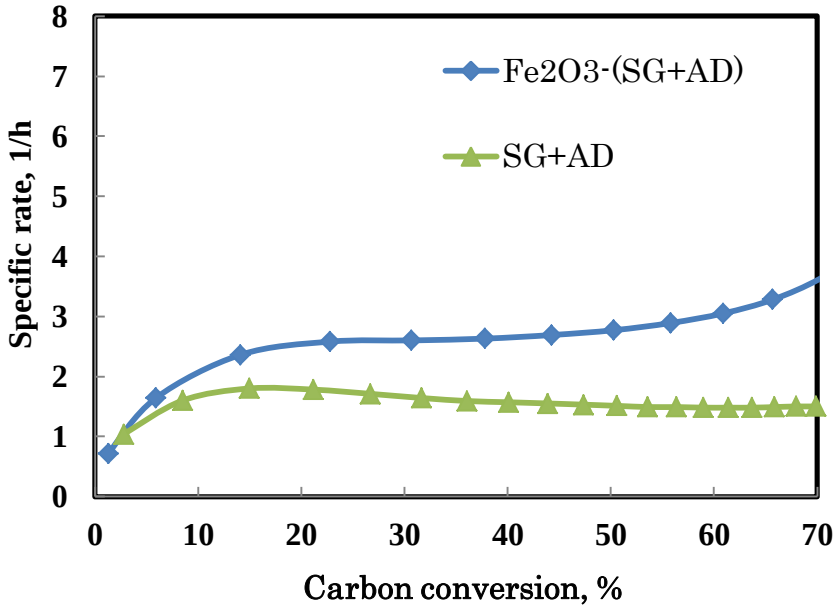

Figure 4.8 Specific rate for mixed samples with and without Fe_2O_3

Figure 4.8 shows the relationship between specific rate and carbon conversion for comparing Fe_2O_3-(SG+AD) and (SG+AD). As illustrated in Figure 4.8, the specific rate of (SG+AD) without iron catalyst is nearly constant during the gasification. The specific rate of Fe_2O_3-(SG+AD) increased with increasing carbon conversion. This indicates that the reactivity of Fe_2O_3-(SG+AD) is very high in the whole gasification.

4.3.6 Change of weight during pyrolysis by Fe_2O_3 addition

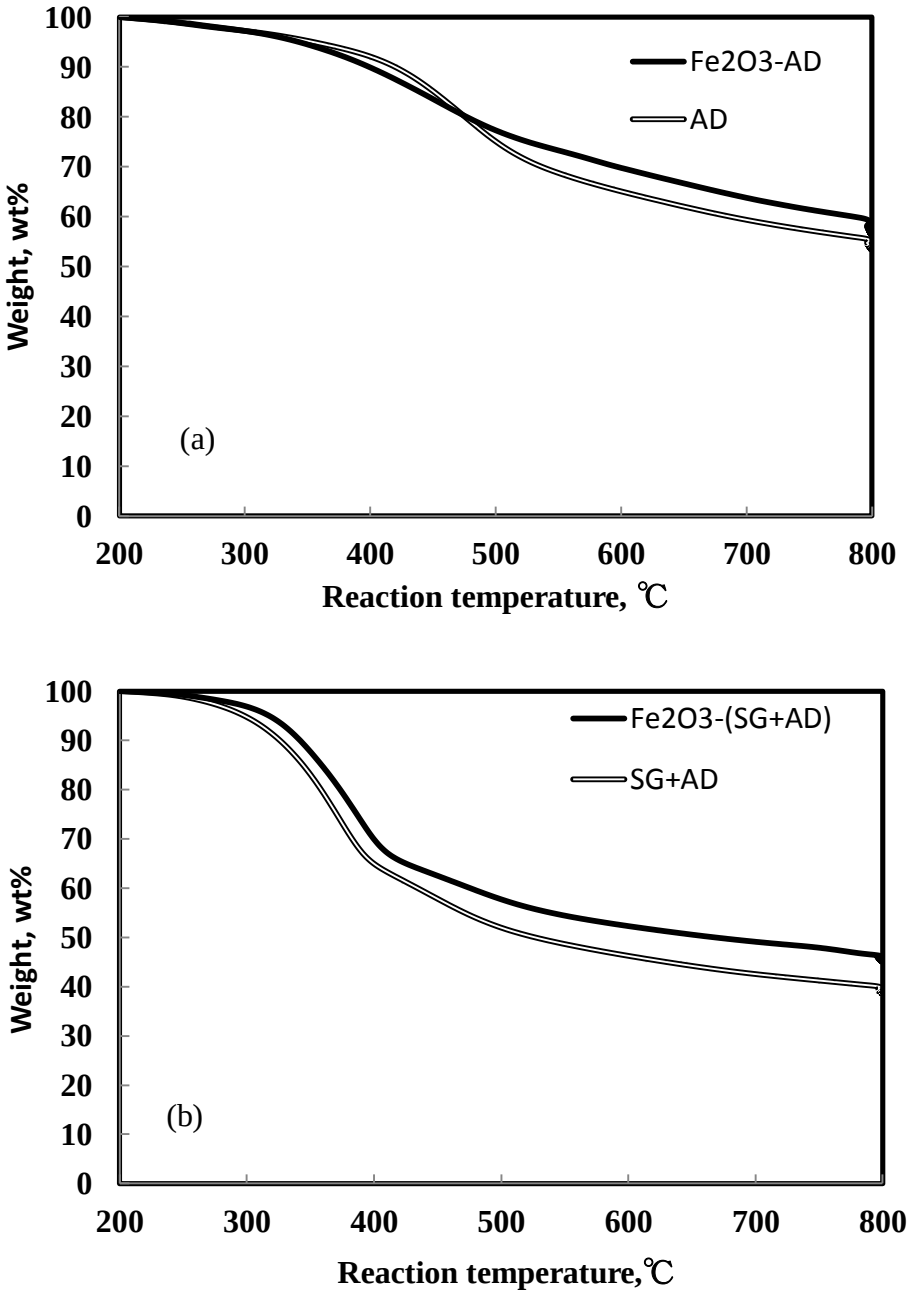

Figure 4.9 The difference in weight change during pyrolysis between samples with and without Fe_2O_3 (a) AD and Fe_2O_3-AD, (b) (SG+AD) and Fe_2O_3-(SG+AD).

Figure 4.9 shows the difference in weight change during pyrolysis between samples with and without Fe_2O_3. In all samples, the weight of char for the Fe_2O_3 mixed samples at 800℃ were higher than the samples without Fe_2O_3. However, a difference in reaction temperature was noted; for Fe_2O_3-AD and AD, the change began at 480℃; for Fe_2O_3-(SG+AD) and

(SG+AD), the change began at approximately 250℃. Therefore, the Fe catalyst became effective at a lower temperature in Fe_2O_3-(SG+AD). Tar formation occurred between 250～500℃, and tar may have been produced by the release of the small fragments in the coal or biomass with hydrogen radicals [80-84]. Fe_2O_3 could react with hydrogen radicals [85].

$$3Fe_2O_3 + 2\ H\cdot \rightarrow 2Fe_3O_4 + H_2O$$

This is probably the reason why Fe_2O_3 in Fe_2O_3-(SG+AD) could be reduced at this temperature range. For Fe_2O_3-AD and AD, there is little difference before 500℃ during pyrolysis. On the other hand, the weight loss before 500℃ for Fe_2O_3-(SG+AD) is lower than that of (SG+AD). This indicates that part of tar from SG maybe incorporated into char by Fe_2O_3 addition. This result is similar with the study of Cahyono et al. [86].

Figure 4.10 shows the XRD patterns of Fe_2O_3-loaded samples during pyrolysis.

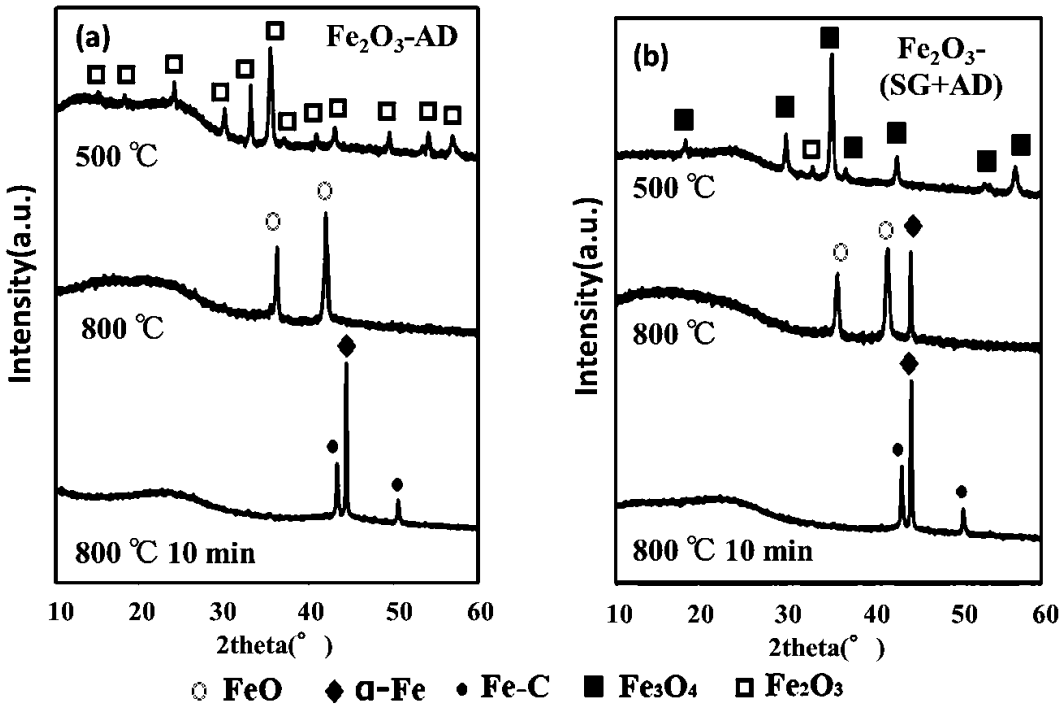

Figure 4.10 XRD patterns of Fe_2O_3 -loaded sample during pyrolysis. (a) Fe_2O_3-AD, (b) Fe_2O_3-(SG+AD)

Compared Fe_2O_3-AD with Fe_2O_3-(SG+AD), SG addition significantly changed reduction rate of iron species. The significant difference between Fe_2O_3-AD and Fe_2O_3-(SG+AD) was seen at 500℃. For Fe_2O_3-AD, Fe catalyst did not change and remained as Fe_2O_3 at 500℃. However, for Fe_2O_3-(SG+AD), Fe catalyst has changed from Fe_2O_3 to Fe_3O_4 at 500℃.

This indicates that SG produces a lot of H radicals, which reacts with Fe_2O_3. From Figure 4.3, it could be known that tar is formed by the reaction of small fragment and H radicals. Therefore, a change from SG after Fe_2O_3 addition resulted in the change of AD during pyrolysis.

Figure 4.11 shows the mechanism of promotion for Fe catalyst. Without adding Fe_2O_3, SG addition offered a large amount of radicals, reacting with active fragments, producing much tar and light gas species (From TG result in Figure 4.2). After adding Fe_2O_3, a part of H radicals offered by SG reacted with Fe_2O_3, but not with fragments (XRD result in Figure 4.10). This made some active fragments which originally would form tar transformed into char (TG result in Figure 4.9). It is considered to be an important reason why char of Fe_2O_3-(SG+AD) showed a good reactivity.

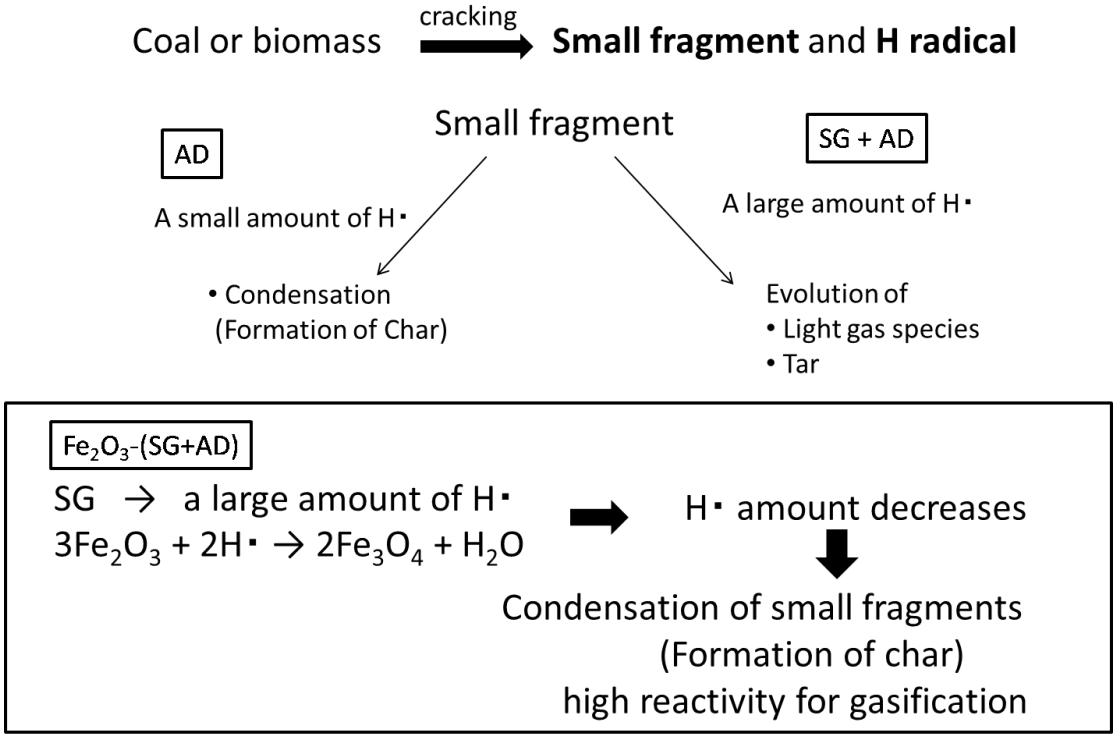

Figure 4.11 A simple diagram for pyrolysis with and without Fe_2O_3

4.3.7 XRD patterns for Fe_2O_3-AD and Fe_2O_3-(SG+AD) during gasification

Figure 4.12 shows that the Fe catalyst changed from a reduced state (α-Fe) to Fe_3O_4 (oxidation state) for Fe loaded samples. This directly corresponded to the change Yu et al. [87] reported.

In the case of gasification by steam without catalyst,

$$C + H_2O \rightarrow CO + H_2. \quad (4.5)$$

In the case of gasification by steam with Fe catalyst,

$$Fe + H_2O \rightarrow Fe(O) + H_2 , \quad (4.6)$$

$$Fe(O) + C \rightarrow C(O) + Fe . \quad (4.7)$$

In the case of gasification by steam with Fe_nO_m,

$$Fe_nO_m + H_2O \rightarrow Fe_nO_m(O) + H_2 , \quad (4.8)$$

$$Fe_nO_m(O) + C \rightarrow C(O) + Fe_nO_m , \quad (4.9)$$

$$C(O) \rightarrow CO. \quad (4.10)$$

Therefore, the Fe catalyst acted as an oxygen transfer agent in steam gasification as described by Yu et al. [87].

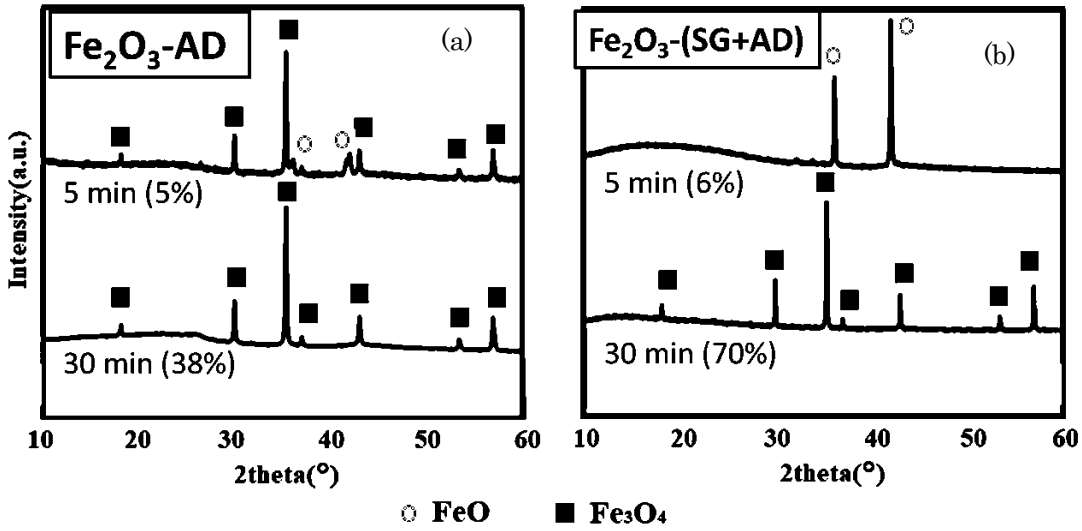

Figure 4.12 XRD patterns during gasification of Fe_2O_3-AD and Fe_2O_3-(SG+AD)

From Figure 4.12, Fe catalyst remained as FeO in Fe_2O_3-(SG+AD) after 5 min, different from the form of Fe_3O_4 in Fe_2O_3-AD. In the chapter 2 and chapter 3, ash of biomass suppressed oxidation of iron species. Therefore, FeO production was probably related to the AAEMs in biomass ash, also considered as a reason why Fe_2O_3-(SG+AD) had a much faster hydrogen

evolution rate.

Carbon conversion during gasification is also shown in Figure 4.12. Carbon conversion for Fe_2O_3-AD was 5% after 5 min gasification and 38% after 30 min gasification; Carbon conversion for Fe_2O_3-(SG+AD) was 6% after 5 min gasification and 70% after 30 min gasification. This also expressed that SG addition largely changed the effect of Fe catalyst.

4.3.8 Influence of biomass mixing ratio on the co-gasification

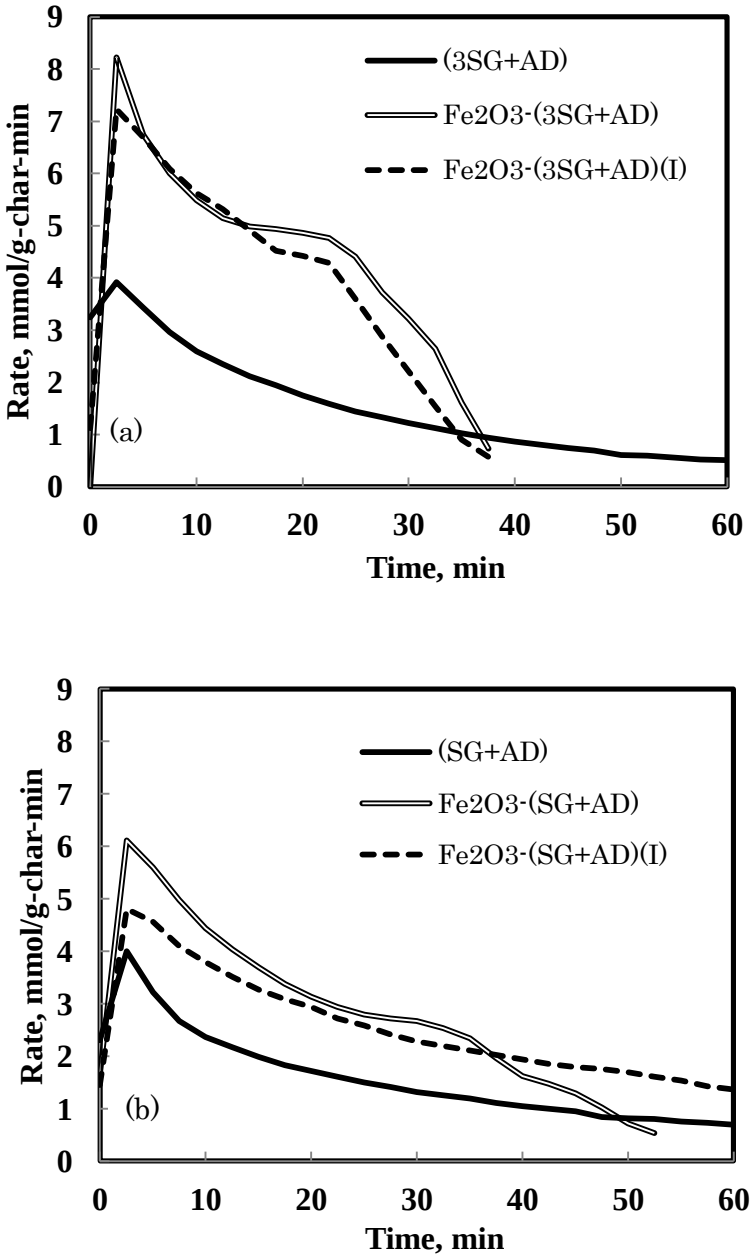

Figure 4.13 The gas evolution rate for (a) Fe_2O_3-(3SG+AD) and (b) Fe_2O_3-(SG+AD)

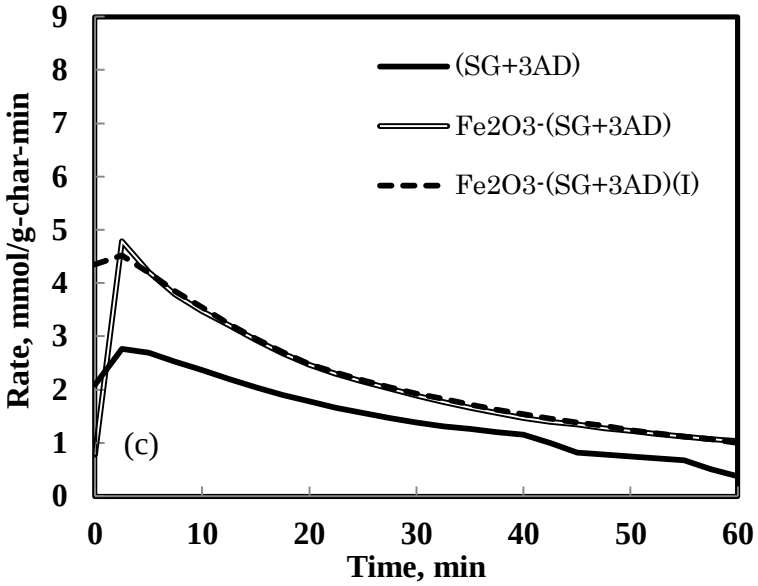

Figure 4.13 The hydrogen evolution rate for (c) Fe_2O_3-(SG+3AD)

Biomass ratio is usually regarded as an important factor which affects co-gasification [88-92]. It is also discussed in this part.

Figure 4.13 shows the hydrogen evolution rate for Fe_2O_3-(SG+3AD), Fe_2O_3-(SG+AD) and Fe_2O_3-(3SG+AD). From this figure, it could be seen that the hydrogen evolution rate increases with increasing SG ratio.

Figure 4.14 shows the relationship between carbon conversion and specific rate. It could be seen that the specific rate increase with increasing SG ratio for both Fe_2O_3-Sample and Fe_2O_3-Sample (I). This is because Fe_2O_3-SG has a higher activity than Fe_2O_3-AD. Without Fe catalyst, there is no big difference by biomass ratio.

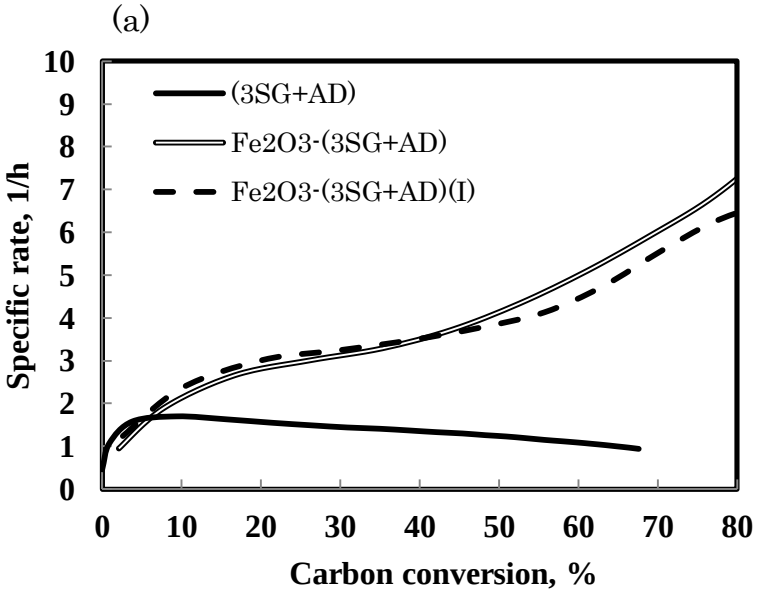

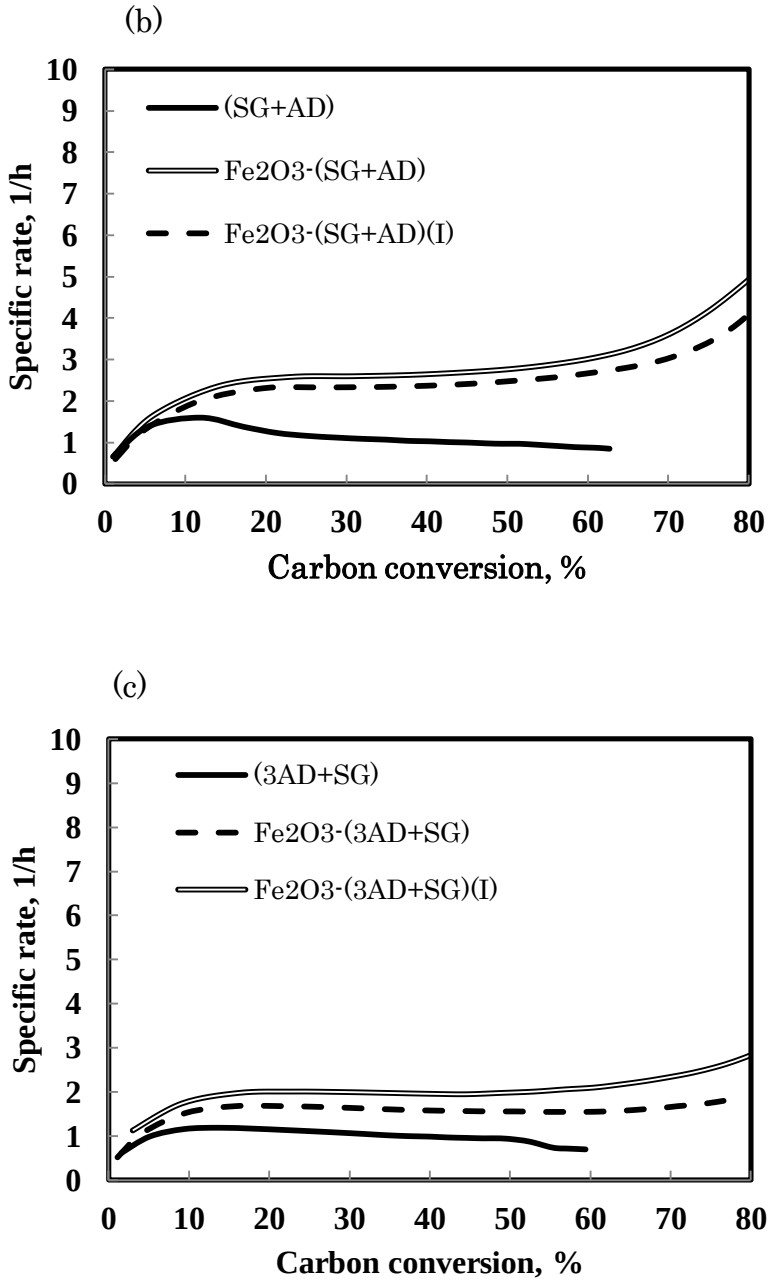

Figure 4.14 Relationship between carbon conversion and specific rate (a) the case of Fe_2O_3-(3SG+AD), (b)the case of Fe_2O_3-(SG+AD), (c) the case of Fe_2O_3-(3AD + SG)

Table 4.1 shows the specific rate when carbon conversion reached 50 %. With the data, the relationship between reactivity index and biochar ratio was compared in Figure 4.15. From the figure, it could be seen that both Fe_2O_3-sample and Fe_2O_3-sample(I) showed higher R_s than the calculation. However, with an increasing of biochar ratio, R_s increased firstly and

decreased gradually. This may be because reactivity is limited by iron loadings [78]. Size of iron particle rises with the increase of catalyst loading, which lead to the reduction of catalytic effect on char.

Table 4.1 The specific rate when carbon conversion reached 50 %

	Fe_2O_3-(SG+3AD)(P)	Fe_2O_3-(SG+3AD)(I)	Fe_2O_3-(SG+AD)(P)	Fe_2O_3-(SG+AD)(I)	Fe_2O_3-(3SG+AD)(P)	Fe_2O_3-(3SG+AD)(I)
Rs	1.5	2	2.8	3	4.34	4.13

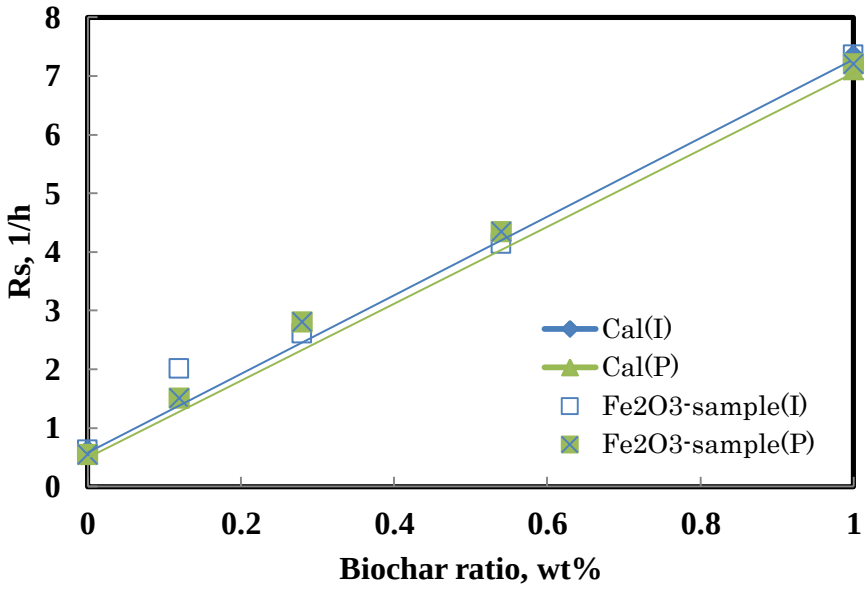

Figure 4.15 The relationship between reactivity index and biochar ratio

4.4 Conclusion

This study conducted steam gasification of Indonesian Adaro coal (AD) and Japanese cedar (SG) at a ratio of 1:1 with the physical addition of a weight ratio of 10% Fe_2O_3 in a volume ratio of 50% H_2O at 800℃ for 1 h. The conclusions are as follows:

1. Without Fe catalyst, SG addition could promote AD gasification slightly.
2. Physical mixing with Fe_2O_3 hardly promoted AD gasification, but largely promoted the gasification of (SG+AD).
3. During pyrolysis, there is an interaction among SG, AD and Fe_2O_3, forming char with difference in structure. This may be the reason why co-gasification with Fe_2O_3 could produce more hydrogen.

Chapter 5 Conclusion

5.1 Conclusion

This doctoral thesis discussed the co-gasification of Fe-SGchar and AD coal, co-gasification of Fe-SGchar and ADchar, and also the co-gasification of Fe-SG and AD. Though the different co-gasification, we discussed the effect of Fe-SGchar (chapter 2), the best mixing timing and ratio of Fe-SGchar addition (chapter 3), effect of physical mixing of Fe catalyst (chapter 4). The conclusions are shown below:

In Chapter 2, mixtures of iron-loaded biochar (pyrolysate of iron-loaded biomass) and AD with weight ratios of 1:10 and 1:5 were gasified with steam at 800 °C in a fixed-bed-type reactor. The conclusions are as follows:
(1) The H_2 production increased by approximately 20 mol% owing to the addition of iron-loaded biochar (20 wt%) to AD.
(2) The specific rates decreased gradually with increasing carbon conversion for AD and 3.2Fe-AD. On the contrary, there was no obvious decrease in the activity of iron catalyst in 1.8Fe-SG/AD and 3.5Fe-SG/AD.
(3) The XRD patterns of char for 3.5Fe-SG/AD were significantly different from those for 3.2Fe-AD. The metallic iron species (α-Fe) existed for the first 30 min of steam gasification for 3.5Fe-SG/AD. In the case of 3.2Fe-AD, the iron species changed to magnetite (Fe_3O_4) after 10 min of steam gasification. The crystallite sizes of Fe_3O_4 for 3.5Fe-SG/AD were slightly smaller than those for 3.2Fe-AD.
(4) The ash in SG samples had the effect of maintaining the iron catalyst activity.

In Chapter 3, mixtures of iron-loaded biochar (the pyrolysate of iron-loaded biomass) and AD coal/ADchar with different weight ratios were gasified with steam at 800 °C in a fixed-bed-type reactor. The conclusions obtained from this work are as follows:
(1) The optimal time to add iron-loaded biochar in this co-gasification system is before the pyrolysis of AD, and the optimal ratio for the addition of Fe-SGchar to ADchar is 1:1 by weight.
(2) Based on the relationships between the specific rate and carbon conversion obtained, the specific rate of Fe-SGchar/AD was always higher than that of Fe-SGchar/ADchar.

(3) According to the XRD patterns of chars pyrolyzed at various temperatures, a transition between α-Fe and Fe_3C occurred in Fe-SGchar/AD but not in Fe-SGchar/ADchar and produced a large amount of highly reactive carbons. Additionally, the XRD patterns of chars gasified at 800 °C for various times revealed that the iron catalyst can be maintained in its reduced form on both Fe-SGchar/AD and Fe-SGchar/ADchar for a longer time than that on Fe-AD. Finally, the oxidation of Fe-SGchar/AD was delayed compared to that of Fe-SGchar/ADchar in the presence of the same amount of iron catalyst.

In Chapter 4, steam gasification of Indonesian Adaro coal (AD) and Japanese cedar (SG) at a ratio of 1:1 with the physical addition of a weight ratio of 10% Fe_2O_3 was conducted in a volume ratio of 50% H_2O at 800℃ for 1 h. The conclusions are as follows:

(1) Without Fe catalyst, SG addition could promote AD gasification slightly.
(2) Physical mixing with Fe_2O_3 hardly promoted AD gasification, but largely promoted the gasification of (SG + AD).
(3) During pyrolysis, there is an interaction among SG, AD and Fe_2O_3, forming char with difference in structure. This may be the reason why co-gasification with Fe_2O_3 could produce more hydrogen.

5.2 Future outlook

Our results are considered to be able to be applied to IGCC process. The main conclusion of our results is that existence of biomass helps to keep high activity of Fe catalyst.

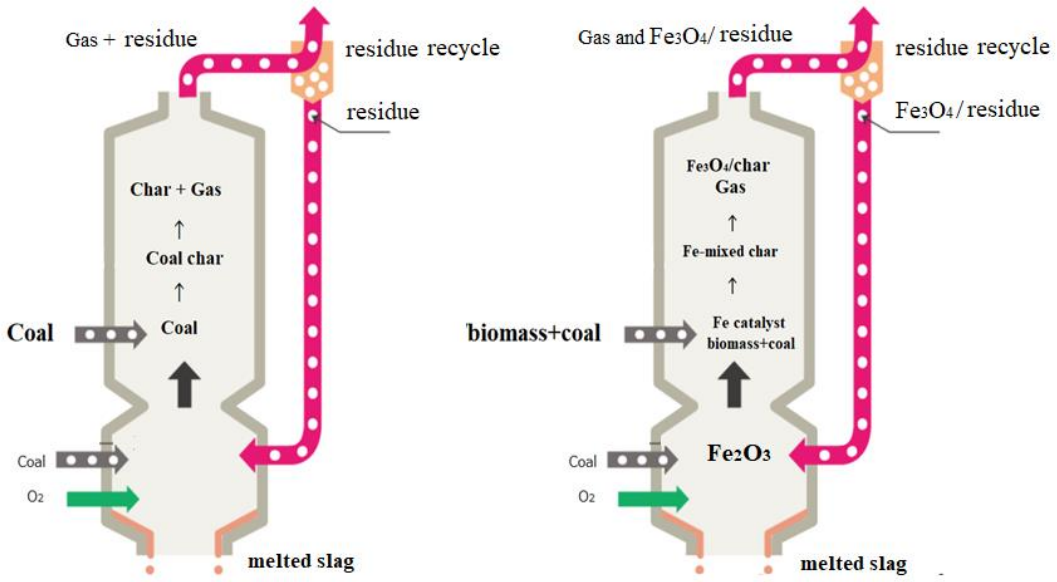

(a) Present IGCC process (b) Considered IGCC process

Figure 5.1 Comparison between present IGCC process and considered

Figure 5.1 shows the comparison between present IGCC process and considered process. In the present IGCC process, coal is only used, so the efficiency is related to the coal reactivity. If the coal with low reactivity is used, the efficiency will be largely affected. In the considered IGCC process, Fe catalyst will be added together with coal and biomass. In the pyrolysis stage, Fe catalyst stabilizes some active fragments from biomass to form char, increases char amount and reactivity. In the gasification stage, AAEMs in biomass ash could keep high activity of Fe catalyst. Therefore, using our results is considered to be able to make some coal with low reactivity usable in practical process.

References

[1] WEC, “Survey of Energy Resources 2013”.
[2] Ding L, Zhou Z, Dai Z, Yu G. Effects of coal drying on the pyrolysis and in-situ gasification characteristics of lignite coals. Applied Energy 2015, 155: 660–670.
[3] Zhang D, Wang S, Ma X, Tian Y. Interaction between coal and distillation residues of coal tar during co-pyrolysis. Fuel Processing Technology 2015, 138: 221–227.
[4] Ellis N, Masnadi MS, Roberts DG, Kochanek MA, Ilyushechkin AY. Mineral matter interactions during co-pyrolysis of coal and biomass and their impact on intrinsic char co-gasification reactivity. Chemical Engineering Journal 2015, 279: 402–408.
[5] Zhang D, Liu P, Lu X, Wang L, Pan T. Upgrading of low rank coal by hydrothermal treatment: Coal tar yield during pyrolysis. Fuel Processing Technology 2016, 141: 117－122.
[6] Fujitsuka H, Ashida R, Miura K. Upgrading and dewatering of low rank coals through solvent treatment at around 350 °C and low temperature oxygen reactivity of the treated coals. Fuel 2013; 114: 16–20.
[7] Stakić M, Cvetinović D, Škobalj P, Spasojević V. An initial study on feasible treatment of Serbian lignite through utilization of low rank coal upgrading technologies. Chemical Engineering Research and Design 2014; 11: 2383–2395.
[8] Ge L, Zhang Y, Xu C, Wang Z, Zhou J, Cen K. Influence of the hydrothermal dewatering on the combustion characteristics of Chinese low rank coals. Applied Thermal Engineering 2015; 90: 174–181.
[9] Pei P, Wang Q, Wu D. Application and research on Regenerative High Temperature Air Combustion technology on low rank coal pyrolysis. Applied Energy 2015; 156: 762–766.
[10] Saha C, Bhattacharya S. Chemical looping combustion of low-ash and high-ash low rank coals using different metal oxides – A thermo gravimetric analyzer study. Fuel 2012; 97: 137–150.
[11] http://www.nedo.go.jp/hyoukabu/articles/201306igcc/index.html.
[12] http://www.nakoso-igcc.co.jp/equipment/.
[13] Xie K. Coal structure and its reactivity (2015).
[14] Li F and Fang Y. The study of the features and factors influencing char gasification. Journal of Heze University 2010; 32, 69－73.
[15] Asami K, Sears P, Furimsky E, Ohtsuka Y. Gasification of brown coal and char with carbon dioxide in the presence of finely dispersed iron

catalysts. Fuel Process Technol 1996; 47:139–51.
[16] Kumari G and Vairakannu P. CO_2-air based two stage gasification of low ash and high ash Indian coals in the context of underground coal gasification. Energy 2018; 143: 822–832.
[17] Li G, Wang C, Wang P, Du Y, Liu X, Chen X, Che D. Ash Deposition and Alkali Metal Migration during Zhundong High-alkali Coal Gasification. Energy Procedia 2017; 105: 1350–1355.
[18] Shang J, Eduardo E. Kinetic and FTIR studies of the sodium-catalyzed steam gasification of coal chars. Fuel 1984; 63: 1604–1609.
[19] Van H, Muhlen J. Aspects of coal properties and constitution important for gasification. Fuel 1985; 64: 1405–1414.
[20] Suzuki T, Yamada H, Yunoki Y, Yamaguchi H. Highly active coal liquefaction catalyst: soluble ruthenium complexes as catalyst precursors. Energy Fuels 1992; 6: 352–356.
[21] Chen S, Yang R. Unified Mechanism of Alkali and Alkaline Earth Catalyzed Gasification Reactions of Carbon by CO_2 and H_2O. Energy Fuels 1997; 11: 421–427.
[22] Chen S, Yang R. The Active Surface Species in Alkali-Catalyzed Carbon Gasification: Phenolate (C-O-M) Groups vs Clusters (Particles). Journal of Catalysis 1993; 141: 102－113.
[23] Ohme H, Suzuki T. Mechanisms of CO_2 Gasification of Carbon Catalyzed with Group VIII Metals. 1. Iron-Catalyzed CO_2 Gasification. Energy & Fuel 1996; 10: 980－987.
[24] Asaki K, Ohtuska Y. Gasification of brown coal and char with carbon dioxide in the presence of finely dispersed iron catalysts. Fuel 1996; 47: 139 –151.
[25] Clemens H, Damiano L, Matheson T. The effect of calcium on the rate and products of steam gasification of char from low rank coal. Fuel 1998; 77: 1017–1020.
[26] Akira T, Yoshihiko W, Takayuki T, Yasuo O, Yasukatus T, Nicked-catalysed gasification of brown coal in a fluidized bed reactor at atmospheric pressure. Fuel 1985; 64: 795–800.
[27] Shen X, Qin L. Study on MSW catalytic combustion by TGA. Energy Conversion and Management 2006; 47: 1429–1437.
[28] Cahyono B, Rozhan N, Yasuda N, Nomura T, Hosokai S, Kashiwaya Y, Akiyama T. Catalytic coal-tar decomposition to enhance reactivity of low-grade iron ore. Fuel Processing Technology 2013; 113: 84–89.
[29] Yu J, Tian F, Chow MC, Mckenzie LJ, Li C. Effect of iron on the

gasification of Victorian brown coal with steam: enhancement of hydrogen production Fuel 2006; 85: 127–133.
[30] Qi X, Guo X, Xue L, Zheng C. Effect of iron on Shenfu coal char structure and its influence on gasification reactivity. Journal of Analytical and Applied Pyrolysis 2014; 110: 401–407.
[31] Li X, Hayashi J, Li C, Volatilisation and catalytic effects of alkali and alkaline earth metallic species during the pyrolysis and gasification of Victorian brown coal. Part VII. Raman spectroscopic study on the changes in char structure during the catalytic gasification in air. Fuel 2006; 85: 1509–1517.
[32] Gong X, Guo Z, Wang Z. Effects of Fe_2O_3 on pyrolysis reactivity of demineralized higher rank coal and its char structure. CIESC Journal 2009; 60: 2321−2326.
[33] Yamashita H, Ohtsuka Y, Yoshida S, Tomita A. Local structures of metals dispersed on coal. 1. Change of local structure of iron species on brown coal during heat treatment. Energy Fuels 1989; 3: 686−692.
[34] Ohtsuka Y, Kuroda Y, Tamai Y, Tomita A. Chemical form of iron catalysts during the CO_2-gasification of carbon. Fuel 1986; 65: 1476–1478.
[35] Ding L, Zhang Y, Wang Z, Huang J, Fang Y. Interaction and its induced inhibiting or synergistic effects during co-gasification of coal char and biomass char. Bioresource Technology 2014; 173: 11－20.
[36] Wei J, Guo Q, Ding L, Ding L, Yu G. Synergy mechanism analysis of petroleum coke and municipal solid waste (MSW)-derived hydrochar co-gasification. Applied Energy 2017; 206: 1354−1363.
[37] Wei J, Guo Q, Ding L, Ding L, Yu G. Synergistic effect on co-gasification reactivity of biomass-petroleum coke blended char. Bioresource Technology 2017; 234: 33−39.
[38] Krerkkaiwan S, Fushimi C, Tsutsumi A, Kuchonthara P. Synergetic effect during co-pyrolysis/gasification of biomass and sub-bituminous coal. Fuel Processing Technology 2013; 115, 11−18.
[39] Kazuhiro K, Toshiaki H, Shinji F, Tomoaki M, Kinya S. Co-gasification of woody biomass and coal with air and steam. Fuel 2007; 86: 684－689.
[40] Brown R, Liu Q, Norton G. Catalytic effects observed during the co-gasification of coal and switchgrass. Biomass & Bioenergy 2000; 18: 499–506.
[41] Chmielniak T, Sciazko M. Co-gasification of biomass and coal for methanol synthesis. Apply Energy 2003; 74: 393–403.

[42] Mclendon R, Lui P, Pineault L, Beer K, Richardson W. High-pressure co-gasification of coal and biomass in a fluidized bed. Biomass Bioenergy 2004; 26: 377–88.
[43] Dong P, Sang K, See K and Jae L. Co-pyrolysis characteristics of sawdust and coal blend in TGA and a fixed bed reactor. Bioresource Technology 2010; 101: 6151–6156.
[44] Zhang L, Xu SP, Zhao W, Liu S. Co-pyrolysis of biomass and coal in a free fall reactor. Fuel 2007; 86: 353–359.
[45] Haykiri-Acma H, Yaman S. Interaction between biomass and different rank coals during co-pyrolysis. Renewable Energy 2010; 35: 288–292.
[46] Vélez F, Chejne F, Valdés F, Emery J, Londoño A. Co-gasification of Colombian coal and biomass in fluidized bed: An experimental study. Fuel 2009; 88: 424－430.
[47] Adeyemi I, Janajreh I, Arink T and Ghenai C. Gasification behavior of coal and woody biomass: Validation and parametrical study. Applied Energy 2017; 185: 1007–1018.
[48] Shen L, Murakami K, "Steam gasification of iron-loaded biochar and sub-bituminous coal mixture", 5th International Conference on Sustainable Energy and Environment (SEE2014) (Bangkok, Thailand), E －007.
[49] Shen L, and Murakami K, "Effects of iron-based catalysts in steam gasification of low rank coal", International Symposium for the 70th Anniversary of the Tohoku Branch of the Chemical Society of Japan (Sendai), 2P128.
[50] Xiao X, Gao J, Meng X, Le D, Li L, Ogawa Y, Sato K, Takarada T. Synthesis gas production from catalytic gasification of waste biomass using nickel-loaded brown coal char. Fuel 2013; 103: 135–140.
[51] Murakami K, Arai M, Shirai M, In situ XAFS study of catalytically active species on brown coal during coal conversion process, Topics in Catalysis 2002; 18: 119–123.
[52] Zhang F, Xu D, Wang Y, Argyle MD, Fan M. CO_2 gasification of Powder River Basin coal catalyzed by a cost-effective and environmentally friendly iron catalyst. Applied Energy 2015; 145: 295–305.
[53] Asami K, Ohtuska Y. Highly active iron catalysts from ferric chloride for the steam gasification of brown coal. I&EC Research 1993; 32: 1631–1636.
[54] Murakami K, Sato M, Sugawara K. Effect of iron and calcium catalysts on steam gasification. International Conference on Coal Science

and Technology (ICCS&T) 2011; B66.
[55] Howaniec N, Smoliński A, Stanczyk K, Pichlak M. Steam co-gasification of coal and biomass derived chars with synergy effect as an innovative way of hydrogen-rich gas production. International journal of hydrogen energy 2011; 36: 14455−14463.
[56] Jeong J, Park S, Hwang J, Co-gasification of coal–biomass blended char with CO_2 at temperatures of 900–1100 °C. Fuel 2014; 116: 465–470.
[57] Zhang Y, Zheng Y, Yang M, Song Y. Effect of fuel origin on synergy during co-gasification of biomass and coal in CO_2. Bioresource Technology 2016; 200: 789–794.
[58] Jiang L, Hu S, Wang Y, Su S, Sun L, Xu B, He L, Xiang J. Catalytic effects of inherent alkali and alkaline earth metallic species on steam gasification of biomass. International Journal of Hydrogen Energy 2015; 40: 15460–15469.
[59] Howaniec N, Smoliński A. Influence of fuel blend ash components on steam co-gasification of coal and biomass — Chemometric study. Energy 2014; 78: 814–825.
[60] Wei J, Guo Q, Chen H, Chen X, Yu G. Study on reactivity characteristics and synergy behaviours of rice straw and bituminous coal co-gasification. Bioresource Technology 2016; 220: 509−515.
[61] Encinar JM, Gonzalez JF, Martinez G, Sanchez N, Sanguino IM. Hydrogen production by means of pyrolysis and steam gasification of glycerol. Fuel Processing Technology 2002; 75: 27–43.
[62] Zamboni I, Courson C, Kiennemann A. Synthesis of Fe/CaO active sorbent for CO_2 adsorption and tars removal in biomass gasification. Catal Today 2011; 176: 197–201.
[63] Felice L-D, Courson C, Kiennemann A. Biomass gasification with catalytic tar reforming: a model study into activity enhancement of calcium and magnesium oxide based catalytic materials by incorporation of iron. Energy Fuels 2010; 24: 4034–45.
[64] Ohtsuka Y, Kuroda Y, Tamai Y, Tomita A. Chemical form of iron catalysts during the CO_2-gasification of carbon. Fuel 1986; 65:1476–1478.
[65] Blanchard J, Abatzoglou N. Nano-iron carbide synthesized by plasma as catalyst for Fischer–Tropsch synthesis in slurry reactors: The role of iron loading and K, Cu promoters, Catalysis Today 2014; 237: 150–160.
[66] Pour AN, Shahri SMK, Bozorgzadeh HR, Zamani Y, Tavasoli A, Marvast MA. Effect of Mg, La and Ca promoters on the structure and catalytic behavior of iron-based catalysts in Fischer–Tropsch synthesis.

Applied Catalysis A: General 2008; 348: 201–208.
[67] Shen L and Murakami K. Steam co–gasification of iron–loaded biochar and low rank coal. International Journal of Energy Research 2016; 40: 1846–1854.
[68] Howaniec N and Smolinski A. Effect of fuel blend composition on the efficiency of hydrogen–rich gas production in co–gasification of coal and biomass. Fuel 2014; 128: 442–450.
[69] Yuan S, Dai Z, Zhou Z, Chen X, Yu G, Wang F. Rapid co–pyrolysis of rice straw and a bituminous coal in a high–frequency furnace and gasification of the residual char. Bioresource Technolodge2012; 109: 188–197.
[70] Jeong HJ, Sang SP, Hwang J. Co–gasification of coal–biomass blended char with CO_2 at temperatures of 900–1100 °C. Fuel 2014; 116: 465–470.
[71] Sun Z, Chen S, et al. Improvement of H_2-rich gas production with tar abatement from pine wood conversion over bi-functional $Ca_2Fe_2O_5$ catalyst: Investigation of inner-looping redox reaction and promoting mechanisms. Applied Energy 2018; 212(15): 931－943.
[72] Zhang J, Yin J, Cao W, Yang L. Characterization of ultrafine particle iron–carbide catalyst and investigation on the catalytic mechanism for F–T synthesis. Journal and fuel chemistry and Technology 1993; 21: 375–379.
[73] Li X, Hui H, Li S, He L, Cui L. Integration of coal pyrolysis process with iron ore reduction: Reduction behaviors of iron ore with benzene–containing coal pyrolysis gas as a reducing agent. Chinese Journal of Chemical Engineering 2016; 24: 811–817.
[74] Qi X, Guo X, Luo Z, Zheng C. Effect of Iron on the Structure of Shenfu Brown Coal Char During Pyrolysis. Journal of Engineering Thermophysics 2014; 4: 796–800.
[75] Zhang Y, Zheng Y, Yang M, Song Y. Effect of fuel origin on synergy during co-gasification of biomass and coal in CO_2. Bioresource Technology 2016; 200: 789–794.
[76] Che D, Li J, Li S, Wang Q. Experimental Investigation of Effect of Biomass Blending Ratio on Coal Gasification. Characteristics Proceedings of the CESS 2013; 33: 35–40.
[77] Yan W, Lu X. Investigation of Effect of the Blending Ratios of Biomass and Lignite on Characteristic of Co-gasification. Proceedings of the CSEE2009; 29: 150－155.
[78] Qi XJ, Guo X, Xue LX, Zheng CG. Effect of iron on Shenfu coal char structure and its influence on gasification reactivity. Journal of

Analytical and Applied Pyrolysis 2014; 110: 401–407.
[79] Shen L, Nakamura A and Murakami K. Effect of adding iron-loaded biochar on steam gasification of subbituminous coal. Global Journal of Engineering Science and Research Management 2017; 4 (1): 23－38.
[80] Kinoshita MC, Wang Y and Zhou J. Tar formation under different biomass gasification conditions. Journal of Analytical and Applied Pyrolysis 1994; 29(2): 169－181.
[81] Palma CF. Modelling of tar formation and evolution for biomass gasification: A review. Applied Energy 2013; 111: 129－141.
[82] Qin Y, Campen A, Wiltowsk T, Feng J, Li W. The influence of different chemical compositions in biomass on gasification tar formation. Biomass and Bioenergy 2015; 83: 77－84.
[83] Yu H, Zhang Z, Li Z, Chen D. Characteristics of tar formation during cellulose, hemicellulose and lignin gasification. Fuel 2014; 118(15): 250－256.
[84] Tursun Y, Xu S, Wang G, Wang C, Xiao Y. Tar formation during co-gasification of biomass and coal under different gasification condition. Journal of Analytical and Applied Pyrolysis 2015; 111: 191－199.
[85] Zhang F, Xu D, Wang Y, Argyle M, Fan M. Tar formation during co-gasification of biomass and coal under different gasification condition. Applied Energy 2015; 145: 295－305.
[86] Cahyono R, Rozhan A, Nomura T, Hosokai S, Kashiway Y, Akiyama T. Catalytic coal-tar decomposition to enhance reactivity of low-grade iron ore. Fuel Processing Technology 2013; 143: 84－89.
[87] Yu J, Tian F, Chow M, Mckenzie L and Li C. Effect of iron on the gasification of Victorian brown coal with steam: enhancement of hydrogen production. Fuel 2006; 85: 127–133.
[88] Mafu L, Neomagus H, Everson R, Okolo G, Strydom C, Bunt J. The carbon dioxide gasification characteristics of biomass char samples and their effect on coal gasification reactivity during co-gasification. Bioresource Technology 2017, in press.
[89] Zhang Z, Pang S and Levi T. Influence of AAEM species in coal and biomass on steam co-gasification of chars of blended coal and biomass. Renewable Energy 2017; 101: 356－363.
[90] Park HJ, Park HW, Choi S, Park DW. Effects of blend ratio between high density polyethylene and biomass on co-gasification behavior in a two-stage gasification system. International Journal of Hydrogen Energy 2016; 41(38): 16813－16822.

[91] Peng W, Ge S, Ebadi AG, Hisoriev H, Esfahani MJ. Syngas production by catalytic co-gasification of coal-biomass blends in a circulating fluidized bed gasifier. Journal of Cleaner Production 2017; 161(1): 1513－1517.
[92] Wang G, Zhang J, Zhang G, Ming X, Li X, Liu Z, Guo J. Experimental and kinetic studies on co-gasification of petroleum coke and biomass char blends. Energy 2017; 131(15): 27－40.

Acknowledgments

The study presented in thesis has been carried out under continuous help and assistance by many people.

I am sincerely grateful to Professor Murakami Kenji, Akita University, for his continuous guidance over the past five years and valuable suggestions throughout this work.

I am deeply indebted to Assistant teacher Ayano Nakamura, Akita University, for her useful suggestions and helping in many aspects during my research work.

I would like to express my thanks to parents, my aunt and my friends for their mental support during my research.

February 2018
Shen Lingbo